ENHANCEMENT OF TRANSPORT PROCESS IN MICRO-CHANNEL

Thesis submitted for the award of the degree of

Doctor of Philosophy (Engg.)

by

SAMPAD GOBINDA DAS

DEPARTMENT OF MECHANICAL ENGINEERING

JADAVPUR UNIVERSITY

KOLKATA-700032, INDIA

2025

INDEX NO. 176/19/E

1. **Title of the Thesis:** ENHANCEMENT OF TRANSPORT PROCESS IN MICRO-CHANNEL

2. **Name Designation & Institution of the Supervisors:**

Dr. Himadri Chattopadhyay
Professor,
Department of Mechanical Engineering,
Jadavpur University, Kolkata-700032, India

Dr. Suvanjan Bhattacharyya
Assistant Professor
Depatment of Mechanical Engineering
BITS Pilani, Pilani, Rajasthan-333031, India

3. List of Journal publications from the thesis

Journals:

- ✓ **Das. S. G.,** Bhattacharyya. S., Chattopadhyay. H., **Benim. A. C. (2021), Transport phenomenon of simultaneously developing flow and heat transfer in twisted sinusoidal wavy microchannel under pulsating inlet flow condition,** Heat Transfer Engineeirng, 43 (3-6), 410 - 422.
- ✓ Bhattacharyya. S., **Das. S. G.**, Chattopadhyay. H. (2020), **Thermohydraulic Characteristics and entropy analysis of a Novel Clockwise and Anti-Clockwise Twisted Sinusoidal Wavy Micro-channel under Pulsating Inlet Condition,** European Physical Journal Applied Physics, 92 (2),

4. **List of Patents**

Nil

5. List of National / International Conferences

- ✓ **Suvanjan Bhattacharyya, Sampad Gobinda Das, Himadri Chattopadhyay, M. A. Moghimi, Ali Cemal Benim, "Transport phenomenon and optimization of simultaneously developing flow and heat transfer in twisted sinusoidal wavy microchannel under pulsating inlet flow condition",** XII International Conference on Computational Heat Mass & Momentum Transfer (ICCHMT 2019), Roma Tre University & University of Rome, Rome, Italy, September 3 – 6, 2019.

- ✓ **Sampad Gobinda Das, Suvanjan Bhattacharyya, Himadri Chattopadhyay,** " Numerical Investigation of Heat Transfer Enhancement for Flow Past Twisted Micro-Channels", International conference on Energy & Sustainable Development (ISCESD 2020), Jadavpur University, Kolkata, India, February 14 – 15, 2020.

- ✓ **Sampad Gobinda Das, Suvanjan Bhattacharyya, Himadri Chattopadhyay, "**Thermo-hydraulic Characteristics of a Stepped Micro-Channel under Pulsating Inlet Flow Condition", 48th National Conference on Fluid Mechanics and Fluid Power (FMFP), BITS Pilani, Pilani Campus, Rajasthan, (India), December 27-29, 2021.

PROFORMA – 1

"Statement of Originality"

I, Sampad Gobinda Das registered on 24/06/2019 do hereby declare that this thesis entitled "ENHANCEMENT OF TRANSPORT PROCESS IN MICRO-CHANNEL" ontains literature survey and original research work done by the undersigned candidate as part of Doctoral studies.

All information in this thesis have been obtained and presented in accordance with existing academic rules and ethical conduct. I declare that, as required by these rules and conduct, I have fully cited and referred all materials and results that are not original to this work.

I also declare that I have checked this thesis as per the "Policy on Anti Plagiarism, Jadavpur University, 2019", and the level of similarity as checked by iThenticate software is 8%.

Signature of Candidate: Sampad Gobinda Das

Date: 27/11/25

Certified by Supervisor(s): (Signature with date, seal)

1. H. Chattopadhyay 27.11.25

Dr. Himadri Chattopadhyay
Professor
Dept. of Mechanical Engg.
JADAVPUR UNIVERSITY
Kolkata-700 032, India

2. Bhattacharyya 27/11/2025

ASSISTANT PROFESSOR
DEPT. OF MECHANICAL Engg.
BITS PILANI
PILANI, RAJASTHAN

CERTIFICATE FROM THE SUPERVISOR

This is to certify that the thesis entitled **"Enhancement of Transport Process in Micro-channel"** submitted by Shri Sampad Gobinda Das who got his name registered on 24/06/2019 for the award of Ph.D. (Engg) degree of Jadavpur University is absolutely based upon his own work under my supervision and guidance and that neither his thesis nor any part of the thesis has been submitted for any degree/diploma or any other academic award anywhere before.

H. Chattopadhyay
23.6.2025

Signature of Supervisor
and date with office Seal
Dr. Himadri Chattopadhyay
Professor
Department of Mechanical Engineering,
Jadavpur University, Kolkata-700032

Dr. Himadri Chattopadhyay
Professor
Dept. of Mechanical Engg.
JADAVPUR UNIVERSITY
Kolkata-700 032, India

Bhattacharyya 23/06/2025

Signature of Co- Supervisor
and date with office Seal
Dr. Suvanjan Bhattacharyya
Assistant Professor
Depatment of Mechanical Engineering
BITS Pilani, Pilani, Rajasthan-333031

Dedicated

to

my Parents

and

Wife

ACKNOWLEDGEMENT

It is my pleasure to express my heartiest gratitude to my supervisors Prof. Himadri Chattopadhyay, Department of Mechanical Engineering, Jadavpur University and prof. Suvanjan Bhattacharyya, Department of Mechanical Engineering, BITS Pilani for their invaluable guidance, thorough encouragement and total involvement in my endeavour through every step to complete my research work. They helped me to broaden my view and knowledge and also guided me to work on the right track for facing the new challenges in achieving the target at the right time by providing an excellent and stirring working atmosphere. Their keen interest on the topic and enthusiastic support on my effort was a source of inspiration and always in my mind to smoothly carry out my research work and make me alert for work ahead. They paid much of the invaluable time for improving the draft manuscript of entire thesis. I consider myself fortunate to work under their careful supervision and guidance that brought me wherever I stand today in my research carrier. They always given me priority to my needs at every step for consultation, discussion and deliberation be it academic or personal. No word is sufficient to explain my indebtedness to them for their pioneering support and dedication to my successful compilation of this thesis.

I am very much thankful to prof. Swarnendu Sen, Mechanical Engineering Department, Jadavpur University for his help and cooperation during my research work in Jadavpur University.

I would like to convey my sincere gratitude to Prof. Anindya Ghosh, OIC, GCETTB, Berhampore for providing me the all-time inspiration, and valuable guidance for this research work.

I would like to express my sincere gratitude to Prof. B. Chakraborti, Principal, RKMGEC, Purulia, whose inspiration and support made it possible for me to complete my Ph.D. I am really thankful to Prof. J Shit, Head of the Department of Mechanical Engineering, RKMGEC, Purulia, who always encouraged me throughout the tenure of this work and helped me as and when required is spite of the many problems.

I am also thankful to my colleagues Prof. Saurav Manna, Prof. Malay Quila, Prof. Dwaipayan Ghosh, Prof. Biswajit Singh Sardar, Prof. suman Mandal, Prof. Asim kumar Batabyal, Pof.

Indraneel Sinha, Prof. Sunil Hasda, Prof. Bijay Kumar Mudi, and Prof. Dilip Sao for their continuous help and support to complete this work successful I am grateful to my parents for their silent support, good wishes and blessings which guided me throughout my life. I would like to express my deepest sense of gratitude to my wife Sayani for her love, patience, understanding and inspiration in spite of all the ups and downs of my life. The completion of this thesis would not have been possible without her sacrifice.

Sampad Gobinda Das
23/06/25

Sampad Gobinda Das

ABSTRACT

Due to rapid shrinking and increased heat flux density, effective thermal management in tiny systems such as microelectronics, MEMS, and biomedical devices has become increasingly important. Because of its great surface area to volume ratio and efficient convective heat transfer properties, micro-channel heat sinks have become a potential approach for high-performance thermal management. Conventional micro-channel designs still suffer in thermal performance, nevertheless, from laminar flow regimes and boundary layer formation. Using Computational Fluid Dynamics (CFD), this thesis examines the improvement of heat transport in micro-channels under constant and pulsating flow conditions. The influence of pulsation frequency, amplitude, and waveform on flow behaviour and thermal performance is investigated in this work therefore offering a thorough knowledge of flow-thermal interactions at the microscale.there are six chapters form the thesis. Microscale heat transmission, the value of micro-channel technology, and the function of flow pulsation in thermal enhancement are thoroughly reviewed in Chapter 2. The chapter also points out current research gaps and drives the necessity of a computer analysis.

Together with the modelling assumptions, Chapter 3 shows the governing equations for heat transfer and fluid flow. The finite volume method (FVM) is the foundation of the numerical technique applied; ANSYS Fluent is used for simulations. Reliability and accuracy of the model are guaranteed by thorough grid independent investigation and validation using benchmark previous literature data.

Using water as the coolant, Chapter 3 addresses the baseline investigation of heat transport in a 2D micro-channel under constant flow circumstances. We investigate in particular how Reynolds number affects Nusselt number, friction factor, and temperature distribution.

Chapter 5 presents flow pulsation into the 3D micro-channel and assesses their effect on thermal and hydrodynamic performance. The work explores a spectrum of pulsation frequencies and amplitudes, emphasizing the regimes whereby pulsation greatly increases the convective heat transfer without causing a major pressure penalty. Also, the chapter investigates pulsing flows the performance of micro-channels with geometric modifications. I investigate synergistic thermal increase techniques by means of the combined influence of geometry-induced turbulence and flow pulsation.

Chapter 6, at last, compiles the main conclusions and contributions of the investigation. It emphasizes that depending on the flow parameters and waveform, pulsing flow can increase the Nusselt number by up to 30–45%. This improvement is accompanied, nevertheless, by a pressure decrease that has to be tuned depending on the intended use.

This work presents insightful analysis of micro-channel heat sink design and optimization for high-performance uses. Engineers and designers hoping to apply active flow control techniques in small-sized thermal systems might find direction in the results. Future research could use phase transition materials or nano-fluids to improve performance even further.

CONTETNS

LIST OF FIGURES

LIST OF TABLES

NOMENCLATURE

A	pulsating flow amplitude Aw Wave Amplitude
Cp	Specific Heat
f	frequency of pulsation
f	friction factor
Dh	Hydraulic diameter of channel
h	heat transfer co-efficient
k	Thermal conductivity
L	Length of the domain (x direction)
Nu	Nusselt number
Re	Reynolds number
St	Strohul number
T	temperature
Ta	ambient temperature t time
Tw	average wall temperature
Uin	inlet velocity
Um	mean velocity
u	velocity component in x direction
v	velocity component in y direction
w	velocity component in z direction

Greek Symbols

η	enhancement ratio
λ	wavelength
μ	dynamic viscosity
ρ	density of working fluid

Subscripts

Avg	averaged over time
in	inlet
m	mean
w	wall
x	local

CHAPTER ONE

INTRODUCTION

1.1 Introduction

The conventional energy sources are anticipated to run out within the next few decades. In order to preserve the traditional energy sources, scientists and researchers are working on energy management concerns. In order to preserve traditional energy sources, it is necessary to use renewable energy sources more frequently and make conventional energy systems more efficient. Modern scientists are paying more attention to the energy system's thermal management. Numerous studies have been conducted to increase the effectiveness of energy systems. One of the cutting-edge approaches to creating energy-efficient systems is miniaturisation. The technology of heat exchangers has been greatly impacted by miniaturization, which makes the heat exchangers more efficient and small. The total effectiveness and lifespan of the thermal energy system are significantly influenced by the efficiency of a heat exchanger. A cutting-edge heat-exchanger device is the micro-channel heatsink. The benefits of the micro-channel heat sink's huge heat transfer surface and great compactness make it the most suited heat dissipation device for electronic cooling applications. The ability of a modern high-powered small electronic component to dissipate heat affects how long it will last. An American company (AI Technology Inc.) located in new jersey conducted a survey on major causes of electronic device failure (Hanafi *et al* 2015). Figure 1.1 illustrates the result they received. Their result manifested that temperature, vibration, dust and humidity are the four major causes of failure of electronic devices. They also found that dust is the least important issue (furnishes only 6% of the total failure) while, temperature (contributing 55% of the total failure) is the major one. According to their study the general purpose electrical devices should maintain a maximum temperature range between 75° - 120° (Faraji and El Qarnia, 2010). It can be concluded that it is essential for the electronic devices to have a dependable thermal management system that can dissipate the heat generated efficiently from the components.

By offering an effective heat dissipation device like MCHS, an electronic component's lifespan is increased. Additionally, MCHS is used in the LED cooling, combustors, refrigeration, fuel cells, chemical, and food industries, among other places. The wealth of MCHS literature is evidence of the technology's promise.

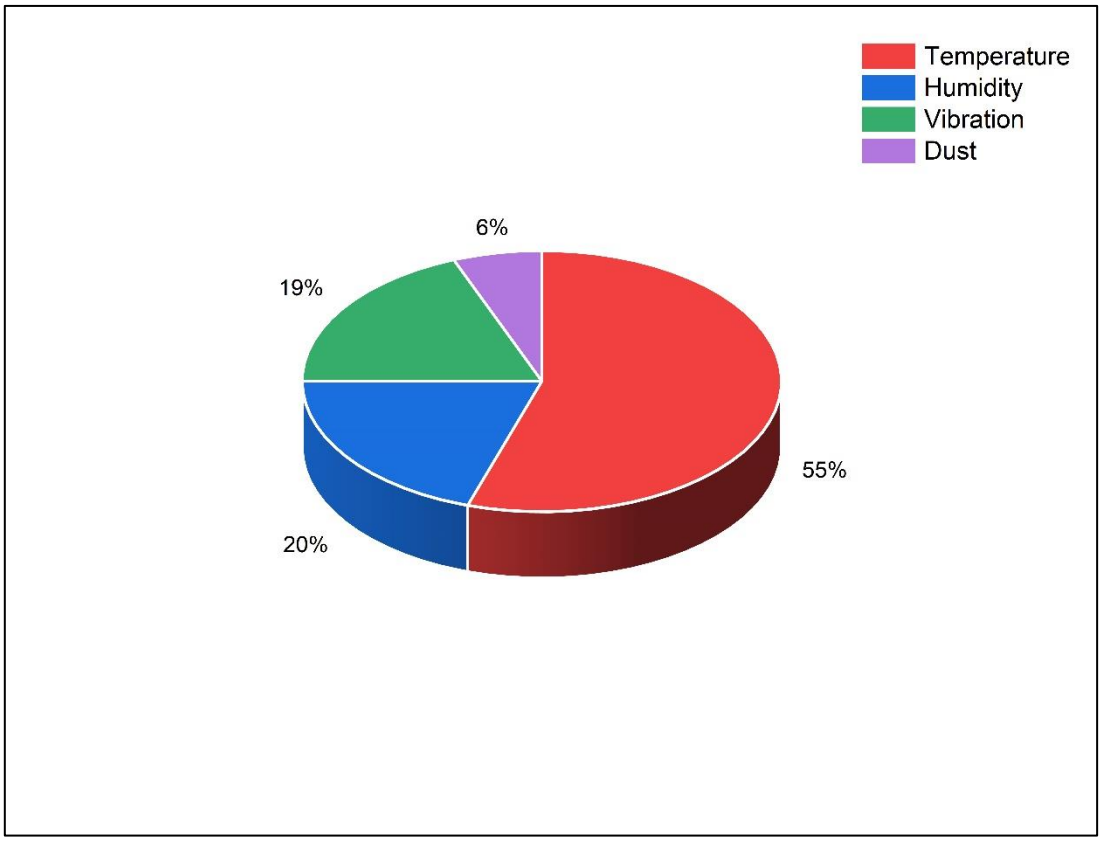

Figure 1.1: Major causes of electronic failure

Micro-channels are classified as per their hydraulic diameter. Different types of classifications are available in literatures. However, the most commonly used classification are provided by Kandilkar and Grande (2010) as follows: -

3mm < D: Conventional Passages

200 μm < D < 3mm: Mini-channels

10 μm < D < 200 μm: Micro-channels

1 μm < D <10 μm: transitional Micro-channels

Some researchers also follow classification by Obot (2002) considering channels with hydraulic diameter less than 1000 μm (1 mm) are all micro-channels.

1.2 Heat Transfer Enhancement Techniques

The heat Transfer Enhancement Techniques can be broadly classified as follows: -

1. Active Techniques.
2. Passive Techniques.

The enhancement techniques that utilizes inputs from some external sources to achieve enhanced heat transfer, are defined as active techniques. Generally, active techniques utilize input from some external sources. The input may be in the form of power, electricity, RF signals or a pump. The methods that falls under the active enhancement technique category are as follows -

a) **Vibration: -** Vibration in the fluid or the surface carrying the fluid can be applied to enhance the heat transfer.
b) **Electrostatic Fields: -** In this method, the flow is exposed to an electrical field. It is studied by a number of researchers and they found enhancement for conventional, as well as mini-channel flows.
c) **Flow Pulsation: -** Applying variable velocity at inlet, and thus varying the mass flow rate through the inlet of the flow passage may also furnish enhanced heat transfer result. Better mixing of the flowing fluid can be achieved by this method, and better mixing can result in heat transfer augmentation.

d) **Variable Roughness: -** In this method, the surface roughness of the channel wall is varied throughout the section.

Passive enhancement techniques are those where the enhancing factors are added inside the channel. Hence no external source is required to enhance heat transfer. These are generally linked with different kind of surface geometry modification or combination of them. Some important methods are: -

a) **Surface Roughness: -** In this method, the surface roughness is increased by surface treatment of the heated channel wall. By increasing the roughness of the heated wall, reduction in boundary layer thickness and early transition to turbulent flow may be obtained. This can increase the heat transfer.

b) **Flow disruption: -** Probably the most popular passive technique. In this method, flow is disrupted using twisted tape, coiled wire, bluff bodies etc. It can accommodate improved fluid mixing and may also beneficial for disruption of the boundary layer causing flow transition as shown in figure 1.2. and 1.3.

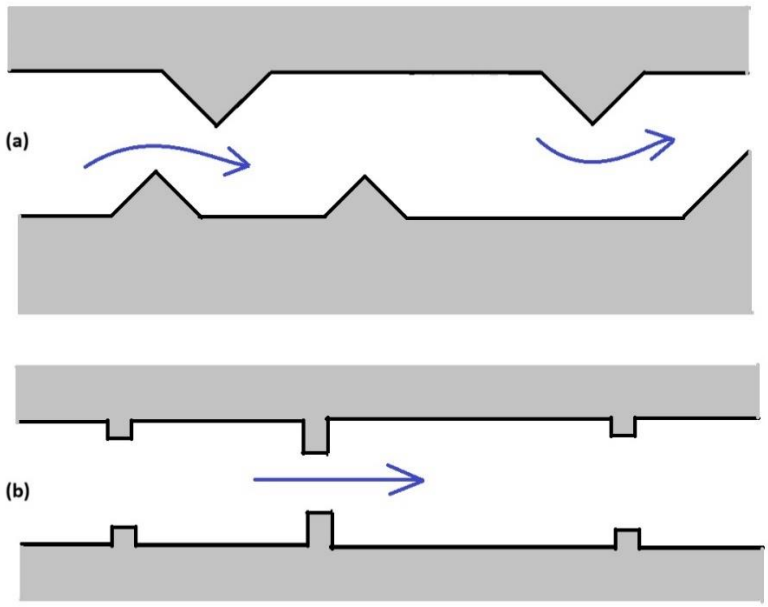

Fig. 1.2 Flow disruption with sidewall flow obstruction
(a) triangular obstructions (b) square obstructions

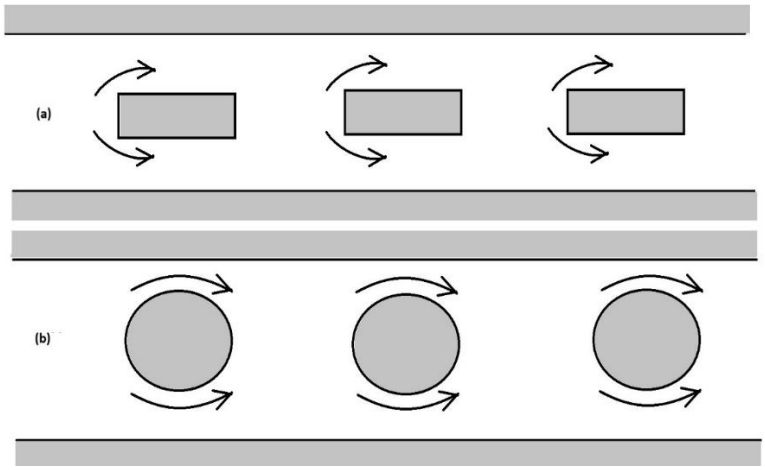

Fig. 1.3 Flow obstruction inside channel

(b) rectangular obstructions (b) circular obstructions

c) **Channel Curvature: -** Several researchers reported heat transfer enhancement using this method. In this method, the working fluid is passed along a curved path. The traditional parabolic velocity profile is distorted by the additional acceleration force. consequently, the angle between the gradient is reduced, thereby, facilitating enhancement.

d) **Re-entrant Obstruction: -** This method enables re-entrance of the same working fluid inside the flow passage to achieve enhanced heat transfer by placing obstruction over flow path (as in figure 1.3). These obstructions disrupt the fluid flow and facilitate redevelopment of thermal boundary layer leading to enriched fluid mixing and higher heat transfer co-efficient.

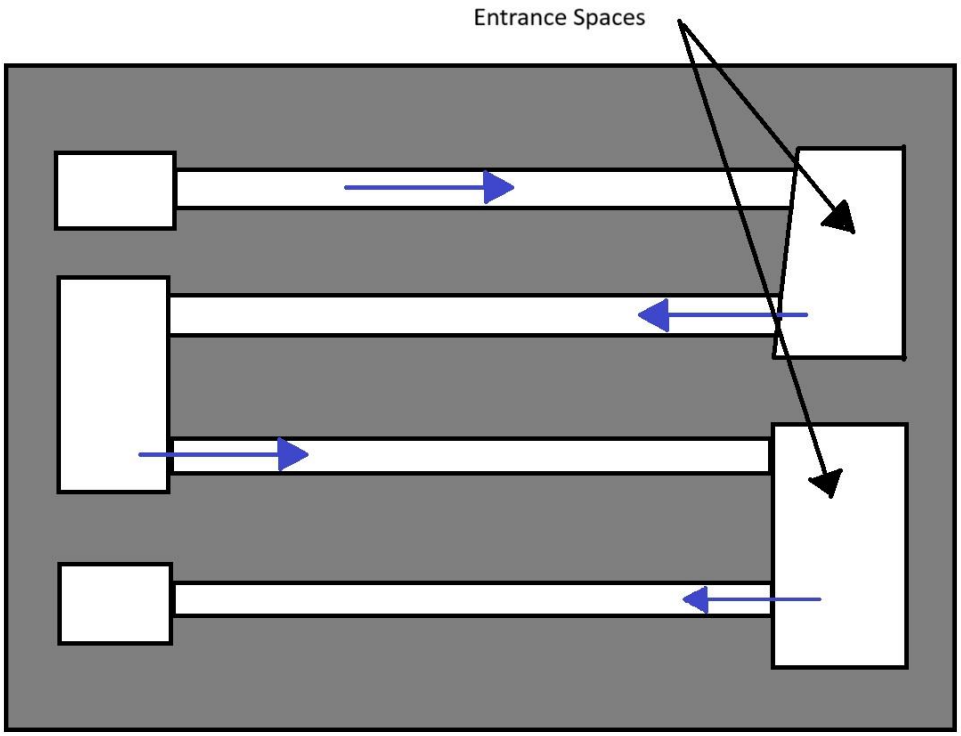

Fig. 1.4 Re-entrant Obstruction

e) **Secondary Flows: -** An extra secondary flow is injected to the main flow in this method as illustrated in figure 1.4. This can improve swirl flow, thus enhancing heat transfer.

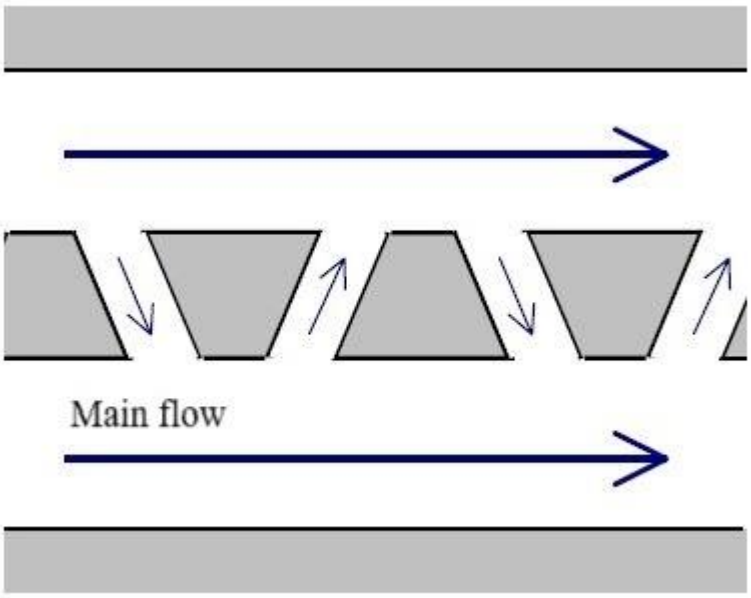

Fig. 1.5 Secondary flow paths

f) **Out of Plane Mixing: -** To increase the binary fluid mixing, this method can be used. the flow axis is changed repeatedly in this method. To enable this, a channel twisted about the flow axis can be incorporated.

g) **Fluid Additives: -** Small particles, containing a phase change material (PCM) are added to the working fluid in this approach. As the fluid temperature rises, the solid particles added with the fluid attain their melting point. The latent heat of fusion necessary for the PCM is taken from the heated surface, hence improving heat transfer.

1.3 Advantages and Disadvantages of Micro-Channel Heat Sink (MCHS)

A Micro-Channel Heat Sink (MCHS) is a specific kind of heat exchanger, designed primarily for the thermal management of electronic equipment involving high heat flux. It employs small channels (about 10–500 micrometres in width) through which a cooling circulates for effectively heat dissipation. An MCHS consists of a base plate with micro-sized parallel channels etched into it, followed by a cover plate to form the enclosure. Water or any other dielectric liquid can be used for a liquid cooling setup. Whereas, air or any other chemically stable gas can be used for gas cooling purpose. Advantages of using MCHS are as follows: -

1. Due to their large surface area to volume ratio, micro-channel heat sinks enjoy inflated heat transfer.
2. Their compact size suits well for the miniaturized electronics and space-constrained systems that accumulates large amount of heat (e.g., laptops, embedded systems).
3. Can handle heat fluxes over 1000 W/cm², which is beyond the capability of traditional cooling methods.
4. Can provide enhanced thermal performance with a range of coolants.

5. Due to large contact surface area and small fluid volume, they response much more quickly towards temperature changes
6. They also enjoy the advantages of reduced thermal resistance, due to short path between the heat source and the cooling fluid.

Though an MCHS enjoys a lot of advantages over conventional heat exchangers, it also possesses specific operational restrictions as outlined below (2020): -

1. The inflated surface area in micro-channels results in an elevated friction factor, causing a greater pressure drop, which is exacerbated when high-viscosity fluids are introduced.
2. When nano-fluids are used to achieve more enhanced heat transfer in MCHS, the performance can severely drop due to fouling effects on channel walls.
3. In MCHS, the fluid flow distribution is non-uniform and that can produce hot spots on the device, which, in turn will reduce the durability of the devices.
4. The MCHS need high surface quality to extract best performance from them. However, it is very much inconvenient to manufacture micro-sized devices with near zero surface roughness.
5. Due to small flow passage, chances of blockage caused by the impurities of the coolant are high.

1.4 Application of Micro-Channel Heat Sink (MCHS)

The application of Micro-Channel Heat Sinks (MCHS) has been widely explored in various industries due to their unique features, such as high heat transfer rate, compact size, light weight etc. Some of the major application of Micro-Channel Heat Sinks are as follows: -

Micro-Channel Heat Sinks in Refrigeration and Air Conditioning

One of the primary application of MCHS is in the field of refrigeration and air conditioning. in this industry, the use of MCHS has been proven to provide significant advantages over traditional heat exchanges. Due to their small size, MCHS can be incorporated into smaller refrigeration systems, resulting in a more compact and efficient design. Additionally, the use of MCHS in refrigeration and air conditioning systems has been found to reduce the amount of refrigerant required, which is an important consideration due to environmental concerns related to refrigerate leakage. MCHSs can also operate at higher heat fluxes, leading to improved performance and efficiency.

Micro-Channel Heat Sinks in Electronic Cooling

Another area where MCHSs have been widely applied is in the field of electronic cooling. With the increasing use of electronic devices, there is a growing need for efficient cooling systems to dissipate the heat generated by these devices. MCHSs are an ideal solution for this application due to their compact size and high heat transfer capabilities. In electronic cooling, MCHSs can be integrated directly into the electronic device, providing efficient cooling while maintaining a small form factor. MCHSs have also been used in heat sinks and cold plates for high performance computing system.

Micro-Channel Heat Sinks in Power Generation

Another area where MCHSs have found application is in the field of power generation. They have been used in the cooling of fuel cells which are a promising technology for the generation of Clean Energy. The use of Micro-Channel Heat Sink in fuel cell cooling has been found to improve the performance and efficiency of the system while reducing the overall size and weight of the system. Micro-Channel Heat Sink have also been used in the

cooling of nuclear reactors, where the high heat fluxes and corrosive environments make traditional heat exchangers impractical.

Micro-Channel Heat Sinks in Aviation

MCHSs have also found application in the aerospace industry. in this industry, the use of MCHS has been explored as a means of improving the efficiency of thermal management systems. The compact size and high heat transfer capabilities of MCHSs make them and ideal solution for use in spacecraft and satellites, where weight and space limitations are critical factors. MCHSs have also been used in the cooling of high power electronic devices in aerospace applications.

Micro-Channel Heat Sinks in Automobile

Due to their compact size and efficient heat dissipation capabilities in limited spaces, they are favoured as heat sinks in various parts of automobiles. They can be used in radiators for engine cooling enhancement, in Electric Vehicle battery thermal management, can also be used in automobile electronic cooling.

1.5 Heat Transfer in Micro-channel with Pulsating Inlet

Pulsating flow can enhance heat transfer performance of micro-channels remarkably as compared to steady one. The oscillating nature of the fluid flow, produces intense mixing effect, thus resulting in augmented convective heat transfer. Therefore, it is imperative to comprehend the unsteady flows within micro-channels. This can be achieved by employing a passive technique that imposes pulsatile flow at the inlet, potentially leading to substantial enhanced heat transfer through the micro-channel. Furthermore, it seeks to induce boundary layer destabilisation in low Reynolds number flows.

Prior studies, which include the work of Nandi et al (2013, 2014), showcased numerical results for overall heat transfer augmentation in some certain micro-channel geometry, considering a wide range of parameters, such as Reynolds number (both steady and pulsating), Strouhal number, amplitude, in comparison to the steady flow scenario.

1.6 Organization of the Thesis

The present thesis accommodates six chapters. The first chapter provides, a brief introduction to microchannel flow, its application and heat transfer enhancement techniques.

Chapter two delivers a brief literature review on micro-channel fluid flow and heat transfer. This chapter is sub-divided into several parts to elaborate different aspects of the field of study. Different parameters like fluid flow characteristics, heat transfer characteristics, vortex generation, boundary layer separation, enhancement techniques are also discussed in literature review. Based on this literature review, specified objectives are enumerated in this chapter.

Chapter three demonstrates the mathematical modeling for the present work. Further, the parameters used to evaluate heat transfer performance (surface averaged Nusselt number, friction factor, PEC, entropy generation, Bejan Number etc) are introduced.

In chapter four, numerical investigation of two different two-dimensional modified micro-channel is showcased. The first channel constitutes sudden contractions in stream-wise direction as geometric modification to promote fluid mixing. While the second one constitutes a converging diverging flow path in stream-wise direction as geometric modification to foster vortex generation. Effect of sinusoidal pulsation at the inlet and geometry modification was described in this chapter.

Chapter five investigate numerically the simultaneously developing unsteady laminar flow and heat transfer inside a twisted sinusoidal wavy microchannel. Moreover,

investigation on simultaneously developing unsteady laminar flow and heat transfer inside a clockwise and counterclockwise twisted sinusoidal wavy microchannel. The channel was made twisted clockwise for the first half of the length of the channel and the remaining half-length is twisted counter-clockwise. At the inlet sinusoidal varying velocity component was applied for both the cases. Varying pulsating amplitude and frequency represented by the Strouhal number studied for Reynolds numbers ranging from 1 to 100.

In chapter six, the conclusions drawn from the studies of the thesis are presented. Future scope of work also discussed here.

CHAPTER TWO

LITERATURE REVIEW

With the modernization of science and technology, daily uses of different electronic circuits and other components are experiencing rapid growth. These appliances require high processing speed and simultaneously comparatively smaller sizes. As a result, a large amount of heat accumulation over these devices has become inevitable. The need for smaller, more powerful electronic circuits has sparked a variety of research initiatives to develop more effective thermal management of these systems. To keep the devices at their ideal temperature and stop them from burning, cooling is necessary. Due to the wide range of applications, improving heat transfer at the microscale is a difficult task for which micro-channels are often employed. In this chapter, a detailed literature survey is presented to understand the current scenario in this regard. The review accumulates a wide range of literature involving fluid flow and heat transfer investigations inside micro-channel heat sinks. Both Passive techniques and Active techniques, and their effects are addressed in this chapter.

2.1 Fluid Flow and Heat Transfer in Micro-channels

Steinke and Kandlikar (2004) summarised the microchannel heat exchange (MCHE) strategy and flow behaviour of micro and mini-channels. Research work involving thermal performance of MCHS was introduced by Tuckerman and Pease (1981). The channel was rectangular in cross-section with 50 μm width and 302 μm depths. Constant heat flux boundary condition with 790 W/cm^2 power densities was engaged.

An experimental study of Gas and liquid flow behaviour through micro-channels was conducted by Pfahler *et al.* (1991). They fabricated channels with rectangular cross-section and area ranging from 80 square nanometre to 7200 square nanometre for the investigation purpose. They found that while the experimental results for large flow channels were somewhat consistent with the predictions made from solving Navier Stokes equations, the variances grew for small channels

Wang and Peterson (1994), conducted heat transfer experiments on rectangular micro-channels with hydraulic diameter ranging from 0.133 mm to 0.367 mm. They deployed water as their cooling fluid. Their result showed that the laminar heat transfer regime falls within a Reynolds number range of 200 – 700. Also, turbulent convective heat transfer regime was found to be within Reynolds number range of 400 – 1500.

Peng and Peterson (1996), also conducted experiments of single phase forced convection heat transfer and fluid flow inside rectangular cross-section micro-channels. Their micro-channel geometry was with hydraulic diameters ranging from 133 – 367μm. Their result showed that hydraulic diameter and channel aspect ratio can influence the friction factor results greatly.

In deep rectangular micro-channels, single-phase forced convention was experimented by Harms *et al* (1999). They evaluated both single channel and multiple channel in two different setups. The channels of the multiple channel system were 25 μm wide, and the walls were 119 μm thick. The channels in both systems are around 1000 μm deep and define a projected area of 2.5 cm x 2.5 cm. Deionized water with a Reynolds number ranging from 173 – 12900 was employed as the working fluid. The local Nusselt number derived through experiments, aligned well with the results from the predictions made by solving Navier-Stokes equations.

Using PIV, Meinhart *et al* (1999) experimentally observed velocity fields with a spatial precision of order 1 m. In a 30 μm × 300 μm rectangular micro channel, ensemble averaged velocity profiles were reported. Their result agreed to be within 2% of the analytical solution obtained from Stokes flow solution in a rectangular micro-channel.

With the use of a micro PIV, Klank *et al.* (2002) studied flow behaviour in a micro-fluidic three dimensional sheathing structure. The structure was silicon made and 1.0-micron orange fluorescent polystyrene particle suspended in water was used as the flowing fluid. They also compared their results with numerical simulation.

Judy *et al* (2002) performed experiments with square and circular cross section micro-channels using distilled water, methanol and isopropanol as the working fluid for the cooling purpose. Their experiment involved micro-channels with hydraulic diameter ranging from 15 – 150 μm. A Reynolds number range of 8 – 2300 was employed in their experiment. Their observation indicated no significant deviation from the expected result from the solution of the Navier-Stokes equation.

Liu and Garimella (2002) performed flow visualization and pressure drop experiments on micro- channels. They also compared their experimental results with numerical simulations. Hydraulic diameter for their experiment was in the range from 244 – 974 μm whereas, Reynolds number ranged from 230 – 6500. They were able to measure the onset of turbulence through their flow visualization, and compared their pressure drop measurements with numerical calculations. Their results showed that both transition mechanism to turbulence and pressure drop behaviors follow the predictions from laminar flow models.

Qu and Mudawar (2002) tested micro channels of 349 μm hydraulic diameter both experimentally and numerically. The rectangular micro-channels were 713 μm in depth and 231 μm in width. They presented a detailed description of the heat transfer characteristics. Their established pressure drop and temperature distribution data agreed well with results from conventional channel flow.

Micron-resolution particle image velocimetry was used by Tretheway and Meinhart (2002) to measure the velocity profile of the water flowing across channels with 30 × 300 μm size.s. The micro-channel surface is 450 nm away from where the velocity profiles were measured. The measured velocity profiles were in agreement with Navier-Stokes solutions and the widely known no-slip boundary condition when the surface was hydrophilic (uncoated glass). However, an apparent velocity was detected immediately above the solid surface when the

micro channel surface was covered with a 2.3 nm thick coating of hydrophobic octa-decyl-trichlorosilane. The slide length is roughly 1 μm and the velocity was about 10% of the free-stream velocity.

Hrnjak and Tu (2007) conducted pressure drop investigation in single phase flow in rectangular micro-channel with hydraulic diameter ranging 69.5 – 304.7 μm. They utilized R314a as their working fluid with Reynolds number range 112 – 9180. They observed that the laminar flow theory predictions aligned with their findings when the channel surface is almost smooth. However, one of the examined channels had a sizable amount of surface abrasion, resulting in an increase in friction and a transition Reynolds number of 1570.

In their experimental investigation, Wu and Cheng (2003) used smooth, trapezoidal silicon micro-channels with different aspect ratios. They experimented with channel of hydraulic diameter ranging from 25.90 – 291 μm. they utilized deionized water as the cooling fluid. Their observations revealed that the Navier-Stokes equations are valid for water flow with no slip boundary condition over channels with hydraulic diameter as low as 25.90 μm. They also found that the friction factor data is significantly influenced by the channel aspect ratio.

Micro-PIV visualizations on micro-channels was carried out by Li and Peterson (2006), who found that there was no early transition to turbulence in their experiments. Micro channels with hydraulic diameters of 320 μm and aspect ratios of 1 to 5.7 were examined over a Reynolds number range of 200 to 3267 as part of some of their experiments. By measuring an increase in centerline velocity fluctuations, they were able to quantify the onset of turbulence and discovered that the transition region occurred for Reynolds numbers between 1765 and 2315. Additionally, they discovered that fully developed turbulent flow started to happen at Reynolds numbers between 2600 and 3200.

Avci and Aydin (2007) presented analysed fully developed mixed convective heat transfer of a Newtonian fluid in an open-ended vertical parallel plate microchannel with asymmetric wall heating. They also took into account the temperature jump near the wall and the velocity slip. They found that with increase in Knudsen number (Kn), velocity slip at wall increases and the maximum velocity decreases.

An experimental analysis of the impact of viscous dissipation in liquids flowing via heated micro-channels was conducted by Morini and Spiga (2007). The viscous dissipation effect, which has been demonstrated to be a characteristic "scaling effect" for micro-channel flow, can become extremely significant for liquid flows when the hydraulic diameter is smaller than 100 µm.

An experimental and theoretical examination on single-phase heat transfer in micro channels was presented by Hetsroni *et al.* (2009) and compared with numerical findings. They discussed regarding pressure drop variation and laminar to turbulent transitions. Data on heat transport in microscopic channels with hydraulic diameters ranging from 60 - 200 mm was examined. Axial heat flux caused by thermal conduction via the working fluid and channel walls, as well as the impacts of geometry and energy dissipation, were also studied. They assumed that under typical flow conditions, the impact of energy dissipation on heat transmission in micro-channels is minimal.

In order to investigate the laminar hydrodynamic development length at the entry region of adiabatic square micro channels, Ahmad and Hassan, (2010) conducted experiments. They measured the flow field using micro particle image velocimetry. Three distinct micro-channels with hydraulic diameters of 500 µm, 200 µm, and 100 µm were examined. Each and every channel had a cross-section of 1. Distilled water served as the working fluid. They

sampled Reynolds numbers between 0.5 and 200. For duct and parallel plates, they found good agreement with results obtained from traditional entrance length correlations.

2.2 Passive Enhancement Technique

It has been already discussed that enhancement can be achieved by active (external input utilized) as well as Passive measures (no external input used). Here, a detailed summary of literatures involving enhancement using passive techniques are presented. Among the passive enhancement techniques, the channel geometry modification is most popular one. Geometry modification includes both channel curvature (enforcing the fluid to flow on a curved path), as well as setting flow obstructing structures over the flow path to disrupt the flow.

Wang and Vanka (1995) investigated with a converging diverging micro-channel. They executed their study in transition zone for heat transfer augmentation. Above Reynolds number 180, they observed self-sustained oscillation inside the flow. This oscillatory flow brought instabilities in laminar thermal boundary layers and replenished the near wall fluid with the core fluid. This enhanced the heat transfer. Ničeno and Nobile (2001) carried out investigations over sinusoidal wavy micro-channel. Their simulation results established that the self-sustained oscillation in flow due to the wavy nature of the wall results in heat transfer augmentation. Guo and Li, (2003) experimented on micro-channels with high relative roughness. They observed that wall roughness may incur early turbulence transition than expected. They also concluded that surface roughness can produce better Nusselt Number results, though, would produce increased friction factor.

Croce *et al* (2007) investigated the effect of surface roughness on and heat transfer and pressure drop in micro-channel flow. A number of three-dimensional conical peaks were used to act as the roughness. These peaks were placed over a perfectly smooth surface of a planar micro channel. Varying Reynolds numbers, varied peak heights and peak

arrangements are taken into consideration. They found that the pressure drop may be considerably impacted by surface roughness. For a relative roughness of 2.65% an increase in Poiseulle number of up to 16% was observed. On the other hand, a maximum Nusselt number increase of about 7.7% was obtained with this kind of setup. Yeh and Yang (2009) carried out experiments with rectangular, air foil shaped micro-heat exchangers. Channel length and channel arrangements were the most important parameters that can influence the overall performance of the device. Their results exhibited that shorter the length and narrower the space, better is the thermal performance of the heat sink. Parida *et al.* (2010). To evaluate the overall cooling performance of the test setup, they used infrared thermography. Their findings indicate that the copper channel yields better thermal performance in terms of time constant i.e. found to be in the range of 1 – 2 seconds.

Three dimensional rectangular wavy micro-channels were numerically investigated by Sui *et al.* (2010). They utilized water as the coolant and conducted the simulation within a Reynolds number range 100 – 500. They found that the wavy channel can deliver improved thermal performance compared to traditional straight micro-channels. In rectangular wavy micro-channel heat sinks (MCHS) Mohammed *et al* (2011) conducted computational analysis. Evaluation of heat transfer and fluid flow characteristics was the main focus of their study. The rectangular channels they studied was with a range of wave amplitude 125 – 500 µm, while implying Reynolds number ranging from 100 -1000. Their results indicated that the proposed wavy micro-channel heat sink yielded significantly higher heat transfer results compared to the straight micro-channel heat sinks. Lu *et al* (2013) investigated micro-channel heat exchangers with wavy walls for heat transfer augmentation purpose. They used deionized water as their working fluid and their experiment involved Reynolds number ranging 10 -100. Channel with hydraulic diameter 500 µm was their flow passage. According to their experimental results, the wavy channel provided about 26% improved overall thermal

performance as compared to the straight micro-channel. Experiments on Aluminium and Copper base microchannel heat exchangers was conducted by Sui *et al* (2012) also investigated heat transfer studies in periodic wavy micro-channels. They utilized water as the coolant and conducted the simulation within a Reynolds number range 200 – 400. They found that the wavy channel can deliver improved thermal performance compared to traditional straight micro-channels.

In a microchannel with a hydraulic diameter of 500 μm, Lu *et al* (2013) executed numerical computation aimed to obtain enhanced cooling efficiency for integrated circuits. They examined micro-channels with dimpled structure for enhanced thermal performance of the heat sink. Channels with hydraulic diameter 500 μm and a constant heat flux of 1 W/mm^2 was deployed for their study. They performed the work within the laminar flow regime at low Reynolds number (100 – 500). Their result established that employing dimpled structure inside channel could be a prospective way to achieve enhanced thermal performance of Micro-Channel Heat Sinks (MCHS). Xie *et al.* (2013) tested wavy micro-channel to assess its effect on heat transfer and pressure drop. They executed numerical simulation with three different kinds of water-cooled, micro-channel heat sinks in their work. They observed that the longitudinal wavy microchannel is inferior to the straight rectangular micro-channel in terms of overall thermal performance. They also reported that transverse wavy micro-channel geometry proposed by them can produce better thermal performance when compared to the conventional straight rectangular cross-section micro-channel heat sink especially at higher wave amplitude. Ghaedamini *et al* (2013) studied the influence of geometrical parameters on heat transfer. They utilized a converging diverging channel as the flow passage for their study. They executed their work for three different Reynolds number (200, 400 and 600). They found that increase in waviness yields better thermal performance.

The effect of geometry on transition in wavy micro-channels was studies by Ramgadia and Saha (2013). They carried out numerical analysis of fully developed fluid flow and heat transfer in a two dimensional wavy micro-channel. They performed the computation for a Reynolds number range from 25 – 1000. They worked with both steady and transient case and observed a decrease in thermal performance factor with increase in Reynolds number for steady case. Whereas, in case of transient one, the thermal performance factor shows rising trend with increase in Reynolds number. Sakanova *et al* (2015) essayed effect of wavy micro-channel heat sink on heat transfer. They utilized pure water and three different types of nano-fluid with volume concentration ranging from 1% - 5% as the cooling medium. They found that channels with higher wave amplitude can provide lesser thermal resistance.

Heat transfer enhancement in wavy micro-channels with constant heat flux boundary condition was investigated by Rostami and Abbassi (2016). They have done detailed study for optimum geometrical parameters. They also assessed effect of nano-fluids on heat transfer rate. They found better thermal performance in their proposed scheme as compared to conventional straight micro-channels.

Huang *et al.* (2020) experimented with micro-channel heat exchangers featuring cavities of two different shapes to assess the thermal performance of the heat sink. They examined Reynolds numbers with low ranges (40 – 120). The hydraulic diameter of the micro-channel they fabricated for the experiment was 300 μm. their experimental results indicated that the cavities fitted in the flow path of the micro-channel heat sink (MCHS) can enhance heat transfer as well as yielding reduced pressure drop compared to straight channels.

The amplitude of the wavy micro-channel has a significant impact on the value of the heat transfer coefficient and the wall shear stress, according to Lori and Vafai (2022). They numerically investigated wavy micro-channels. Additionally, they found a significant rise in

pressure drop and friction factors, caused by the micro-channel heat sink's growing wavy amplitude. Wang *et al.* (2022) used Wavy micro-channels with secondary branches, in their study regarding heat transfer performance of the heat sink. They performed the computation within a Reynolds number range of 50 -700. They found good result in terms of heat transfer at high values of amplitude to wavelength ratio and Reynolds number.

Numerical simulation of micro-channel heat sink fitted with semi elliptical pin fin structures were conducted by Ali *et al.* (2024). They utilised semi elliptical shaped pin fin with different aspect ratios to examine the effect geometry over heat transfer and fluid flow behaviour. They found enhanced heat transfer result, though it was coupled with increased pressure drop also.

Sakkay *et al.* (2024) conducted numerical analysis of thermal performance with micro-structure pillars inserted in a micro-channel heat sink. They conducted their work with Reynolds number range 300 – 740. They varied the spacing of the pillars, diameter of the pillars and number of pillars to assess the effect on heat transfer performance. They found that the insertion of pillars could increase the heat transfer up to four times.

Huang *et al.* (2024) experimented with three different flat plate micro-oscillating heat pipes with alternatively arranged ratchet micro-channels for heat transfer augmentation. Their result indicated that the improved flow boiling and stronger flow disruption induced by the ratchet micro-channel resulted in better convective heat transfer.

Zhang *et al.* (2024) conducted experimental investigation on flow boiling heat transfer with a hybrid of finned and porous coating micro-channel heat sink. They evaluated the heat transfer characteristics with three more micro-channels i.e. a smooth micro-channel, a finned micro-channel and a hybrid channel with both finned surface and smooth surface. They observed increased heat transfer co-efficient for their proposed configuration as compared to the other

micro-channels. Experimental investigation on flow boiling heat transfer and pressure drop characteristics were conducted by Wu *et al.* (2024). They examined five different fin heights and a range of heat fluxes for the study purpose. They found significant increase in heat transfer co-efficient. Haider *et al.* (2025) numerically investigated the effect of secondary channels and micro-ribs, in micro-channel heat sinks to obtain augmented heat transfer. The dimensionless performance indicators such as Nu/Nu_0, f/f0, were the parameters they computed for this purpose. Their Reynolds Number range was 100 - 500. Their result indicated that only the secondary channel may not improve the thermal performance of the heat sink remarkably. But when micro-ribs are fitted on the side walls of the heat sink, it produced significant enhancement in its thermal performance due to increased heat transfer surface area.

Wu, Zhao and Dong, (2025) conducted numerical simulation of a micro-channel heat sink fitted with flexible micro-column array on the side walls of the channel. they explored the influence of column height, width and spacing over the heat transfer performance of the heat sink. They found improved thermal performance. Al-Neama, (2025) incorporated a dynamically deforming upper wall in a micro-channel heat exchanger, intending to avert overheating and sustain performance of electronic circuits. They developed a numerical model to study the effect of sinusoidal oscillation of the wall on hydro thermal performance of the heat sink. They found that with increase in oscillation frequency and amplitude, the convective heat transfer coefficient increased exponentially. Yan *et al.* (2025) conducted experimental investigation on micro-channel with ribs and rectangular cavities for heat transfer augmentation. Three different combination of ribs and cavities were their subject of examination. Their result indicated that the presence of offset rectangular cavities improved heat transfer performance of the micro-channel in both single phase and two phase domains. Zhang *et al.* (2025) experimented on flow boiling heat transfer over a ribbed micro-channel

with porous decorated sidewalls of 100 μm and 200 μm thickness. The results were compared with conventional smooth ribbed micro-channels and porous ribbed micro-channels. Their result showed that the capillary pressure on the near wall fluid created a slip between the bubbles and the fluid near the wall. This enables the fluid to move through the porous region and enables reentrance and better mixing of the flowing fluid. They obtained better heat transfer result in their study.

The hydrodynamic and thermal performance of a bifurcated, divergent micro-channel was investigated by Cui *et al.* (2026). They assessed the effect width and height of the bifurcated plate on heat transfer and fluid flow. They found that the modified geometry resulted reduced flow resistance and thus enhanced heat transfer. Effect of multiple elastic flaps in the downstream of a micro-channel was investigated by Zhou, Xin and Wang (2026). They also proposed an optimal layout of the flaps.

2.3 Active Enhancement Technique

Maynes and Webb (2003) inspected fully developed electro-osmotic flow in micro-channel and its consequences on heat transfer. They applied both constant wall temperature and constant wall heat flux as boundary condition for their study purpose. The flow was established by a voltage gradient along the tube's length. They received enhanced Nusselt number results.

Morini *et al.* (2006) assessed the effect of electro-kinetically driven flow on heat transfer in a micro-channel heat sink in their computational study. They used channels with two different cross-sections i.e. rectangular and trapezoidal respectively. They found significant enhancement in heat transfer. They also reported that the trapezoidal channel provided better thermal performance compared to rectangular cro-section channel.

Chen and Cho (2007) investigated numerically, the effect of electro-kinetically driven flow mixing in micro-channels. They used channel with wavy surface for this purpose. Their result suggested that the wavy nature of the flow passage, increased interfacial contact area, thus providing enhance fluid mixing as well as heat transfer. Their work also indicated that the wave amplitude increased fluid mixing and thermal performance of the channel.

The thermal performance of trapezoidal micro-channel heat sink was investigated by Han *et al* (2013). They utilized various techniques, including experimental, analytical and numerical methods. The applied pure pressure driven flow (PDF), pure electro-osmotic flow (EOF) and combined flow for their study. The effect of side wall angle and channel height-width ratio was also analysed and compared for different flow condition. They received a decrease in thermal resistance about 17.94% when the electric potential increased from 1kV/cm. to 6 kV/cm. Their result also exhibited an enhanced Nusselt number result as good as around 21.87%.

Ganguly *et al.* (2015) investigated the combined effect of pressure driven flow, electro-osmotic flow and magnetic field in a micro-channel. They found that the magneto-hydrodynamic effects reduced the advective transport of the flowing fluid inside the channel, thus decreasing thermal performance of the channel.

Ganguly *et al.* (2015) looked into electro-osmotic blood flow in a hydrophobic micro-channel and heat transfer associated to it. A magnetic field was applied externally to enhance transport. applied The effect of hydrodynamic slip as well as temperature slip was taken into account. The non-Newtonian viscoelastic fluid model was used for the computation purpose. They reported that the external magnetic field can control the axial velocity. They also concluded that the temperature distribution of blood flow is significantly affected by the thermal radiation.

Study of two-phase nanofluid double diffusion convection in the presence of an induced magnetic field was done by Sheikholeslami and Rokni (2017). They utilizing the Runge-Kutta method for their numerical solutions. The findings indicated that the temperature gradient is enhanced by increasing the suction parameter, while thermos-phoretic parameters reduce it. Additionally, nanofluid motion diminishes with higher Schmidt and Hartmann numbers but increases with increase in buoyancy ratio and thermos-phoretic parameters. They also provided valuable insights into the effects of induced magnetic fields on heat and mass transfer.

Yang *et al.* (2019) studied the effects of a lateral electric field, a vertical magnetic field, alongside an axial electric field, in a rectangular micro-channel. They derived analytical expressions for non-dimensional velocity, temperature, and Nusselt number, to estimate the effect of parameters like Hartmann number (Ha), Brinkmann number (Br), and the intensity of the lateral electric field on them. Results indicate that the lateral electric field significantly impacts flow control and the fluid velocity decreases with increasing Ha, in the absence of that electric field. Their study also revealed that both velocity and temperature profiles exhibit an increasing-decreasing trend based on a critical Hartmann number. They also highlighted the importance of viscous dissipation and Joule heating in thermal transport processes.

For enhancement of heat transfer introduction of pulsation has been found to be an effective way as observed by Nandi & Chattopadhyay. Chattopadhyay *et al* (2006) conducted numerical study of laminar fluid flow and heat transfer in an isothermal circular tube. There was a sinusoidal varying time dependent velocity component superimposed over the average inlet velocity to examine whether there comes an improvement in the heat transfer performance of the tube. The study was conducted at Reynolds number 200 and pulsation

frequency ranging 0 -20 Hz. The amplitude taken was below 1. They found no beneficial effects on heat transfer accomplished by the pulsation at the inlet.

Though for conventional channels pulsation did not bring any improvement in thermal performance of heat sinks, MCHSs manifested some good outcomes in terms of heat transfer as well as pressure drop. Persoons *et al.* (2009) conducted experimental investigation on rectangular microchannel for single phase heat transfer performance with sinusoidal pulsating flow at the inlet. They developed a pulsator device to supply fluctuating fluid velocity with controlled amplitude and frequency at the inlet. They performed the study with Reynolds number range 50 – 400, whereas, Womersley number ranging from 2 to 17. They observed improved heat transfer about 40 % as compared to the steady case. Nandi and Chattopadhyay (2013) investigated two dimensional wavy micro-channel with sinusoidal velocity component applied at inlet. They studied fluid flow and heat transfer characteristics for simultaneously developing laminar region. Water was the cooling fluid with Reynolds number range of 0.1 to 100. They performed the simulation with different amplitude and frequency of simulation. They compared their results with steady flow inside wavy micro-channel and observed enhance heat transfer results. Later, Nandi and Chattopadhyay (2014) executed similar kind of study in a two dimensional raccoon type micro-channel. They found an optimum heat transfer at a Strouhal number value 5. They also reported that the pulsating velocity at inlet provided better thermal performance compared to steady case. numerical investigation of laminar, pulsating flow along a three dimensional helical type micro-channel heat sink (MCHS) was carried out by Narrein *et al* (2016) to assess heat transfer. The computation was performed in very low Reynolds number (6 – 25) and Al_2O_3 – water based nano-fluid was used as the working fluid. The amplitude of the pulsation was in the range 1 – 3. Whereas, frequency was ranging 5 – 20. They reported significant heat transfer improvement as effect of implementation of sinusoidal pulsation at inlet. Later, Sivasankaran and Narrein, (2016)

worked with same kind of computational analysis in a helically twisted micro-channel heat sink filled with a porous medium with 40% porosity. They utilized the same nano-fluid with same pulsating frequency and wave amplitude as before. They reported that porous medium and inlet pulsation enhanced the thermal performance of the MCHS. Numerical analysis of heat transfer performance of a micro-channel heat sink with sinusoidal velocity pulsation at inlet was performed by Ebrahim Qomi *et al* (2020) The heat sink was fitted with two heat source and a MHD nano-fluid was used as the working fluid. They found that with increase in Reynolds number 100 to 500, the proposed setup yields a 350% inflated heat transfer although, furnishing two times increase in pressure drop.

Binuyo (2020) carried out computational analysis of heat transfer characteristics in a three dimensional micro-channel fitted with ribs. They deployed Al_2O_3 – water base nano fluid as the cooling medium and fluctuating velocity at inlet for their study. A range of Reynolds nmber 200 -1000 and pulsating frequency ranging from 100 – 500 Hz was engaged for their research work. Their result illustrated that the sinusoidal inlet velocity can improve heat transfer result significantly.

Wang *et al.* (2020) investigated the effect of flow pulsation on laminar forced convective heat transfer in a louvered microchannel heat sink (MCHS). The MCHS featured louver-like microstructures with varying pitch ratios from 0.25 to 1.75 and Reynolds numbers ranging from 100 – 300. The inlet velocity was fluctuated in a triangular waveform, with Strouhal numbers from 0 – 2.8. they observed that the micro-structures disrupted the main flow and increased the efficiency of the MCHS.

Xu *et al.* (2021) conducted experimental investigation on microchannel for heat transfer performance with pulsating flow at the inlet. They inspected thermal characteristics of the micro-channel heat sink with four different types of input wave signals applied at inlet. They

used graphene – oxide – platelets - water Nano fluid to act as the cooling medium. They found the square pulsating wave signal to yield best heat transfer performance.

Das *et al.* (2021), explored the heat transfer and fluid flow characteristic in a twisted sinusoidal wavy micro channel. The channel was square cross sectioned with 0.5 mm hydraulic diameter and was made twisted and sinusoidal wavy to enhance recirculation and mixing within the flow. A range of Reynolds number 1 to 100 and varying pulsation amplitude, as well as frequency were incorporated to assess thermal performance of the proposed geometry. At lower Reynolds number and pulsation amplitude, the Nusselt number exhibited similar results to that of study case. However, at higher values of the above, the result unveiled significant rise in Nusselt number. The Pressure drop analysis designate that at different frequencies and amplitudes of pulsation, the improvised design can furnish pressure drop within acceptable limit. The analysis also show that the inlet flow pulsation can bring down the thermal entropy generation, leading to better thermal performance as compared to the study one.

Nandi and Duari (2022) studied the effect of inlet flow pulsation over the heat transfer performance of a two dimensional ribbed micro-channel heat sink. The pulsating inlet velocity maintained with a frequency, represented by dimensionless Strouhal number. A Strouhal number value 10 and amplitude of 0.8 was utilized in this computational study. The channel walls were kept at constant temperature condition. Their investigation was kept within a Reynolds number range of 100 – 500. They found significant augmented heat transfer result at higher Reynolds number.

Huang *et al.* (2024) introduced an innovative modified micro channel geometry to encounter the escalating thermal challenges associated with integrated circuits. They examined with different bottom angle and nano-fluid concentration for their purpose. They achieved

significant improvement in the thermal performance of the micro-channel heat sink. Zhang *et al.* (2024) explored the effect of ultrasound on heat transfer characteristics in rectangular micro-channels. They conducted a large number of experiments with varying fluid velocity and heat flux. They found a maximum 12.9% improved thermal performance with the use of ultrasound while no negative impact on pressure drop.

2.4 Closure

The state-of-art survey as presented in the preceding sections clearly shows that most of the previous studies were confined to geometrical modification of channels for enhancement of heat transfer and mixing. While inlet flow pulsation could bring in augmentation in transport, very few studies dealt with this aspect. The present computational investigation concentrates on the performance of twisted microchannel with inlet flow pulsation thus combining the effect of geometry and pulsation for bringing out enhanced performance.

The present work is a numerical investigation of fluid flow and heat transfer for micro-channels. Detailed transport phenomena is reported by solving full Navier-Stokes equation. The objectives can be elaborated as –

1. To explore heat transfer & fluid flow over a geometrically modified two dimensional stepped micro-channel. The channel cross-section was made contracted for enhancement purpose. The length of the narrowed down part was varied to investigate the effect of the modified geometry.
2. To examine the effect of introduction of a convergent-divergent section in the micro-channel on heat transfer. The length of the modified two dimensional convergent-divergent micro-channel section was varied to observe geometry effect over heat transfer.

3. To investigate heat transfer enhancement over a twisted micro-channel. The channel was made twisted about its own axis for enhancement purpose. The pitch and the twist directions of the channel was also varied to investigate the effect of the modified geometry.
4. To assess the combined effect of both active and passive enhancement method using a twisted channel and pulsating flow at inlet.

CHAPTER THREE

METHODOLOGY

3.1 Introduction

Fluid flow of pulsating nature can trigger convective heat transfer when there is presence of flow instability or when reciprocating type device is used to pump the fluid along the flow passage. Micro-pumps with vibrating diaphragm pumping mechanism can be employed for this purpose.

Micro-channel flow with inlet pulsation has garnered considerable interest in thermal engineering research because of its potential to improve heat transfer performance. The thermal limitations of standard rectangular micro-channels utilising water for high heat dissipation had been examined by a number of researchers, and flow pulsation has been emerged as one of the most promising heat transfer enhancement techniques for micro-channels. Nonetheless, the existing findings regarding heat transfer, resulting from pulsation are inconsistent, leaving the inquiry unresolved: Does pulsation improve or diminish heat transfer in comparison to steady flow? The previous chapter emphasised the necessity for research endeavours in this regard. This section discusses the methodology of numerical computation.

The equations that utilised to model the fluid flow and heat transfer in micro-channel are the Navier-Stokes equations. These equations were non-dimensionalized for the simulation work. The non-dimensionalized parameters are presented as follows: -

Length – using diameter D

Velocity – using average inlet velocity U_m

Time – $t = D / U_m$

Temperature – $T^* = (T – T_{in}) / (T_w – T_{in})$ [* is used to denote non-dimensional values]

In all the cases, usual no slip wall boundary conditions are applied. At the inlet, a sinusoidal pulsating velocity component added with the main uniform velocity profile. The inlet velocity profile is given by –

$$u_{in} = u_m \{1 + A \sin(2\pi f_r t)\} \quad (3.1)$$

Here 'A' is the non-dimensional amplitude and the frequency 'f_r' is represented by a dimensionless number called Strouhal number. ($St = f_r.D_h / U_m$). The channel surface was assumed to be isothermal. The local convective heat transfer co-efficient 'h' is given by the following equation –

$$q = h\,(T_w - T_b) \quad (3.2)$$

Here T_b is the local bulk temperature whereas T_w is the temperature at wall.

The incompressible assumption complicates the solution to the governing equation due to the absence of an independent equation for pressure. For every momentum equation, the pressure gradients contribute to the fluid flow. The three momentum equations along with the continuity equation could be sufficient for solving four dependent variables e.g. u, v, w and p. But there is no independent transport equation for pressure. This, restricts the possibility of solution for these 4 unknowns using Navier Stokes equation. Under these conditions, the continuity equation serves as a kinetic constraint on the velocity field rather than a dynamic equation. Formulating the pressure field ensures adherence to the continuity equation and helps to correlate pressure with velocity in an incompressible flow.

The governing equations, derived from the basic heat and fluid flow principles, are named as the continuity equation, momentum equation and energy equation respectively. The continuity and momentum equations are used to calculate the velocity vector, whereas, the energy equation is employed to calculate the temperature distribution and wall heat transfer

co-efficient. There are some simplified assumptions that are made while applying the Navier-Stokes equation to model the fluid flow and heat transfer process. The assumptions may be sum up as –

1. The Knudsen number lies in the continuum flow regime ($Kn < 10^{-3}$) which implies that the continuum model based conservation equation of motion (Navier-Stokes Equation) can be used to model the flow.
2. The fluid is Newtonian and incompressible.
3. Both the fluid and the solid possess constant property.
4. There is no internal heat generation.
5. There is no radiative heat transfer.
6. Second order effects are negligible.

3.2 Computational Domain

In a Computational Fluid Dynamics (CFD) simulation, precise definition of the geometry largely affects the accuracy of the results. To generate accurate mesh, to employ proper boundary conditions and to interpret the flow field precisely, the detailed definition of the flow geometry is necessary. The geometrical parameters, affects the flow behaviour and other performance parameters. So, while investigating an MCHS for enhanced heat transfer results, the detailed description of the heat sink geometry is crucial. As already discussed, different types of channel geometry were proposed and assessed in this thesis, to bring out augmented heat transfer results. A detailed summary of the geometries associated in this thesis is presented in the following table (table 3.1). Along with schematic diagrams of the geometries, table 3.1 also elaborates the dimensions and associated boundary conditions of all the geometries taken into consideration in this thesis. These geometric specifications play pivotal role in generating mesh and for subsequent CFD analysis.

Geometry	Dimension	Boundary condition
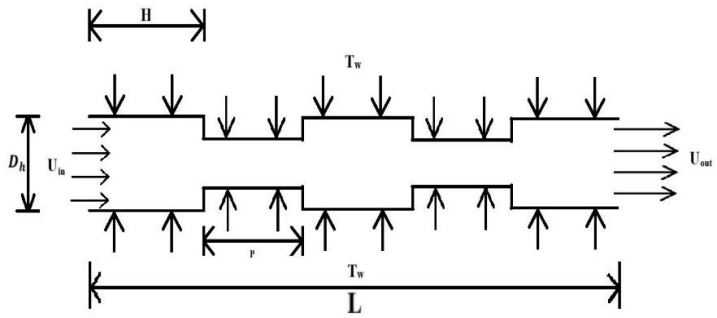	**Stepped Channel** Length (L) = 25 mm Pitch (P) = 5 mm, 8 mm, 10 mm Contraction Ratio (α) = P/D_h = 10, 16, 20 Length (L) = 2P + 3H	**Velocity** Inlet - Re = 100 – 500 Outlet - p_{exit} = 0 Wall – no slip Pulsating inlet – $u_{in} = u_m\{1 + A\ \sin(2\pi f_r t)\}$ **Temperature** Inlet – ambient Temperature fluid Wall - T_w = 330 K
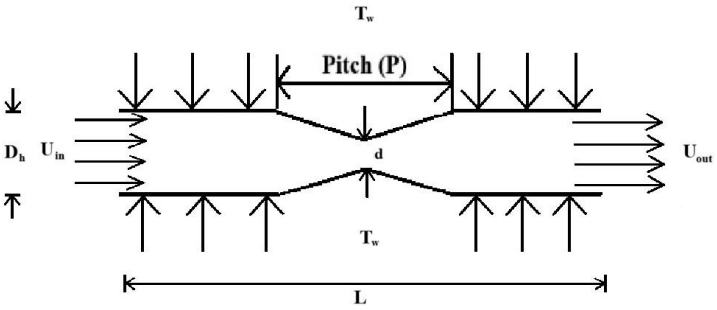	**Converging Diverging Channel** Length (L) = 50 mm Pitch (P) = 15 mm, 20 mm, 25 mm Contraction Ratio (α) = P/D_h = 30, 40, 50	**Velocity** Inlet - Re = 100 – 500 Outlet - p_{exit} = 0 Wall – no slip Pulsating inlet – $u_{in} = u_m\{1 + A\ \sin(2\pi f_r t)\}$ **Temperature** Inlet – ambient Temperature fluid Wall - T_w = 330 K
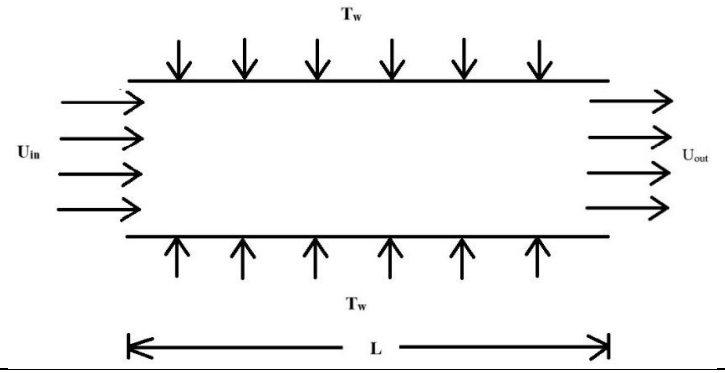	**Plain Channel** Length (L) = 25 mm	**Velocity** Inlet - Re = 100 – 500 Outlet - p_{exit} = 0 Wall – no slip Pulsating inlet – $u_{in} = u_m\{1 + A\ \sin(2\pi f_r t)\}$ **Temperature** Inlet – ambient Temperature fluid Wall - T_w = 330 K

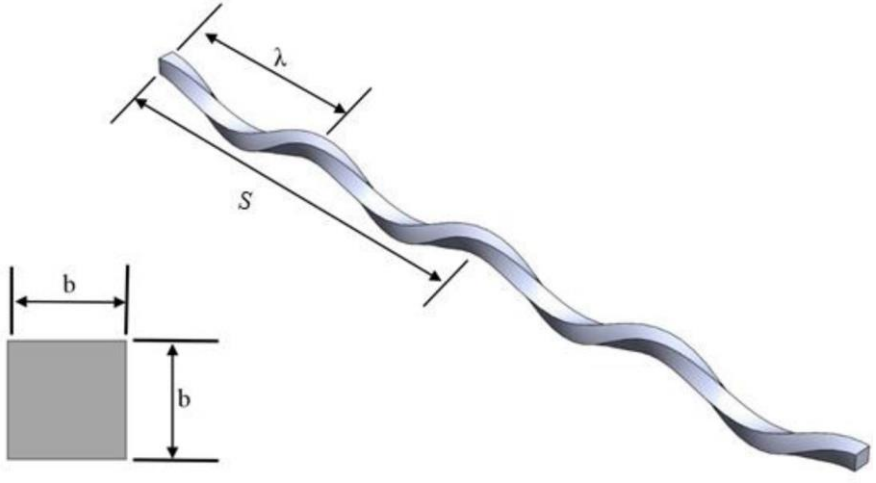	**Clockwise Twisted Micro-channel** Length (L) = 25 cm Wave Amplitude (A_w) = 1 mm Pitch (S) = 5 cm Wavelength (λ) = 2.5 cm	**Velocity** Inlet - Re = 10 – 100 Outlet - p_{exit} = 0 Wall – no slip Pulsating inlet – $u_{in} = u_m\{1 + A\ \sin(2\pi f_r t)\}$ **Temperature** Inlet – ambient Temperature fluid Wall - T_w = 343 K
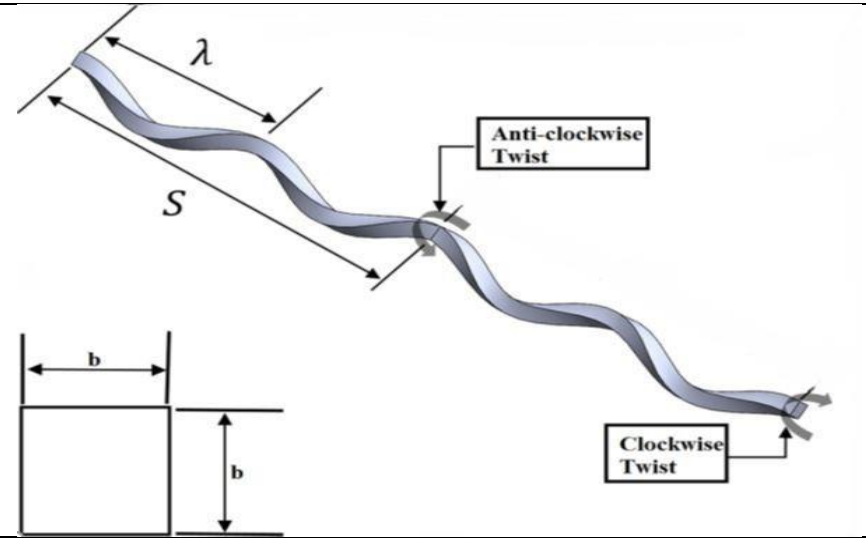	**Clockwise-anticlockwiseTwisted Micro-channel** Length (L) = 25 cm Wave Amplitude (A_w) = 1 mm Pitch (S) = 5 cm Wavelength (λ) = 2.5 cm	**Velocity** Inlet - Re = 10 – 100 Outlet - p_{exit} = 0 Wall – no slip Pulsating inlet – $u_{in} = u_m\{1 + A\ \sin(2\pi f_r t)\}$ **Temperature** Inlet – ambient Temperature fluid Wall - T_w = 343 K

Table 3.1. Table for the geometries involved and their dimensions and respective boundary conditions

3.3 Governing equations

Mass conservation equation –

The mass conservation equation for problems involving two-dimensional, Cartesian geometry may be written as

$$\frac{\partial \rho}{\partial t} + \frac{\partial (\rho u)}{\partial x} + \frac{\partial (\rho v)}{\partial y} + \frac{\partial (\rho w)}{\partial z} = 0 \tag{3.3}$$

where, x, y and z are the coordinate directions, u, v and w are the velocity components in those coordinate directions, respectively.

Momentum conservation equations –

The x momentum in Cartesian coordinates may be written as,

$$\frac{\partial (\rho u)}{\partial t} + \frac{\partial (\rho u^2)}{\partial x} + \frac{\partial (\rho uv)}{\partial y} + \frac{\partial (\rho uw)}{\partial z} = -\frac{\partial \rho}{\partial x} + \frac{1}{Re}\left(\frac{\partial \tau_{xx}}{\partial x} + \frac{\partial \tau_{xy}}{\partial y} + \frac{\partial \tau_{xz}}{\partial z}\right) \tag{3.4}$$

Similarly, the y momentum equation in Cartesian Coordinates may be written as,

$$\frac{\partial (\rho v)}{\partial t} + \frac{\partial (\rho uv)}{\partial x} + \frac{\partial (\rho v^2)}{\partial y} + \frac{\partial (\rho vw)}{\partial z} = -\frac{\partial \rho}{\partial y} + \frac{1}{Re}\left(\frac{\partial \tau_{xy}}{\partial x} + \frac{\partial \tau_{yy}}{\partial y} + \frac{\partial \tau_{yz}}{\partial z}\right) \tag{3.5}$$

Also, the z momentum equation in Cartesian co-ordinate can be written as,

$$\frac{\partial (\rho w)}{\partial t} + \frac{\partial (\rho uw)}{\partial x} + \frac{\partial (\rho vw)}{\partial y} + \frac{\partial (\rho w^2)}{\partial z} = -\frac{\partial \rho}{\partial z} + \frac{1}{Re}\left(\frac{\partial \tau_{xz}}{\partial x} + \frac{\partial \tau_{yz}}{\partial y} + \frac{\partial \tau_{zz}}{\partial z}\right) \tag{3.6}$$

In Eqn. (3.4), eqn. (3.5) and (3.6), the viscous stresses appear explicitly and for Newtonian fluids they are given as follows: -

$$\tau_{xx} = 2\mu \frac{\partial u}{\partial x} \tag{3.7a}$$

$$\tau_{yy} = 2\mu \frac{\partial v}{\partial y} \tag{3.7b}$$

$$\tau_{zz} = 2\mu \frac{\partial w}{\partial z} \tag{3.7c}$$

$$\tau_{xy} = \tau_{yx} = \mu(\frac{\partial u}{\partial y} + \frac{\partial v}{\partial x}) \quad (3.7d)$$

$$\tau_{xz} = \tau_{zx} = \mu(\frac{\partial u}{\partial z} + \frac{\partial w}{\partial x}) \quad (3.7e)$$

$$\tau_{zy} = \tau_{yz} = \mu(\frac{\partial w}{\partial y} + \frac{\partial v}{\partial z}) \quad (3.7f)$$

Energy conservation equations –

The energy conservation equation on Cartesian coordinate for negligible viscous dissipation and pressure work may be written as,

$$\rho c_p \left[\frac{\partial T}{\partial t} + u\frac{\partial T}{\partial x} + v\frac{\partial T}{\partial y} + w\frac{\partial T}{\partial z}\right] = -\left[\frac{\partial q_x}{\partial x} + \frac{\partial q_y}{\partial y} + \frac{\partial q_z}{\partial z}\right] + q^{\dot{I}II}{}_g \quad (3.8)$$

Absorbing ρ in the derivatives, the above equation may also be written in a conservative form as,

$$c_p \left[\frac{\partial(\rho T)}{\partial t} + \frac{\partial(\rho u T)}{\partial x} + \frac{\partial(\rho v T)}{\partial y} + \frac{\partial(\rho w T)}{\partial z}\right] = -\left[\frac{\partial q_x}{\partial x} + \frac{\partial q_y}{\partial y} + \frac{\partial q_z}{\partial z}\right] + q^{\dot{I}II}{}_g \quad (3.9)$$

For a fluid that obeys Fourier's heat conduction law, the components of heat q_x, q_y and q_z may be written as,

$$q_x = -k\frac{\partial T}{\partial x} \quad (3.10a)$$

$$q_y = -k\frac{\partial T}{\partial y} \quad (3.10b)$$

$$q_z = -k\frac{\partial T}{\partial z} \quad (3.10c)$$

Where $q^{\dot{I}II}{}_g$ is the volumetric heat generation , which, in principle, could be a function of both space & time.

3.4 Dimensionless Quantities

Reynolds number: It is a dimensionless number defined as the ratio of inertia force to viscous force. It can help to anticipate the flow behaviour in different conditions. It is denoted by Re and given by-

$$Re = \frac{\rho v l}{\mu} \tag{3.11}$$

Prandtl Number: The Prandtl number is a dimensionless quantity represented as the ratio of momentum diffusivity to thermal diffusivity. It does not contain any length scale (such as Reynolds number) and is a function of only the fluid properties. It is denoted by 'Pr', Where,

$$Pr = \frac{\nu}{\alpha} = \frac{Viscous\ diffusion\ rate}{Thermal\ diffusion\ rate} = \frac{c_p \mu}{k} \tag{3.12}$$

Nusselt Number: It is also a dimensionless number represented by the ratio of convective to conductive heat transfer across the boundary in a fluid. It is a measure of the convective heat transfer compared to conductive heat transfer. In simple cases the value of local Nusselt number and average Nusselt number is denoted as Nu_L and Nu_{AV} and this can be written as,

$Nu = \frac{hL}{k}$ For plain microchannel (3.13)

Now the dimensionless variables are as follows -

The normalised x-coordinate with respect to height of the enclosure = X = x/H, (3.14a)

The normalised y-coordinate with respect to height of the enclosure = Y = y/H, (3.14b)

The normalised time = t* = t/t_w (3.14c)

The normalised x-component velocity = u* = u/u_m (3.14d)

The normalised y-component velocity = v* = v/v_m (3.14e)

The normalised z-component velocity = w* = w/w_m (3.14f)

The normalised Pressure = p* = $p/\rho u_m{}^2$ (3.14g)

The normalised temperature = θ = (T – T_w) / (ΔT_w) (3.14h)

Under the present scheme of non-dimensionalization, Nu boils down to dimensionless temperature gradient in normal direction

$$Nu = -\frac{\partial T}{\partial n}$$

3.5 Solution Methodology

The governing equations cannot be solved directly due to their non-linear nature. Therefore, they should be solved numerically. A differential equation's numerical solution consists of a set of values from which distribution of the dependent variable can be obtained. Unknown values of the dependent variables are assigned at a finite number of locations (the grid points) in the calculation domain. This can provide a set of algebraic equations for these unknowns to solve the equations. These algebraic equations comprised of the unknown values of the dependent variables at chosen grid points are called discretized equations. Three well accepted methods to discretize the governing equations are Finite Volume Method, Finite Difference Method and Finite Element Method.

Finite Volume Method

Finite Volume Method is a standard and one of the most versatile technique to discretize partial differential equations especially the equations involving conservation law. In this approach, the domain is sub-divided into a number of small finite control volumes. Then the differential equations are integrated over each control volume.

$$\frac{\partial}{\partial t}\iiint_V QdV + \iint_A FdA = 0 \quad (3.15)$$

Where Q is the vector of conserved variables, F is the vector of fluxes, V is the cell volume, and A is the cell surface area.

Finite Element method

In this approach, the domain is divided into a finite number of smaller simple elements. This method is popular for structural analysis of solids, but is also applicable to problems in fluid dynamics. Within these elements, using a set of basis function, the solution is made. It is very common method used for structural analysis of solids. In this method a weighted residual equation is formed as

$$R_i = \iint WQdV \tag{3.16}$$

Where Ri is the equation residual at an element vertex I, Q is the conservation equation expressed on an element basis, W is the weight factor and V is the volume of the element.

Finite Difference Method

This method is a numerical method where the differential equations are solved by approximating derivatives using finite differences. Though, it is simplest to program, it is currently only used in few specialized codes. In this method, the domain is subdivided into a number of intervals. Modern finite difference codes make use of an embedded boundary for handling complex geometries making these codes highly efficient and accurate. Other ways to handle geometries are using overlapping grids, where the solution is interpolated across each grid.

$$\frac{\partial Q}{\partial t} + \frac{\partial F}{\partial x} + \frac{\partial G}{\partial y} + \frac{\partial H}{\partial z} = 0 \tag{3.17}$$

Where Q is the vector of conserved variable, and F, G and H are the fluxes in the x, y and z directions respectively

The present study adopted the finite volume method (FVM) to discretize the governing equations. Figure 3.1 illustrates a typical control volume. The computational domain is sub

divided into a number of control volumes. The control volumes are non-overlapping and chosen in such manner that there is one control volume surrounding each grid point. The differential equations are integrated over each control volume.

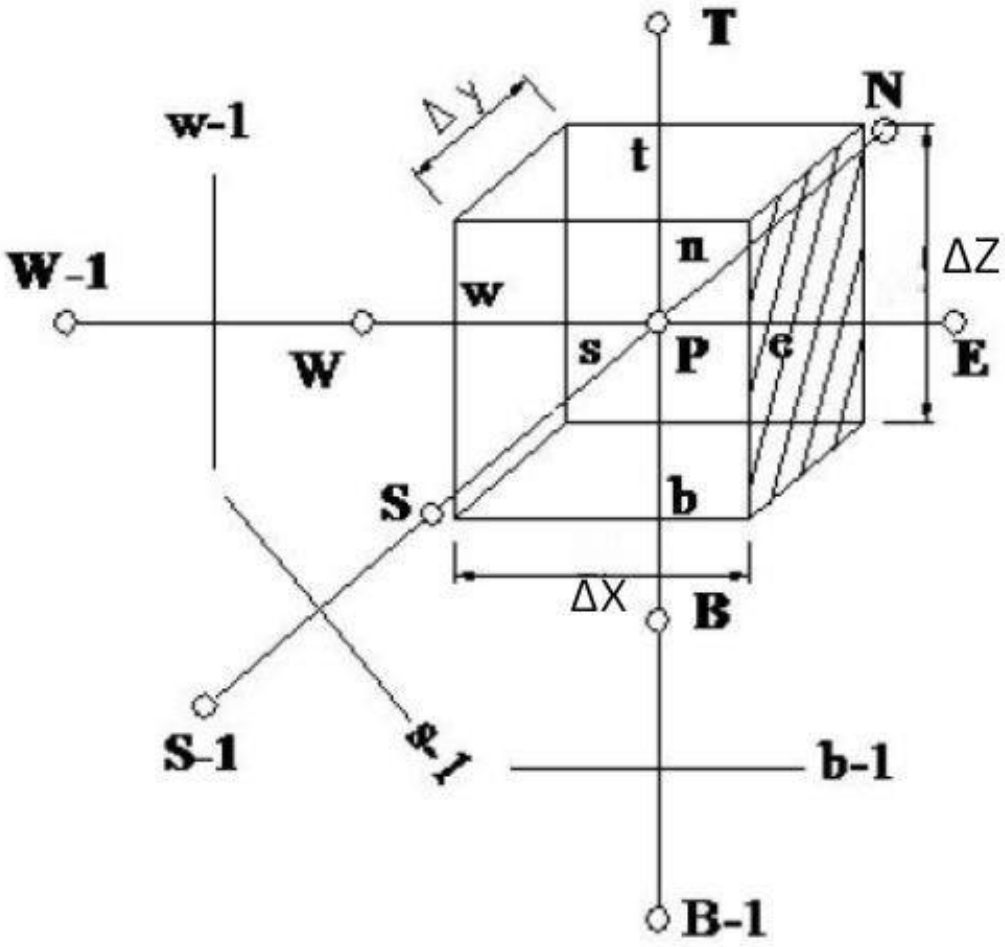

Figure 3.1: A typical control volume

Discretization of the continuity equation

Considering continuity equation of any fluid under observation can be written in Cartesian co-ordinate as,

$$\frac{\partial(\rho)}{\partial t} + \frac{\partial(\rho u)}{\partial x} + \frac{\partial(\rho v)}{\partial y} + \frac{\partial(\rho w)}{\partial z} = 0 \qquad (3.18)$$

Integrating the differential equation (3.18) with respect to time and space over the control volume, we get -

$$\int_t^{t+\Delta t}\int_{CV}\frac{\partial(\rho)}{\partial t}dVdt+\int_t^{t+\Delta t}\int_{CV}\frac{\partial(\rho u)}{\partial x}dVdt$$

$$+\int_t^{t+\Delta t}\int_{CV}\frac{\partial(\rho v)}{\partial y}dVdt$$

$$+\int_t^{t+\Delta t}\int_{CV}\frac{\partial(\rho w)}{\partial z}dVdt=0 \qquad (3.19)$$

Equation (3.19) can be discretized using implicit scheme for time discretization over the control volume and can be written as -

$$[(\rho uA)_e-(\rho uA)_w]+[(\rho vA)_n-(\rho vA)_s]+$$

$$[(\rho wA)_t-(\rho wA)_b]=0 \qquad (3.20)$$

Now, First Order Upwind interpolation scheme can be applied to interpolate volume fraction at cell faces and equation (3.20) can be rewritten as -

$$[F_eA_e-F_wA_w]+[F_nA_n-F_sA_s]+$$

$$[F_tA_t-F_bA_b]=0 \qquad (3.21a)$$

Where mass fluxes are as follows -

$$F_e=(\rho u)_e,\ F_w=(\rho u)_w,\ F_n=(\rho v)_n,\ F_s=(\rho v)_s,\ \ F_t=(\rho w)_t,$$

$$F_b=(\rho w)_b \qquad (3.21b)$$

We can rewrite the equation (3.21a) in the form -

$$a_pf_p=a_Ef_E+a_Wf_W+a_Nf_N+a_Sf_S+a_Tf_T+a_Bf_B+\mathrm{B} \qquad (3.22)$$

Where,

$$a_E=0 \qquad (3.22a)$$

$$a_W = F_w A_w \tag{3.22b}$$

$$a_N = 0 \tag{3.22c}$$

$$a_S = F_s A_s \tag{3.22d}$$

$$a_T = 0 \tag{3.22e}$$

$$a_B = F_b A_b \tag{3.22f}$$

$$a_p = F_e A_e + F_n A_n + F_t A_t + \rho_p \frac{\Delta V}{\Delta t} \tag{3.22g}$$

Discretization of the momentum equations

The momentum equation for the same fluid under observation can be written as -

$$\frac{\partial}{\partial t}(\vec{u}) + \nabla.(\vec{u}\vec{u}) = -\nabla p + \nabla.\bar{\bar{\tau}} + U_{lij} \tag{3.23}$$

Considering only x-momentum in Cartesian co-ordinate, x momentum for said fluid can be written from equation (3.23) as,

$$\frac{\partial}{\partial t}(\rho u) + \frac{\partial}{\partial x}(\rho u u) + \frac{\partial}{\partial y}(\rho v u) + \frac{\partial}{\partial z}(\rho w u) = \frac{\partial p}{\partial x} + \frac{\partial}{\partial x}\left(\mu \frac{\partial u}{\partial x}\right) + \frac{\partial}{\partial y}\left(\mu \frac{\partial u}{\partial y}\right) + \frac{\partial}{\partial z}\left(\mu \frac{\partial u}{\partial z}\right) + U_s + U_a \tag{3.24}$$

Integrating the equation (3.24) with respect to time and space over the control volume, we can write –

$$\int_t^{t+\Delta t}\int_{CV}\frac{\partial}{\partial t}(\rho u)dVdt + \int_t^{t+\Delta t}\int_{CV}\frac{\partial}{\partial x}(\rho u u)dVdt + \int_t^{t+\Delta t}\int_{CV}\frac{\partial}{\partial y}(\rho v u)dVdt +$$

$$\int_t^{t+\Delta t}\int_{CV}\frac{\partial}{\partial z}(\rho w u)dVdt = -\int_t^{t+\Delta t}\int_{CV}\frac{\partial p}{\partial x}dVdt + \int_t^{t+\Delta t}\int_{CV}\frac{\partial}{\partial x}\left(\mu\frac{\partial u}{\partial x}\right)dVdt +$$

$$\int_t^{t+\Delta t}\int_{CV}\frac{\partial}{\partial y}\left(\mu\frac{\partial u}{\partial y}\right)dVdt+\int_t^{t+\Delta t}\int_{CV}\frac{\partial}{\partial z}\left(\mu\frac{\partial u}{\partial z}\right)dVdt+\int_t^{t+\Delta t}\int_{CV}U_s dVdt+\int_t^{t+\Delta t}\int_{CV}U_a dVdt$$

(3.25)

Here also, equation (3.25) can be discretized over the control volume using implicit scheme for time discretization as -

$$(\rho u-\rho^0 u^0)\Delta V+[(\rho uAu)_e-(\rho uAu)_w]\Delta t+[(\rho vAu)_n-(\rho vAu)_w]\Delta t+[(\rho wAu)_t-(\rho wAu)_b]\Delta t=-[(Ap)_e-(Ap)_w]\Delta t+[(\mu Au)_e-(\mu Au)_w]\Delta t+[(\mu Au)_n-(\mu Au)_s]\Delta t+[(\mu Au)_t-(\mu Au)_b]\Delta t+\bar{U}\Delta V\Delta t \quad (3.26)$$

Applying second-order upwind scheme to interpolate convective flux and central difference scheme to interpolate diffusive flux, equation (3.26) can be rewritten as -

$$\left(\rho_p u_p-{\rho_p}^0{u_p}^0\right)\frac{\Delta V}{\Delta t}+\left[F_e A_e\left(u_p+\frac{u_p-u_W}{\Delta x_{pW}}\Delta x_{pe}\right)-F_w\left(u_{pW}+\frac{u_{pW}-u_{pW-1}}{\Delta x_{WW-1}}\Delta x_{Ww}\right)\right]+\left[F_n A_n\left(u_p+\frac{u_p-u_S}{\Delta y_{pS}}\Delta y_{pn}\right)-F_s A_s\left(u_s+\frac{u_s-u_{s-1}}{\Delta y_{ss-1}}\Delta y_{Ss}\right)\right]+[F_t A_t\left(u_p+\frac{u_{p+u_s}}{\Delta z_{PB}}\Delta z_{Pt}\right)-F_b A_b\left(u_B+\frac{u_B-u_{bb-1}}{\Delta z_{BB-1}}\Delta z_{Bb}\right)$$

$$=-[(\mathrm{A}p)_e-(Ap)_w]+[\mu_e A_e\frac{u_E-u_p}{\Delta x_{PE}}-\mu_w A_w\frac{u_p-u_w}{\Delta x_{PW}}]+$$

$$[\mu_n A_n\frac{u_N-u_p}{\Delta y_{PN}}-\mu_s A_s\frac{u_p-u_s}{\Delta y_{PS}}]$$

$$+[\mu_t A_t\frac{u_T-u_P}{\Delta z_{PT}}-\mu_b A_b\frac{u_p-u_b}{\Delta z_{PB}}]+\overline{U}\Delta V \quad (3.27)$$

Where mass fluxes are as follows -

$$F_e=(\rho u)_e,\ F_w=(\rho u)_w, F_n=(\rho v)_n, F_s=(\rho w)_s, F_t=(\rho w)_t\ and$$

$$F_b=(\rho w)_b \quad (3.28)$$

Where, Viscosity at the cell faces are the interpolated value between adjacent cell centres, e.g.

$$\mu_e = \frac{\mu_g + \mu_p}{2} \tag{3.29}$$

although, variation of viscosity is absent in the present work.

Now, equation (3.25) can be written in the form,

$$a_P u_P = a_E u_E + a_W u_W + a_N u_N + a_S u_S + a_T u_T + a_B u_B$$
$$+a_{W-1} u_{W-1} + a_{S-1} u_{S-1} + a_{B-1} u_{B-1} + [(AP)_w - (AP)_e] + S \tag{3.30}$$

Where,

$$a_p = \left(\frac{\Delta V}{\Delta t} + F_e A_e + F_e A_e \frac{\Delta x_{Pe}}{\Delta x_{PW}} + F_n A_n + F_n A_n \frac{\Delta y_{Pn}}{\Delta y_{PS}}\right.$$
$$+F_t A_t \frac{\Delta z_{Pt}}{\Delta z_{PB}} + \frac{\mu_e A_e}{\Delta x_{PE}} - \frac{\mu_w A_w}{\Delta x_{PW}} + \frac{\mu_n A_n}{\Delta y_{PN}} - \frac{\mu_s A_s}{\Delta y_{PS}} \tag{3.31a}$$
$$\left. + \frac{\mu_t A_t}{\Delta z_{PT}} - \frac{\mu_b A_b}{\Delta z_{PB}}\right)$$

$$a_N = \left(\frac{\mu_n A_n}{\Delta y_{PN}}\right) \tag{3.31b}$$

$$a_E = \left(\frac{\mu_e A_e}{\Delta y_{PE}}\right) \tag{3.31c}$$

$$a_W = \left(\frac{\mu_e A_e \Delta x_{Pe}}{\Delta x_{PW}} + F_w A_w F_w A_w \frac{\Delta x_{Ww}}{\Delta x_{WW^{-1}}} - \frac{\mu_w A_w}{\Delta x_{PW}}\right) \tag{3.31d}$$

$$a_S = \left(\frac{\mu_n A_n \Delta y_{Pn}}{\Delta y_{PS}} + F_s A_s + F_s A_s \frac{\Delta y_{Ss}}{\Delta y_{SS^{-1}}} - \frac{\mu_s A_s}{\Delta y_{PS}}\right) \tag{3.31e}$$

$$a_B = \left(\frac{\mu_t A_t \Delta z_{Pt}}{\Delta z_{PB}} + F_b A_b + F_b A_b \frac{\Delta z_{Bb}}{\Delta z_{BB^{-1}}} - \frac{\mu_b A_b}{\Delta z_{PB}}\right) \tag{3.31f}$$

$$a_{W-1} = \left(-F_w A_w \frac{\Delta x_{Ww}}{\Delta x_{WW^{-1}}}\right) \tag{3.31g}$$

$$a_{S-1} = \left(-F_s A_s \frac{\Delta y_{Ss}}{\Delta y_{SS^{-1}}}\right) \tag{3.31h}$$

$$a_{B-1} = \left(-F_b A_b \frac{\Delta z_{Bb}}{\Delta z_{BB^{-1}}}\right) \tag{3.31i}$$

$$S = \rho_p^0 u_p^0 \frac{\Delta V}{\Delta t} + \overline{U}\Delta V \tag{3.31j}$$

Similar to the equation (3.30), discretized equation for v-velocity will be -

$$a_p v_p = a_E v_E + a_W v_W + a_N v_N + a_S v_S + a_T v_T + a_B v_B$$

$$+a_{W^{-1}} v_{W^{-1}} + a_{S^{-1}} v_{S^{-1}} + a_{B^{-1}} v_{B^{-1}} + [(Ap)_s - (Ap)_n] + S \tag{3.32}$$

The discretized equation for z-velocity will be,

$$a_p w_p = a_E w_E + a_W w_W + a_N w_N + a_S w_S + a_T w_T + a_B w_B$$

$$+a_{W^{-1}} w_{W^{-1}} + a_{S^{-1}} w_{S^{-1}} + a_{B^{-1}} w_{B^{-1}} + [(Ap)_b - (Ap)_t] + S \tag{3.33}$$

Considering the u−, v−, w− together, the equation (3.27), (3.28) and (3.29) can be written in the compact form as

$$a_P u_P = \sum_{nb} a_{nb}\, u_{nb} + \sum pA\hat{\imath} + b \tag{3.34}$$

Discretization of the energy equations

Differential form of Energy equation for the said fluid may be written as -

$$\frac{\partial}{\partial \mathrm{t}}(\rho \mathrm{h}) + \frac{\partial}{\partial \mathrm{x}}(\rho \mathrm{uh}) + \frac{\partial}{\partial \mathrm{y}}(\rho \mathrm{vh}) + \frac{\partial}{\partial \mathrm{z}}(\rho \mathrm{wh}) = -\frac{\partial \mathrm{p}}{\partial \mathrm{t}} + \mathrm{M} + \frac{\partial}{\partial \mathrm{x}}\left(\mathrm{k}\frac{\partial \mathrm{T}}{\partial \mathrm{x}}\right) + \frac{\partial}{\partial \mathrm{y}}\left(\mathrm{k}\frac{\partial \mathrm{T}}{\partial \mathrm{y}}\right) +$$

$$\frac{\partial}{\partial \mathrm{z}}\left(\mathrm{k}\frac{\partial \mathrm{T}}{\partial \mathrm{z}}\right) + \mathrm{Q_s} + \mathrm{Q_a} \tag{3.35}$$

Here, M represents strain energy or viscous dissipation.

Since the flow is incompressible, pressure term in (3.33) becomes zero and in terms of temperature we can write equation (3.33) as -

$$\frac{\partial}{\partial t}(\rho c_p T) + \frac{\partial}{\partial x}(\rho u c_p T) + \frac{\partial}{\partial y}(\rho v c_p T) + \frac{\partial}{\partial z}(p w c_p T) = M + \frac{\partial}{\partial x}\left(k\frac{\partial T}{\partial x}\right) + \frac{\partial}{\partial y}\left(k\frac{\partial T}{\partial y}\right) +$$

$$\frac{\partial}{\partial z}\left(k\frac{\partial T}{\partial z}\right) + Q_s + Q_a \qquad (3.36)$$

Integrating equation (3.55) over the control volume, we can write -

$$\iint_{t\,CV}^{t+\Delta t} \frac{\partial}{\partial t}(\rho c_p T)dVd + \iint_{t\,CV}^{t+\Delta t} \frac{\partial}{\partial x}(\rho u c_p T)dVdt + \iint_{t\,CV}^{t+\Delta t} \frac{\partial}{\partial y}(\rho v c_p T)dVdt + \iint_{t\,CV}^{t+\Delta t} \frac{\partial}{\partial z}(\rho w c_p T)dVdt$$

$$= \iint_{t\,CV}^{t+\Delta t} M dVdt + \iint_{t\,CV}^{t+\Delta t} \frac{\partial}{\partial x}\left(k\frac{\partial T}{\partial x}\right)dVdt + \iint_{t\,CV}^{t+\Delta t} \frac{\partial}{\partial y}\left(k\frac{\partial T}{\partial y}\right)dVdt + \iint_{t\,CV}^{t+\Delta t} \frac{\partial}{\partial x}(k\frac{\partial T}{\partial x})dVdt$$

$$+\iint_{t\,CV}^{t+\Delta t} Q_S dVdt + \iint_{t\,CV}^{t+\Delta t} Q_a dVdt \qquad (3.37)$$

Applying implicit scheme for time and, e.g. using first order Upwind scheme for convective flux interpolation and Central difference scheme for diffusive flux interpolation, equation (3.37) can be rewritten as -

$$(\rho_P c_{PP} T_P - \rho_P{}^{\circ} C_{PP}^0 T_P^0)\frac{\Delta V}{\Delta t} + [(\rho u A c_P T)_e - (\rho u A c_P T)_w] + [(\rho v A c_P T)_{ne} - (\rho v A c_P T)_s] +$$

$$[(\rho w A c_P T)_t - (\rho u A c_P T)_b] = \overline{M}\Delta V + [(kA\frac{\partial T}{\partial x})_e - (kA\frac{\partial T}{\partial x})_w] + [(kA\frac{\partial T}{\partial x})_n - \left(kA\frac{\partial T}{\partial x})_s\right] +$$

$$[(kA\frac{\partial T}{\partial x})_t - \left(kA\frac{\partial T}{\partial x})_b\right] + \overline{Q}\Delta V \qquad (3.38)$$

Or,

$$(f_P\rho_P c_{PP}T_P - f_p^0\rho_P{}^\circ C_{PP}^0 T_P^0)\frac{\Delta V}{\Delta t} + [f_e c_{Pe}F_e A_e T_P - f_w c_{Pw}F_w A_w T_w] +$$

$$[f_n c_{Pn}F_n A_n T_P - f_s c_{Ps}F_s A_s T_s] + [f_t c_{Pt}F_t A_t T_P - f_b c_{Pb}F_b A_b T_B]$$

$$= \overline{M}\Delta V + \left[f_e k_e A_e \frac{T_P - T_s}{\Delta y_{Ps}} - f_w k_w A_w \frac{T_P - T_w}{\Delta x_{Pw}}\right] +$$

$$\left[f_n k_n a_n \frac{T_N - T_P}{\Delta y_{PN}} - f_s k_s A_s \frac{T_P - T_s}{\Delta x_{Ps}}\right] + \left[f_t k_t A_t \frac{T_T - T_P}{\Delta z_{PT}} - f_b k_b A_b \frac{T_P - T_B}{\Delta z_{PB}}\right] + \overline{Q}\Delta V \quad (3.39)$$

Where, F is the convective flux at cell faces.

$$F_e = (\rho u)_e, F_w = (\rho u)_w, F_n = (\rho v)_n, F_s = (\rho w)_s, F_t = (\rho w)_t, F_b = (\rho w)_b \quad (3.40)$$

Where, the values of thermal conductivity k and specific heat C_p at the cell faces are again interpolated between two adjacent cell centres.

Now, we can write equation (3.39) as,

$$a_p T_P = a_E T_E + a_W T_W + a_N T_N + a_S T_S + a_T T_T + a_B T_B + B \quad (3.41)$$

Where,

$$a_p = \rho c_{PP} f_p + c_{Pe} f_e F_e A_e + c_{Pn} f_n F_n A_n + c_{Pt} f_t F_t A_t + D_e A_e +$$

$$D_w A_w + D_n A_n + D_s A_s + D_t A_t + D_b A_b \quad (3.42a)$$

$$a_E = D_e A_e \quad (3.42b)$$

$$a_N = D_n A_n \quad (3.42c)$$

$$a_T = D_t A_t \quad (3.42d)$$

$$a_W = f_w c_{Pw} F_w A_w + D_w A_w \quad (3.42e)$$

$$a_s = f_s c_{Ps} F_s A_s + D_s A_s \quad (3.42f)$$

$$a_B = f_b c_{Pb} F_b A_b + D_b A_b \quad (3.42g)$$

$$B = \overline{M}\Delta V + \overline{Q}\Delta V + \rho_P{}^{\circ}C_{PP}^{0} f_P^{0}) \frac{\Delta V}{\Delta t} \quad (3.42h)$$

And,

$$D_e = \frac{k_e}{\Delta x_{PE}}, D_W = \frac{k_w}{\Delta x_{PW}}, D_n = \frac{k_n}{\Delta x_{PN}}, D_s = \frac{k_s}{\Delta x_{PS}}, D_t = \frac{k_t}{\Delta x_{PT}}, D_b = \frac{k_b}{\Delta x_{PB}} \quad (3.42i)$$

Pressure-velocity correction using SIMPLE algorithm

As already discussed earlier, SIMPLE is the acronym for Semi Implicit Pressure Linked Equation. It is a procedure to solve a system of equations representing fluid transport. One of the advantages of this scheme is it can easily be employed for two or three dimensional cases. A brief description of the pressure correction methodology is presented here.

The discretized form of the continuity equation given in equation (3.20) is -

$$[J_e A_e - J_w A_w] + [J_n A_n - J_s A_s] + [J_t A_t - J_b A_b] = 0 \quad (3.43)$$

Or,

$$\sum_f^{N_{faces}} J_f A_f = 0 \quad (3.44)$$

Where fluxes at the control volume faces are**,**

$$J_e = (\rho u)_e, J_w = (\rho u)_w, J_n = (\rho u)_n, J_s = (\rho u)_s, J_t = (\rho u)_t, J_b = (\rho u)_b \quad (3.45)$$

To relate the face velocity, $u_e, u_w, v_n, v_s, w_t, w_b$, to the stored values of velocity at the cell centres, linear interpolation of cell-centered velocities to the faces will result in unphysical

checker boarding of pressure. To avoid checker boarding, the face value of velocities is not averaged linearly. In spite of, momentum-weighted averaging using weighting factors based on the a_P coefficient from equation (3.34), are performed as proposed by Rhie and Chow (1983). Using this procedure, the face flux for any face of the control volume, J_f, may be written as -

$$J_f = f_f\left(\rho_f \frac{a_{P,co}v_{n,co}+a_{p,cl}v_{n,cl}}{a_{P,co}+a_{p,cl}} + d_f[(P_{CO} + (\nabla P)_{co}.\overrightarrow{r_0}) - (P_{cl} + (\nabla p)_{cl}.\overrightarrow{r_1})]\right) \quad (3.46)$$

$$J_f = \widehat{J_f} + d_f\,(P_{CO} - P_{cl}) \quad (3.47)$$

Where,

$$\widehat{J_f} = f_f\left(\rho_f \frac{a_{P,co}v_{n,co}+a_{p,cl}v_{n,cl}}{a_{P,co}+a_{p,cl}} + d_f[(\nabla P)_{co}.\overrightarrow{r_0}) - (P_{cl} + (\nabla p)_{cl}.\overrightarrow{r_1}]\right) \quad (3.48)$$

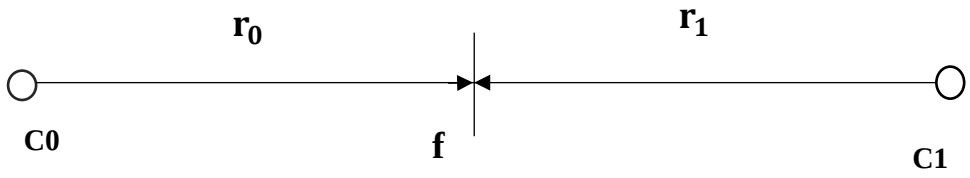

Figure 3.2: Control volume centroids of each control volume on either side of face f

Referring to figure 3.2, P_{CO} and P_{Cl} are the pressures and $v_{n,CO}$ and $v_{n,Cl}$ are the normal velocities respectively within the two cells on either side of the face f . The term $\widehat{J_f}$ contains the influence of velocities in these two adjacent cells and d_f is a function of the average of the momentum equation (3.36) a_P coefficients for the cells on either side of facef . Accordingly, for the control volume as shown in figure 3.2,

$$J_e = \widehat{J_e} + d_e(P_p - P_E) \quad (3.49a)$$

$$J_w = \widehat{J_w} + d_w(P_W - P_P) \quad (3.49b)$$

$$J_n = \widehat{J_n} + d_n (P_P - P_N) \quad (3.49c)$$

$$J_s = \widehat{J_s} + d_s (P_S - P_P) \quad (3.49d)$$

$$J_t = \widehat{J_t} + d_t (P_p - P_r) \quad (3.49e)$$

$$J_b = \hat{j}_b + d_b (p_B - p_P) \quad (3.49f)$$

Now for a guessed pressure field p^*, resulting east face flux from equation (3.49a), will be as follows -

$$J_e^* = \hat{J}_e^* + d_e (p_P^* - p_E^*) \quad (3.50)$$

Which does not satisfy the volume continuity equation (3.42), a correction $\acute{J}_e$ is added to the face flux J_e^* so that the corrected face flux J_e becomes -

$$J_e = J_e^* + \acute{J}_e \quad (3.51)$$

Similarly, a pressure correction $\acute{p}$ is added to the guessed pressure p^* so that the corrected pressure p becomes -

$$p = p^* + \acute{p} \quad (3.52)$$

From the Semi Implicit Method for Pressure Linked Equation (SIMPLE) algorithm, we can write -

$$\acute{J}_e = d_e (\acute{p}_P - \acute{p}_E) \quad (3.53)$$

Substituting the $\acute{J}_e$ in equation (3.48a), we get -

$$J_e = J_e^* + d_e (\acute{p}_P - \acute{p}_E) \quad (3.54a)$$

Similarly,

$$J_w = J_w^* + d_w (\acute{p}_W - \acute{p}_P) \quad (3.54b)$$

$$J_n = J_n^* + d_n(p'_P - p'_N) \quad (3.54c)$$

$$J_s = J_s^* + d_s(p'_S - p'_P) \quad (3.54d)$$

$$J_t = J_t^* + d_t(p'_P - p'_T) \quad (3.54e)$$

$$J_b = J_b^* + d_b(p'_B - p'_P) \quad (3.54f)$$

Now putting the value of $J_e, J_w, J_n, J_s, J_t, J_b$ in the continuity equation (3.42), we get -

$$\left[\left(J_e^* A_e + d_e A_e(p'_P - p'_E)\right) - \left(J_w^* A_e + d_w A_w(p'_W - p'_P)\right)\right] +$$

$$\left[\left(J_n^* A_n + d_n A_n(p'_P - p'_N)\right) - \left(J_s^* A_s + d_s A_s(p'_S - p'_P)\right)\right] + \quad (3.55)$$

$$\left[\left(J_t^* A_t + d_t A_t(p'_P - p'_T)\right) - \left(J_b^* A_b + d_b A_b(p'_B - p'_P)\right)\right] = 0$$

Rearranging equation (3.54) we can write as follows -

$$a_P p'_P = a_E p'_E + a_W p'_W + a_N p'_N + a_S p'_S + a_T p'_T + a_B p'_B + b \quad (3.56)$$

Where,

$$a_P = d_e A_e + d_w A_w + d_n A_n + d_s A_s + d_t A_t + d_b A_b \quad (3.57a)$$

$$a_E = d_e A_e \quad (3.57b)$$

$$a_W = d_w A_w \quad (3.57c)$$

$$a_N = d_n A_n \quad (3.57d)$$

$$a_S = d_s A_s \quad (3.57e)$$

$$a_T = d_t A_t \quad (3.57f)$$

$$a_B = d_b A_b \quad (3.57g)$$

$$b = J_e^* A_e + J_n^* A_n + J_t^* A_t - J_w^* A_w - J_s^* A_s - J_b^* A_b + (f_P^0 \rho_P^0 - f_P \rho_P)\frac{\nabla V}{\nabla t} \quad (3.57h)$$

Equation (3.56) represents the discretized continuity equation as an equation for pressure correction $\acute{p}$. From equation (3.56) we get the pressure correction $\acute{p}$ and putting the value of $\acute{p}$ in equation (3.52) we get correct pressure field p which satisfy the continuity equation (3.44). Then putting this pressure field in the momentum equation (3.56) we get the correct velocity.

3.6 Boundary Condition

Three different types of boundary conditions have been used in this current numerical investigation. At the inlet of the channel, where the fluid flows into the flow passage, velocity inlet boundary condition is employed. The pressure outlet boundary condition has been used at the exit, where the fluid leaves the channel and flushed to ambient. All other sides of the computation domain were taken as wall boundary.

Velocity inlet boundary condition

This type of boundary condition is used at the inlet section to set the flow velocity and other scalar parameters of the flow at the entry of the flow passage. It computes the mass flow into the domain through the inlet based on the input supplied at the boundary. It also figures out the momentum and energy fluxes and the volume fraction through the inlet. In this present work, a sinusoidal pulsating velocity component is superimposed over the uniform velocity profile. The resultant velocity profile can be expressed in the form –

$$u_{in} = u_m \{1 + A \sin(2\pi f_r t)\} \quad (3.58)$$

Here A is the amplitude of pulsation and f_r is the frequency of pulsation which is represented by the dimensionless Strouhal number (St) for this computation. The Strouhal number is defined as –

$$St = \frac{f_r D_h}{u_m} \quad (3.59)$$

Where D_h is the hydraulic diameter of the channel and u_m is the mean velocity of flow.

Pressure outlet boundary condition

The pressure outlet boundary condition defines the input pressure as the static pressure of the fluid at the outer surface and derive all other condition from the interior of the domain. This can be represented as –

$$p_{exit} = 0 \tag{3.60}$$

Wall boundary condition

The wall boundary condition is used to apply no slip condition on duct boundary. Isothermal wall was assumed as the thermal wall boundary condition. The velocity conditions applied at wall can be written in the form –

$$u = v = w = 0 \tag{3.61}$$

The governing equation were solved using ANSYS – FLUENT version 19.2. For momentum equation, third order accurate QUICK scheme was used, and for energy equation MUSCL scheme was used. Relaxation factor used for continuity, momentum and energy were between 0.1 – 0.9. In time domain, second order implicit formulation was used.

3.7 Data Reduction

Since, constant specific heat capacity of fluid is used to measure the energy absorbed, T_b (Bulk Temperature) could be assumed as the average of the temperatures at channel inlet and channel outlet, which in return is accounted for the calculation of fluid properties.

$$T_b = \frac{T_i + T_o}{2} \tag{3.62}$$

The convective heat transfer coefficient (h) is represented as follows (Nandi and Chattopadhyay, 2013),

$$h = \frac{q_w}{T_w - T_b} \tag{3.63}$$

The Nusselt number (Nu) is defined in terms of heat transfer coefficient and hydraulic diameter, represented as -

$$Nu = \frac{h\, D_h}{k} \tag{3.64}$$

Here D_h = hydraulic diameter.

The friction factor (f) is evaluated from,

$$f = \frac{2}{\frac{L}{D_h}} \frac{\Delta p}{\rho {u_{in}}^2} \tag{3.65}$$

where V is time average bulk velocity used in case of pulsating flow.

The performance enhancement criteria, η is given, as per Chang et al. (Chang, Jan and Liou, 2007)

$$\eta = \frac{Nu}{Nu_0} \Big/ \left(\frac{f}{f_0}\right)^{0.33} \tag{3.66}$$

where the subscript '0' denotes a plain channel with similar dimensions.

Entropy generation is the measure of the summation of the entropy generated in any irreversible process due to temperature. This is a function of temperature only. A reducing trend of thermal entropy generation fabricates a high rate of heat transfer. The total entropy generation equation can be written as (Awad, 2015)

$$S_{gen} = \dot{Q} \left[\frac{1}{T_0} - \frac{1}{T_b}\right] + \frac{\dot{V}}{T_0} \Delta P \tag{3.67}$$

To assess the overall thermal performance triggered by the inlet flow pulsation, Augmentation entropy generation number (AEGN) is reported. It is the ratio of entropy generation with pulsation at inlet (S_{gen}) to the entropy generation of the steady case ($S_{gen,0}$). It is represented by the following equation –

$$AEGN = \frac{S_{gen}}{S_{gen,0}} \tag{3.68}$$

3.8 Closure

The full Navier-stokes equation must be solved in order to find the flow and energy field. This chapter illustrates the procedure of solving the equations using the finite volume method. Also, the discretization methodology involving these solution process is discussed in this chapter. For this. Patankar's SIMPLE scheme was used for pressure correction purpose, whereas, Rhie and Chow's (1983) momentum interpolation scheme was also utilized.

In this work, the governing equations were solved using ANSYS – FLUENT 19.2. For momentum equation, third order accurate QUICK scheme was used and for energy equation, MUSCL scheme was used. For continuity, momentum and energy equations, a relaxation factor between 0.1 – 0.9 was used. In time domain, second order implicit formulation was used. To implement sinusoidal velocity fluctuation at the inlet boundary, a User Defined Function (UDF) was written and applied at the inlet. The UDF is shown in figure 3.3

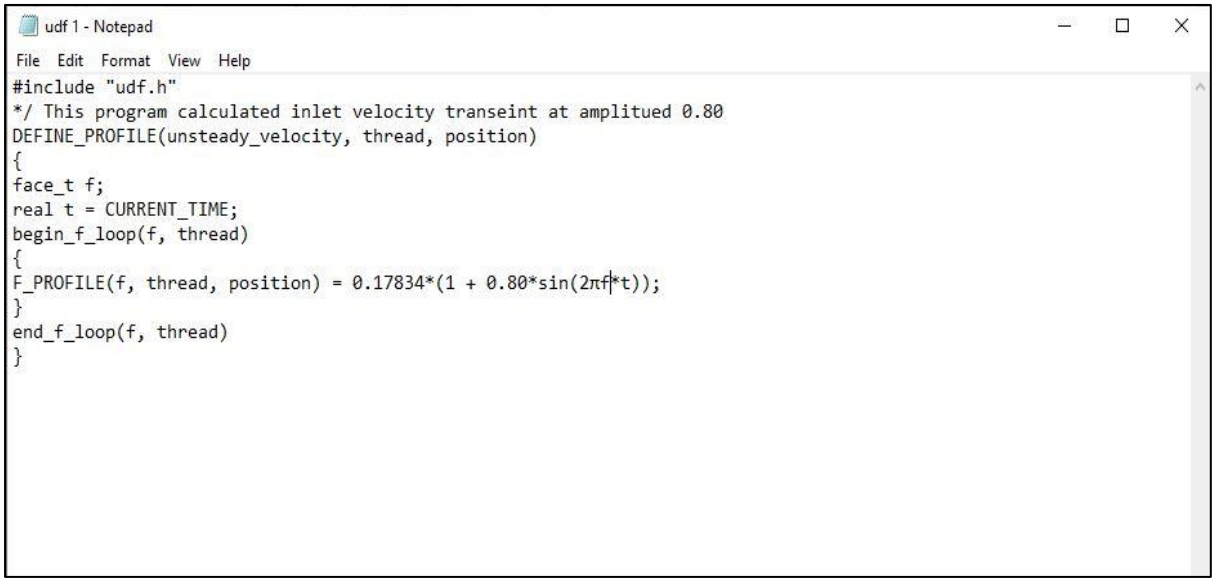

Figure 3.4: User Defined Function (UDF) for implementing sinusoidal velocity fluctuation at inlet

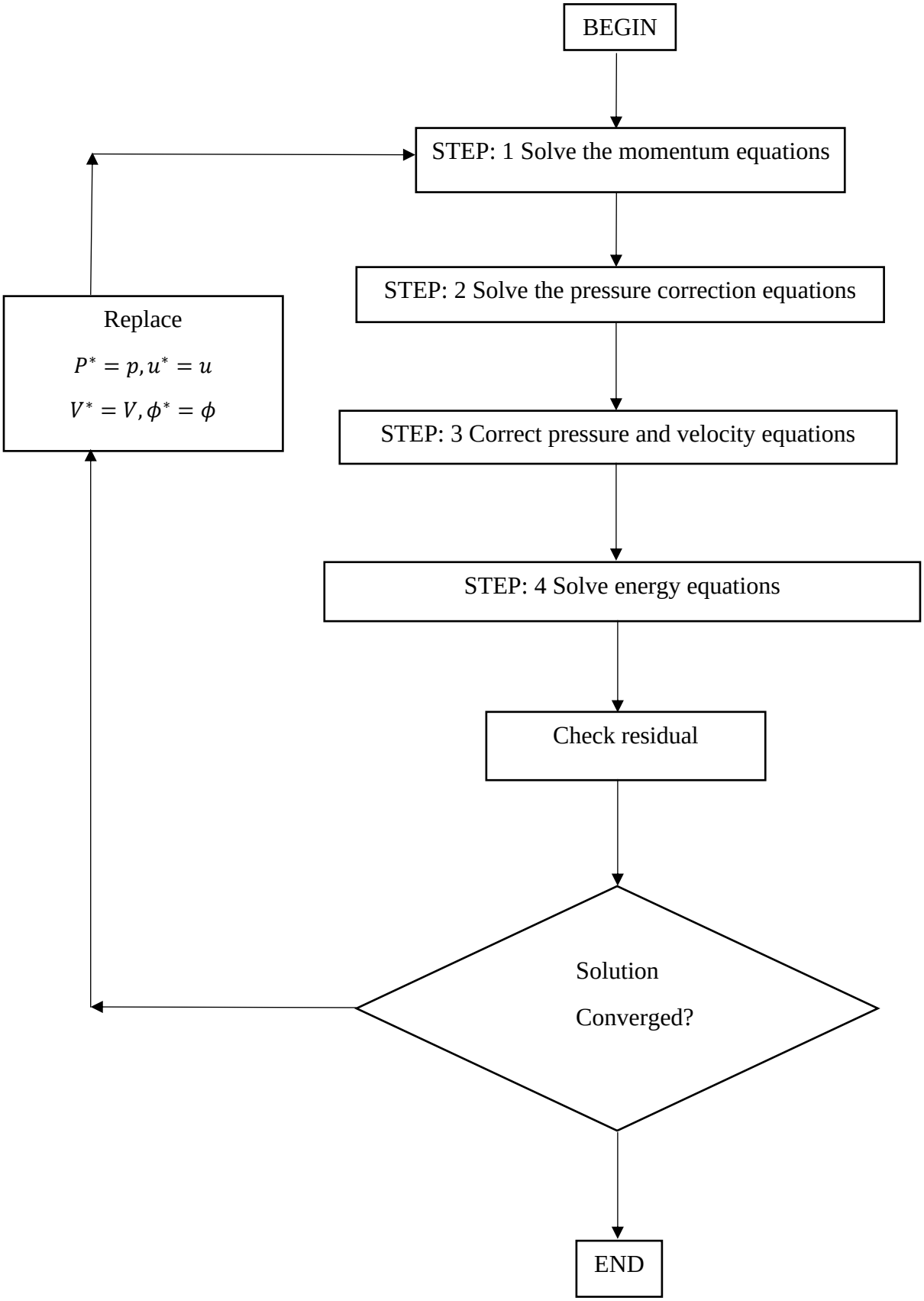

Figure 3.5: Flow chart of computational scheme (at a particular time step)

CHAPTER FOUR

ENHANCED HEAT TRANSFER OVER TWO DIMENSIONAL STEPPED AND CONVERGING DIVERGING MICRO-CHANNELS

4.1 Introduction

A number of geometrically modified micro-channels with pulsating velocity at inlet, were examined in this present research. A vast number of computational work were conducted to assess the transport phenomena and heat transfer in micro-channels. The numerical results were compared with the results obtained from plain micro-channels using same numerical scheme. Both two dimensional and three dimensional micro-channels were designed for the computation purpose. In this preliminary work of this thesis, two dimensional modified geometries were used to evaluate transport phenomena and heat transfer enhancement in micro-channel. The two dimensional micro-channels, involved in this section were modified by providing contractions over the flow path, thus forcing the working fluid to flow along a shrinked passage. Two different types of contraction were provided i.e. sudden contraction (stepped channel) and gradual contraction (converging diverging channel). Along with geometry modification, a sinusoidal inlet flow pulsation was also administered at the channel inlet to evaluate the combined effect of passive and active enhancement technique. Dimensionless Nusselt number and friction factor was reported to portray convective heat transfer and pressure drop results. A performance enhancement criterion, that combines the Nusselt number (Nu) results with pressure drop result, was also reported to estimate the overall thermal performance of the proposed channels.

4.2 Problem statement

Figure 4.1(a) and 4.1(b) exhibit the schematic diagram of both the micro-channels involved in this work. The first channel constitutes two stepped sections (sudden contracted sections) over its length in stream-wise direction. The hydraulic diameter (D_h) of the channel was made 500 μm. The ratio of pitch of the contraction (i.e. the length of the contracted part of the channel represented by 'P') to the hydraulic diameter (D_h) of the channel defined as contraction ratio (α). Channels with three different contraction ratio (α = 10, α = 16, α = 20

respectively) was designed for the analysis purpose. Figure 4.1(b) portray the schematic diagram of the second channel involved in the present work. The channel constitutes a converging diverging section (section with gradual contraction) over its length in stream-wise direction. The throat diameter is specied as 'd'. the study was conducted for three different throat diameter i.e d=0.10, d=0.20 and d=0.30. The hydraulic diameter (D_h) of the channel was made 500 μm. The ratio of pitch of the contraction (i.e. the length of the contracted part of the channel represented by 'P') to the hydraulic diameter (D_h) of the channel defined as contraction ratio (α). Channels with three different contraction ratio (α = 30, α = 40, α = 50 respectively) was designed. The cooling fluid was taken as water for both the cases. The following assumptions were taken up for the analysis: - (i) The flow is steady, (ii) The flow is laminar, (iii) The flow is incompressible, (iv) The fluid is inviscid, (v) There is negligible radiation heat transfer, (vi) All the fluid properties are constant with respect to temperature change.

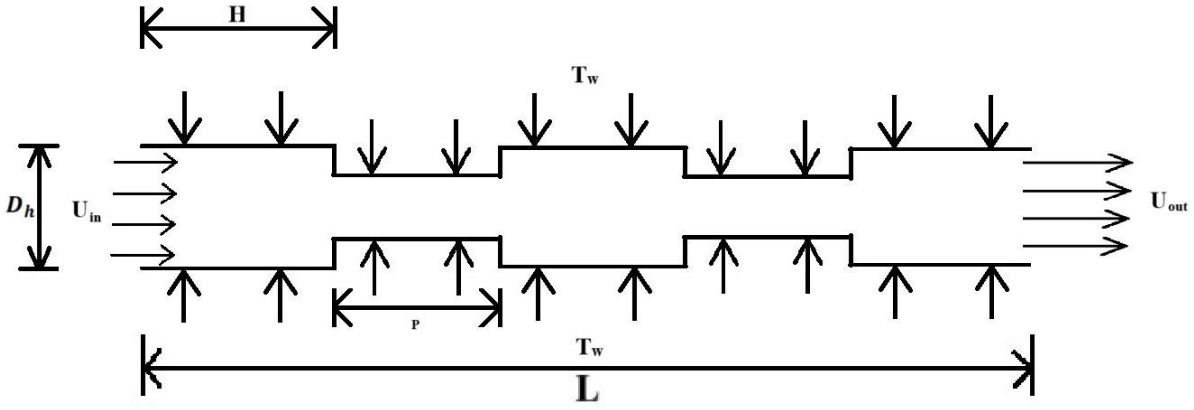

Figure 4.1(a). Schematic diagram of the stepped micro-channel

Dirichlet type of boundary conditions was applied for the MCHS wall. Constant wall temperature boundary condition, which induces isothermal boundary, was imposed. Also, no slip wall boundary, which impose zero velocity at wall was established to conduct the simulation. As per the planning of the investigation criteria, the outlet of the computational

domain was to be kept at free fluid exit to the atmosphere. Hence, pressure outlet boundary condition was applied to the outlet which represents atmospheric pressure. The inlet fluid velocity was to be represented by Reynolds number which is defined as –

$$Re = \frac{uD_h}{\nu} \quad (4.1)$$

For the cases, where a sinusoidal velocity component was super-imposed at the inlet, the inlet velocity was assumed to be in the form of –

$$u_{in} = u_m \{1 + A \sin(2\pi f_r t)\} \quad (4.2)$$

The above equation represents a sinusoidal time variation of the inlet velocity where –

u_{in} = bulk inlet velocity

u_m = average inlet velocity (represented by dimensionless Reynolds Number)

A = amplitude of pulsation

f_r = frequency of pulsation (represented by dimensionless Strouhal Number, $St = f_r D_h/u_m$)

It should be noted that identical inlet conditions have been documented in the literature earlier, e.g. by Nandi and Chattopadhyay (2013).

4.3 Grid Independence Test and Validation

In numerical method, dependent variables are solved at finite number of locations, known as grid points. These are specific locations in the calculation domain, that provides a set of algebraic equations for the unknown dependent variables so that they can be solved numerically using any of the three finite methods. For the present investigation, Finite Volume Method (FVM) has been used. If the distance between the Grid points becomes very close, solution provided by the numerical method becomes very close to the exact solution of the governing differential equations, while, larger distance between the grid points produce

significant difference between exact solution and numerical solution. So, it can be assumed that the solution accuracy depends upon grid spacing in the calculation domain. Less the grid spacing, higher the accuracy of the solution, but it also increases computation time. Also, beyond certain grid density, the solution does not improve and this situation is called grid independent situation and the solution is called "grid independent solution". In numerical methods, grid independence test is conducted to obtain the optimum grid size so that grid independent solution conjugated with least possible computation time may come out. In the present study, intensive grid independence test has been carried out to ensure the optimum grid size.

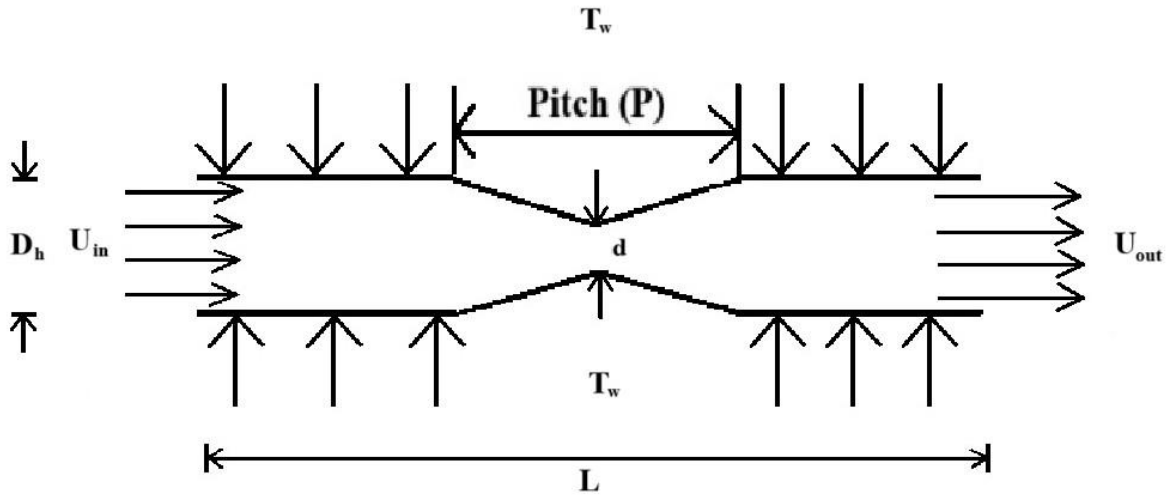

Figure 4.1(b). Schematic diagram of the converging diverging micro-channel

The set of equations was solved using a finite volume based solver ANSYS Fluent 19.2. Simulations were carried out for various Reynolds number between 100 and 500. Uniformly structured mesh was generated for the computation. Meticulous grid independence (GIS) study was performed to pick up the optimum one (displayed in Table 4.1). Pressure drop was the parameter involved for the grid independence study. Table 4.1 demonstrates the GIS for a plain channel without steps. The optimization was done for different nodes and the the results

were compared with previous well established work of Nandi et al. The selection of grid with 20040 nodes produces results that are regarded adequate because additional refinement has little effect on the output. A close-up view of the mesh is shown in Figure 2. The SIMPLE algorithm was used to find solutions [(Patankar *et al* (1977)]. In accordance with Nandi and Chattopadhyay (Chang *et al* (2007), the QUICK scheme was used for momentum equations and the MUSCL scheme for energy equations. In order to achieve convergence, it was made sure that the residual values for the momentum and energy equations, were less than 10^{-5} and 10^{-8} respectively.

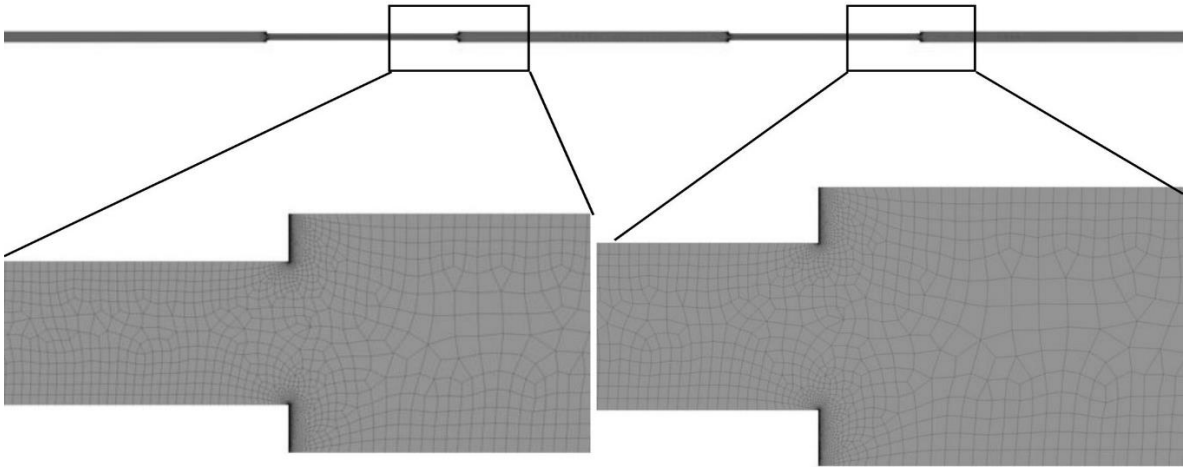

Figure 4.2(a) Mesh of the stepped micro-channel

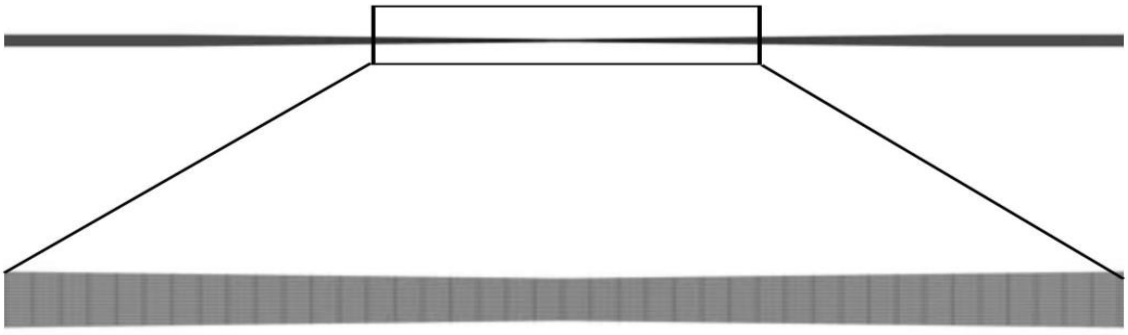

Figure 4.2(b) Mesh of the converging micro-channel

The present numerical model was compared and validated with the previous well established work. Figure 4.3 displays the Nusselt number results of plain micro-channel with the results of Nandi and Chattopadhyay (2013). The results exhibited reasonable agreement with the previous one. The plain channel Nusselt nuber data of the present scheme falls within a variation range of 2% -4% of the previous work. Also, the plain channel friction factor data were compared with the same previous established work. Figure 4.4, portrays the comparison between the friction factor data of the two. The friction factor results also exhibits well agreement (within a range of 2% – 5%) with the previous result.

4.4 Result & Discussion

Figure 4.2(a) and figure 4.2(b) exhibits the mesh of both the channels. Figure 4.5 illustrates the variation of surface average Nusselt number (Nu) with Reynolds number (Re) for the stepped channel. It is evident from figure 4.5 that the modified stepped channel geometry produces accountable increased Nusselt number results as compared to the plain channel. Also, it is clear from the figure that with increasing contraction ratio, the Nusselt number is also increasing.

Table 4.1: Grid Independence Test, Plain Channel, A = 0.8, St = 5, Re = 100

Nodes	Pressure Drop (Pa) (Present Study)	Pressure Drop (Pa) (Nandi et al)	Refinement	Error Percentage
25551	10.25	9.55	0.08	7.33
20040	9.82	9.55	0.09	2.83
16441	9.02	9.55	0.10	5.55

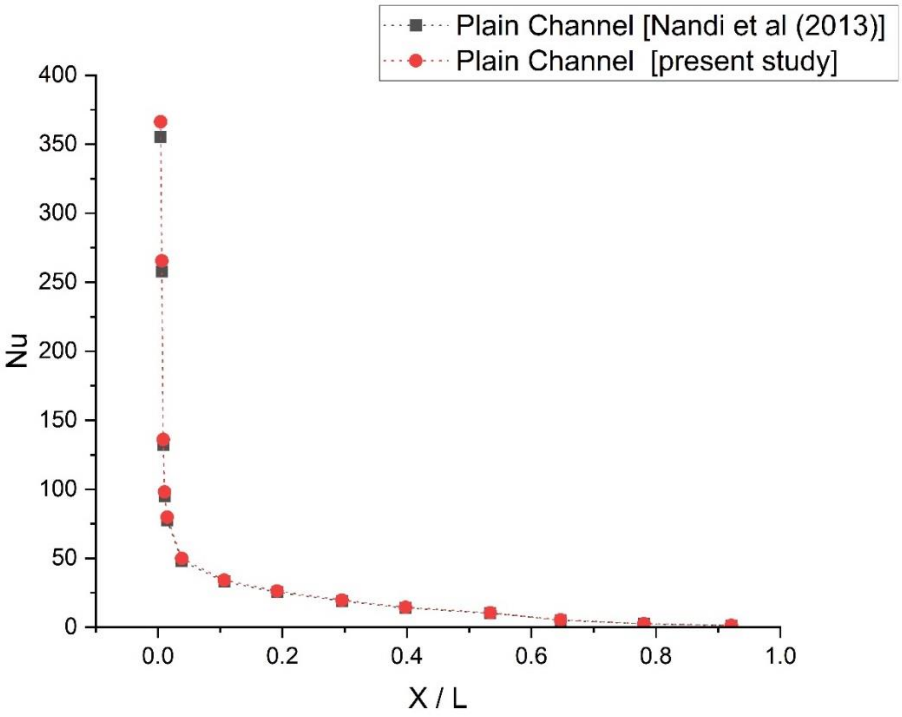

Figure 4.3 Variation of Nu with X/L for plain channel steady case for Re = 100

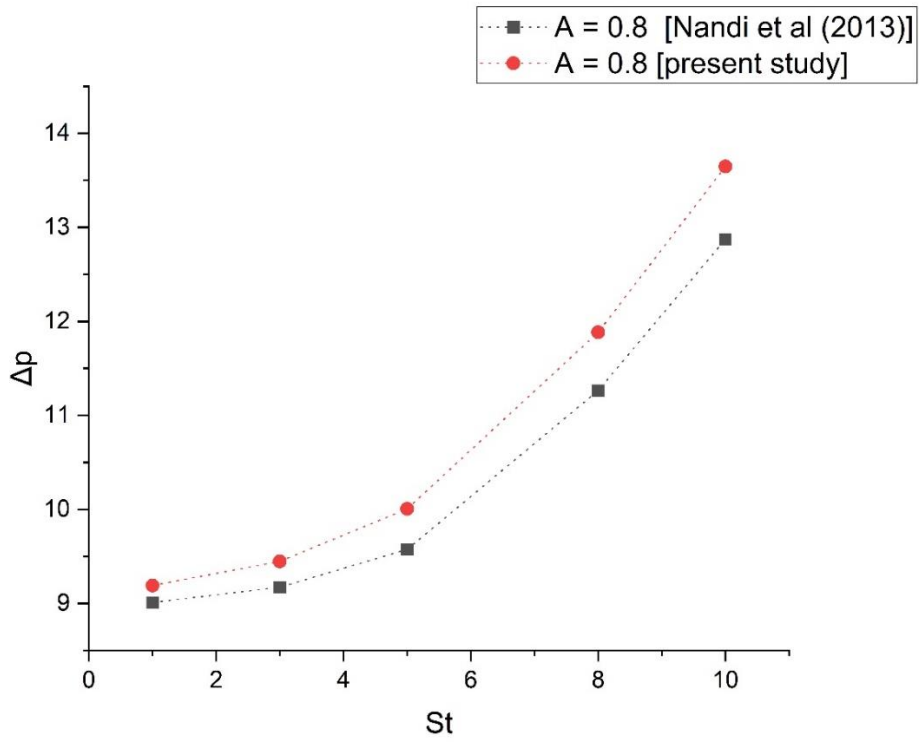

Figure 4.4 Variation of pressure drop with Strouhal Number for plain channel A = 0.8, Re = 100

It may be credited to the flow disruption caused by the sudden contraction in the flow passage. The sudden contraction over the flow path caused creation of recirculation zones as well as better mixing of the core fluids with the near wall fluid, causing elevated Nusselt number results. It can also be observed from the figure that with increase in Reynolds number, the difference between Nuseelt number results of modified geometry and plain channel is also increased. This may be because of the fact that at higher fluid velocity, formation of recirculation along the flow is also higher.

Pressure drop is the price paid for improved heat transfer when using modified channel geometry, i.e. suddenly contracted flow passage in this case. Particularly at low Reynolds numbers, the flow passage's narrowness and fluctuation impede fluid mixing, which results in a large pressure drop. Figure 4.6 depicts the fluctuation of pressure drop inside the stepped channel represented by dimensionless friction factor (*f*) as a function of Reynolds number. It can be narrated from the figure that the stepped geometry produces elevated friction factor results as compared to the plain channel. It is also observed that the friction factor result is getting higher with increase in the contraction ratio.

Figure 4.7 represents the relationship between the Colburn (*j*) factor and Reynolds number (Re) of the stepped channel. The figure clearly shows that the altered shape leads to significant rise in heat transfer compared to the base case. It is also evident from the figure that as the contraction ratio increases, the Colburn (*j*) factor also produces higher values. The augmented heat transfer may be originated from the flow disruption due to the sudden contraction in the flow passage. Due to the abrupt narrowing along the flow path, recirculation zones were formed leading to improved mixing of the core fluids with the near wall fluid, resulting in higher heat transfer outcomes.

Figure 4.8 portrays the variation of Performance Enhancement Ratio (η) with Reynolds number for the stepped channel geometry. It is designated as the ratio of Nusselt number ratio (ratio of nusselt number of the modified geometry to the nusselt number of the plain channel)

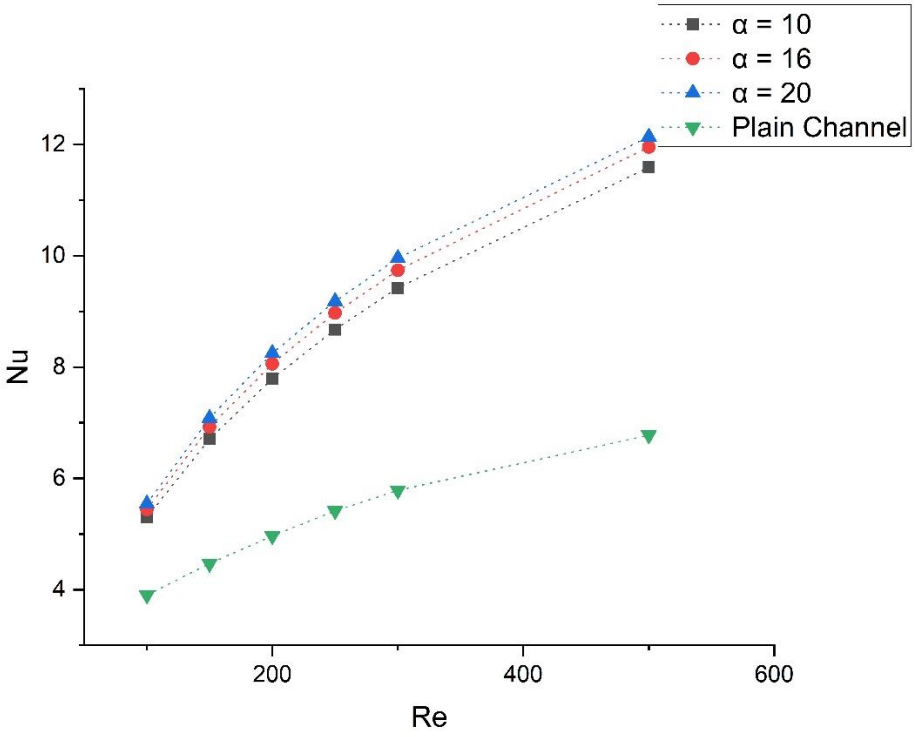

Figure 4.5. Comparison of Nu with Re (Stepped Channel)

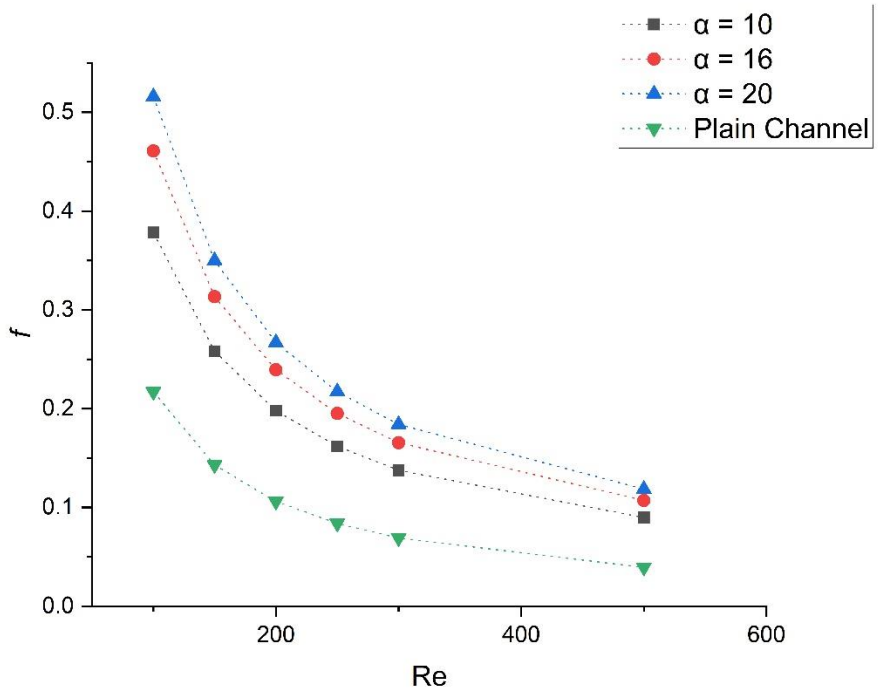

Figure 4.6. Comparison of *f* with Re (Stepped Channel)

to the cube root of friction factor ratio (again ratio of friction factor of the modified geometry to the friction factor of the plain channel). From figure 4.5 and figure 4.6 it is crystal clear that though the modified geometry boosts up the heat transfer performance of the MCHS, it comes at the cost of inflated friction factor. So, to evaluate the overall performance of the stepped channel, the PEC (η) can be utilized. Figure 4.8 unfolds that the PEC (η) values show a steep rise with increase in Reynolds number up to 300. Though it may also be noted that above Re = 300, the PEC value increase very little. This can be attributed to the fact that at high Reynolds number, there is very high friction factor increase and thus affecting the PEC (η) values. Also, it is perceived from the figure that the lowest contraction ratio providing the best result and increase in contraction ratio produces gradual decrement in the PEC (η) values. Hence, modified geometry with least contraction ratio (α) is giving the best performance, whereas channels with increasing contraction ratio (α) yielding degradation in performance.

Expecting further improvement in heat transfer performance of the prescribed modified geometry, additional time dependent sinusoidal velocity fluctuation was implemented at the inlet of the stepped channel. The target was to enhance recirculation zones inside the flow and manipulate fluid mixing. The instantaneous axial velocity inside the microchannel should exhibit periodic changes in nature as a result of the addition of periodic pulsation at the intake. Figure 4.9 displays the input velocity signal as a function of time. The instantaneous axial velocity was monitored at the middle position of the channel to study the nature of the velocity and several such monitors were used. The sinusoidal nature of the above mentioned curve establishes the fact that the velocity field was time dependent and fully periodic in nature, following sinusoidal velocity fluctuation at the channel inlet.

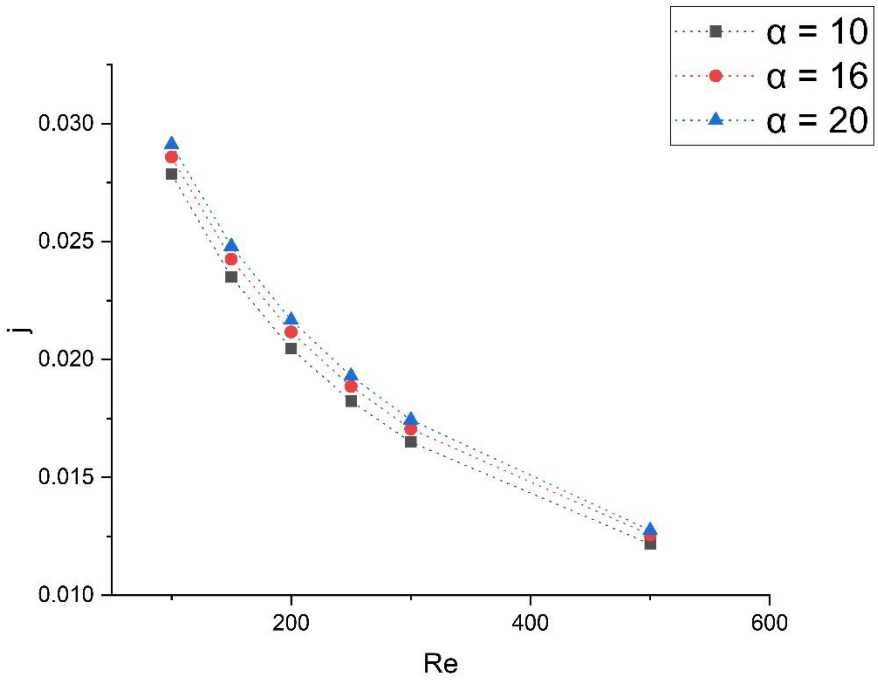

Figure 4.7. Variation of Colburn (j) factor with Re (Stepped Channel)

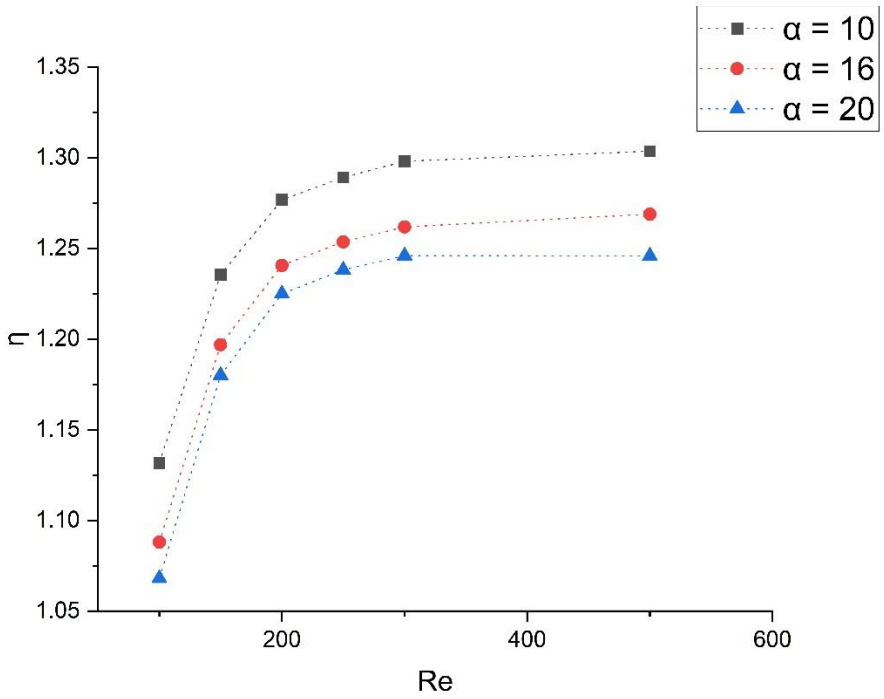

Figure 4.8. Variation of η with Re (Stepped Channel)

Nusselt number variation with and without inlet pulsation against Reynolds number of the stepped channel displayed in figure 4.10. The figure shows that at lower values of Re, the Nusselt number results with inlet pulsation, doesn't deviate much as compared to the case without inlet pulsation. At low Reynolds number the inlet pulsation cannot disrupt the flow accountably. But at higher Reynolds number, the stepped geometry with inlet pulsation is producing much higher Nusselt number result as compared to the case of the stepped geometry without inlet pulsation. The flow pulsation seizes over the viscous force at high values of Re. also, better fluid mixing and the channel's improved geometry allows for the creation of recirculation zones. Thus it can be interpreted that the stepped geometry with inlet pulsation can provide better heat transfer results. It can also be observed from the figure that with increasing concentration ratio, the Nusselt number is also greatly increased.

The friction factor variation against Reynolds number for both with and without pulsation, is displayed in figure 4.11 for the stepped channel. It can clearly be observed from the figure that the velocity pulsation applied to the inlet flow velocity greatly elevates the friction factor values as compared to the modified geometry without inlet pulsation. That can be attributed to the fact that the pulsatile nature of the inlet flow velocity forcing larger amount of fluid into the narrow and fluctuation natured flow passage. Thus one can deduce that though the inlet pulsation enhances the heat transfer along the modified stepped channel geometry, it comes with high pressure drop.

Figure 4.12 represents the relationship between the Colburn (j) factor and Reynolds number (Re) of the stepped channel. The figure clearly shows that the altered shape leads to significant rise in heat transfer compared to the base case. It is also evident from the figure that as the contraction ratio increases, the Colburn (j) factor also produces higher values. The augmented heat transfer may be originated from the flow disruption due to the sudden contraction in the flow passage. Due to the abrupt narrowing along the flow path,

recirculation zones were formed leading to improved mixing of the core fluids with the near wall fluid, resulting in higher heat transfer outcomes.

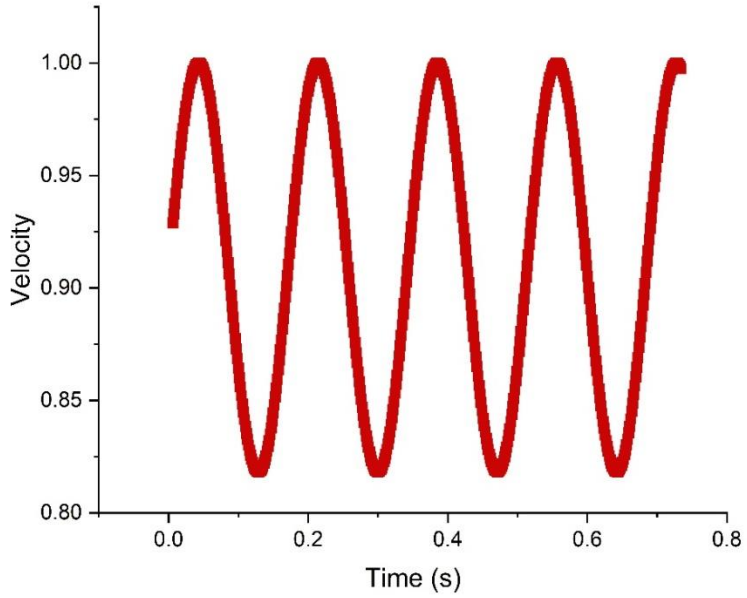

Figure 4.9. Periodical non dimensional velocity magnitude inside the stepped channel

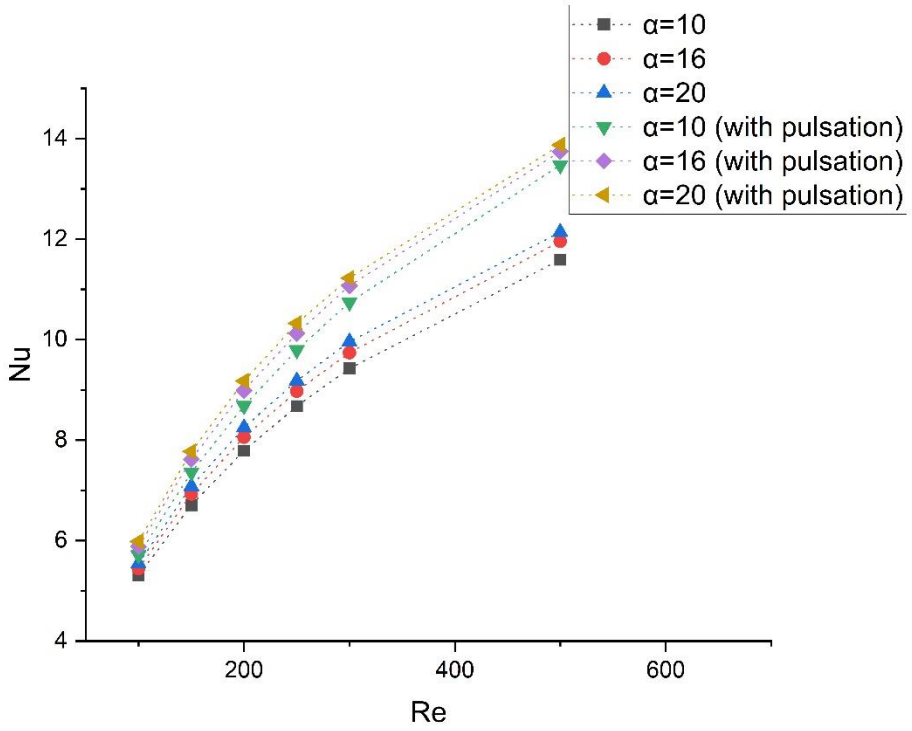

Figure 4.10. Comparison of Nu with Re (Stepped Channel)

Figure 4.13 demonstrates the character of entropy generation against Reynolds number for the suggested geometry. The figure distinctly indicates that with the Reynolds number (Re) increases, there is a noticeable decline in entropy generation, which is preferable as far as heat transfer augmentation is concerned. To compare the thermal performance of the MCHE with inlet flow pulsation to the steady one, a dimensionless quantity, composed of the ratio of entropy generation of the modified geometry to the entropy generation developed by the reference one i.e. the plain channel, taken into consideration. The quantity is termed as Augmentation Entropy Generation Number (AEGN). Figure 4.14 unfolds the variation of this quantity with increase in Reynolds number. As a matter of fact, to achieve greater heat transfer result, reduced value of thermal entropy generation is the objective. Therefore, a lower value of augmented entropy generation, less than one, would indicate a more favourable outcome. The figure illustrates that the present geometry with pulsating flow applied at inlet, consistently exhibits Augmented Entropy Generation Number values below unity.

Figure 4.15 presents the PEC variation with Reynolds number. The figure narrates that the use of inlet pulsation is providing a good overall thermal performance as it is showing values greater than unity for all the cases. However, it is also observed that with increase in contraction ratio, the PEC values are reducing. While the geometry with least contraction ratio i.e. d = 10 is furnishing best results. Also it can be noted from the figure that, though the PEC values showing upward trend primarily with increase in Reynolds number, it declines above Re = 250. However, these may be attributed to the high friction factor comes with high Reynolds number and high contraction ratio.

The focus of using inlet flow pulsation along with the modified geometry was to magnify the amount of heat transfer. As for result, it was noted that though it can provide

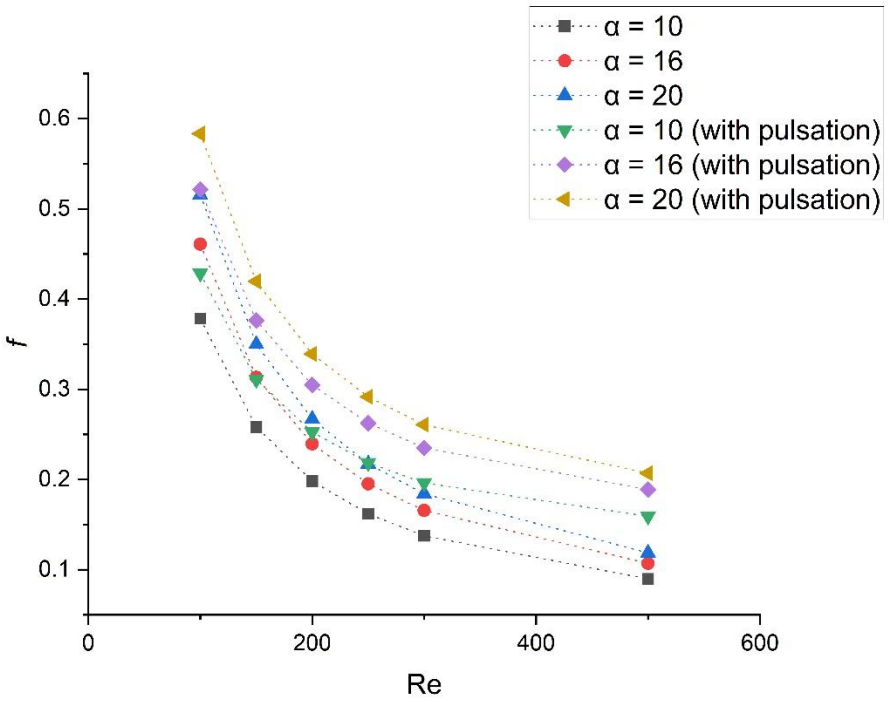

Figure 4.11. Comparison of *f* with Re (Stepped Channel)

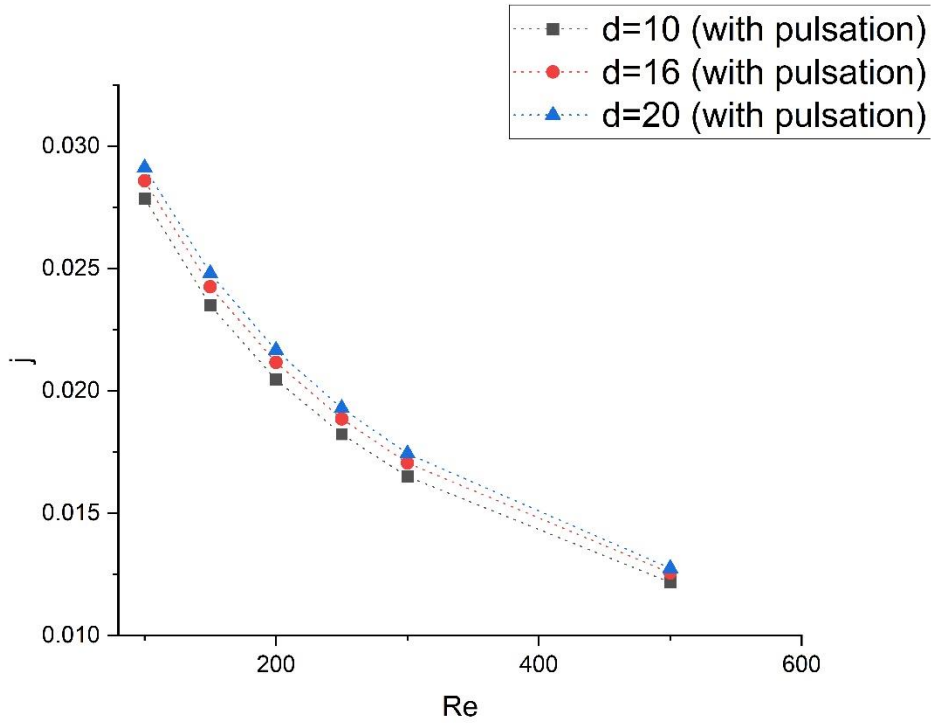

Figure 4.12. Comparison of Colburn (j) factor with Re (Stepped Channel)

elevated Nusselt number result, the pressure drop penalty comes with, is quite high. To predict whether the inlet pulsation can provide overall better thermal performance or not, PEC ratio, i.e. ration PEC without pulsation to PEC with pulsation, is plotted against Reynolds number, which is illustrated in figure 4.16. The figure conveys that, though the ratio is showing greater than unity (it means cases with inlet pulsation ensure greater PEC values) for most of the cases, but it is showing a downward trend. Also, above Re = 250, it is coming down below unity.

Figure 4.17(a), 4.17(b) and 4.17(c) illustrates the variation of surface average Nusselt number (Nu) with Reynolds number (Re) for the converging diverging channel for contraction ratio 30, 40 and 50 respectively. Both the cases with and without inlet pulsation was assessed It is evident from the figures that the modified converging diverging geometry produces accountable increased Nusselt number results as compared to the plain channel. The figure also shows that the inlet pulsation increased the Nusselt number results. Also, it is clear from the figure that geometry with least throat diameter (d=0.10) provided the best Nusselt number result. It may be credited to the flow disruption caused by the sudden contraction in the flow passage. The sudden contraction over the flow path caused creation of recirculation zones as well as better mixing of the core fluids with the near wall fluid, causing elevated Nusselt number results. It can also be observed from the figure that with increase in Reynolds number, the difference between Nuseelt number results of modified geometry and plain channel is also increased. This may be because of the fact that at higher fluid velocity, formation of recirculation along the flow is also higher.

Pressure drop is the price paid for improved heat transfer when using modified channel geometry, i.e. converging diverging flow passage in this case. Particularly at low Reynolds numbers, the flow passage's narrowness and fluctuation impede fluid mixing, which results in a large pressure drop. Figure 4.18(a), 4.18(b) and 4.18(c), depicts the

fluctuation of pressure drop represented by dimensionless friction factor (*f*) as a function of Reynolds number for both steady and pulsating case. It can be narrated from the figure that the modified geometry produces elevated friction factor results as compared to the plain channel. It is also observed that the friction factor result is higher with the least throat diameter. It can also be noted that, though at d=0.10 the pulsating case provided the maximum friction factor result, with increase in Re it showed a steep fall in friction factor data. It can be attributed to the fact that at higher velocity, the pulsating nature of the incoming flow providing reduction in pressure drop.

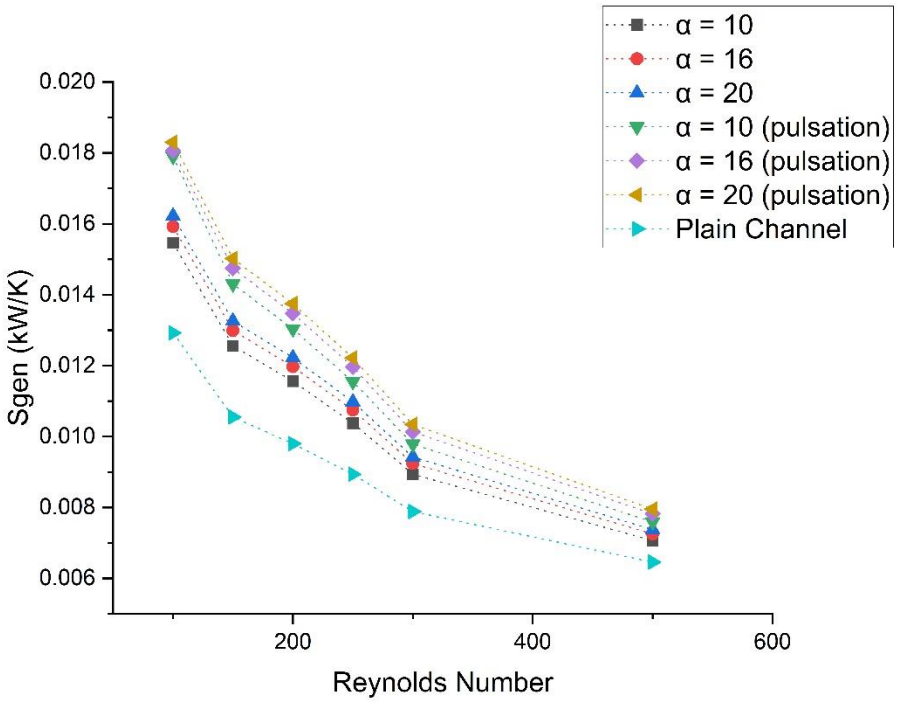

Figure 4.13. Comparison of total entropy generation with Re (Stepped Channel)

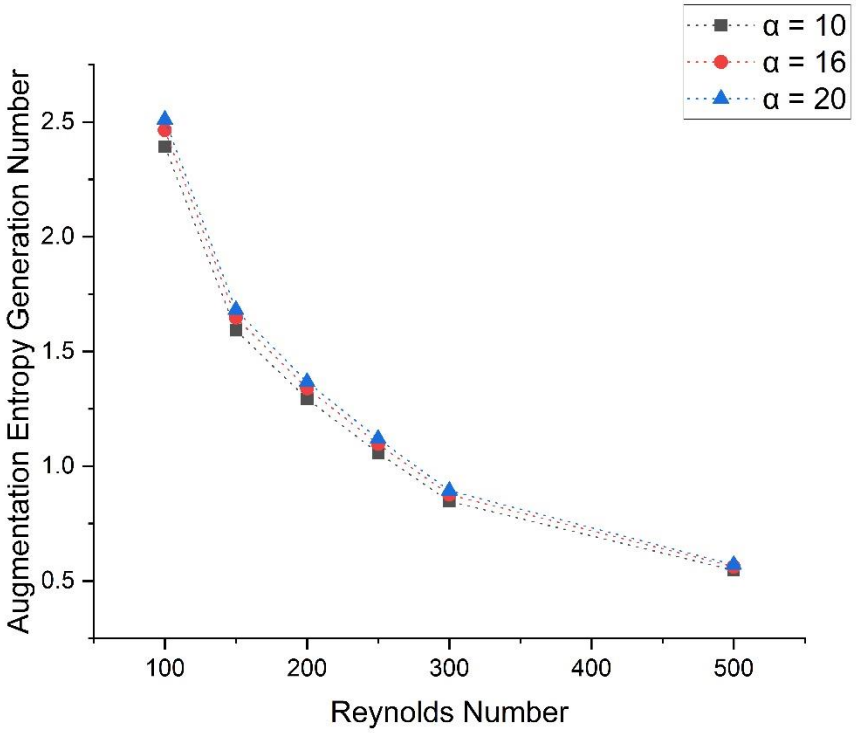

Figure 4.14. Comparison of AEGN Re (Stepped Channel)

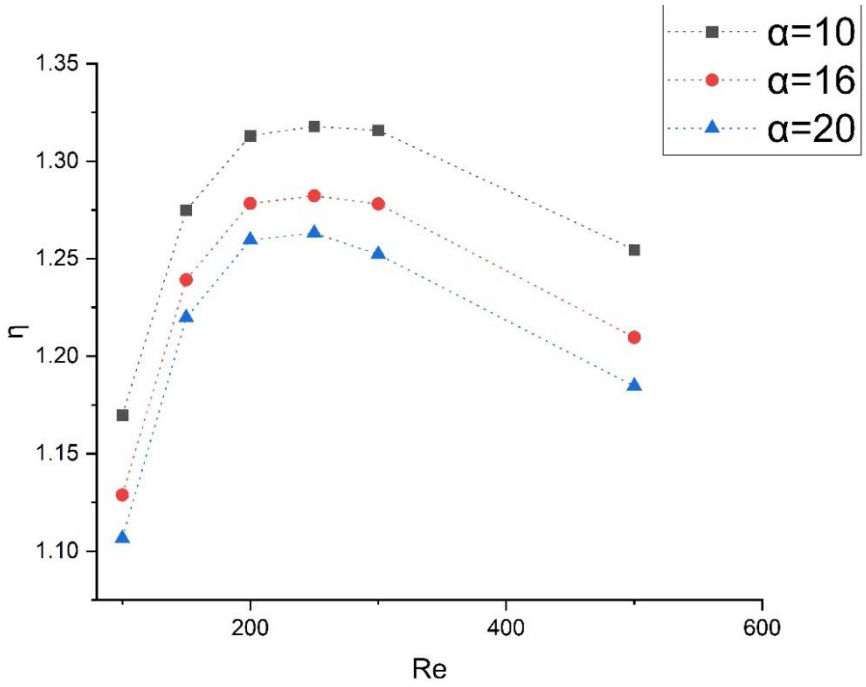

Figure 4.15. Variation of η with Re (Stepped Channel with inlet pulsation)

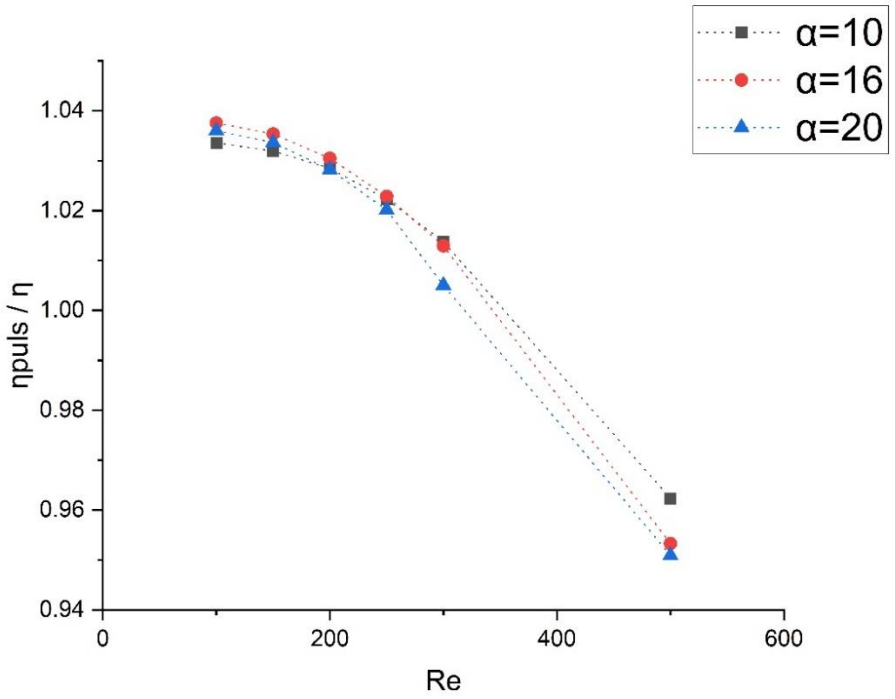

Figure 4.16. Variation of η_{puls} / η with Re (Stepped Channel)

Figure 4.19(a), 4.19(b) and 4.19(c) represents the relationship between the Colburn (*j*) factor and Reynolds number (Re) of the converging diverging micro-channel. The figure clearly shows that the altered shape leads to significant rise in heat transfer compared to the base case. It is also evident from the figure that for the least throat diameter (d=0.10) with pulsating inlet, provided best Colburn (*j*) factor data. The augmented heat transfer may be originated from the flow disruption due to the gardual contraction in the flow passage. Due to the abrupt narrowing along the flow path, recirculation zones were formed leading to improved mixing of the core fluids with the near wall fluid, resulting in higher heat transfer outcomes.

Figure 4.20(a), 4.20(b) and 4.20(c) portrays the variation of performance enhancement ratio (η) with Reynolds number for the present modified geometry. From figure 4.17 and figure 4.18 it is crystal clear that though the modified geometry boosts up the heat transfer performance of the MCHS, it comes at the cost of inflated friction factor. So, to

illustrate the overall performance of the prescribed channel, the performance enhancement criteria (η) can be utilized. Figures unfold that the η values shows a steep rise with increase in Reynolds number up to 400. Though it may also be noted that above 400, the performance enhancement criteria (η) value showed a downward trend. This can be attributed to the fact that at high Reynolds number, there is very high friction factor increase and thus affecting the PEC values. Also, it is perceived from the figure that the highest throat diameter with transient condition giving the best result. Also it can be noted that in most of the cases, the proposed converging diverging geometry produced performance enhancement criteria (η) values less than unity. Form this, we can conclude that, the proposed geometry modification could not enhance overall thermal performance at all. Whereas, the other geometry (the stepped channel) provided an enhanced thermal performance about 10 – 30 %.

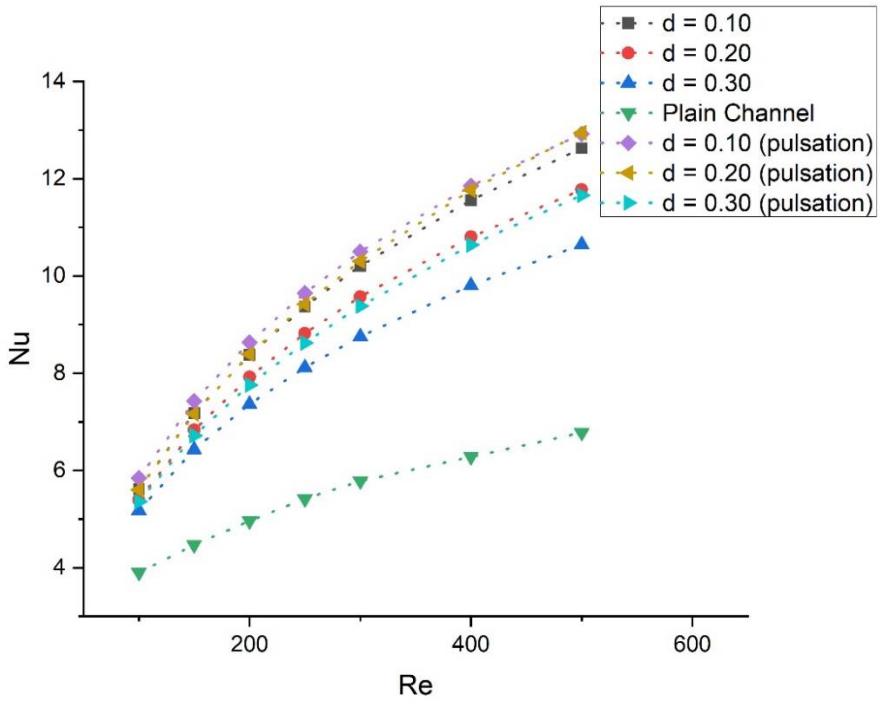

Figure 4.17(a). Comparison of Nu with Re for α=30 (converging diverging channel)

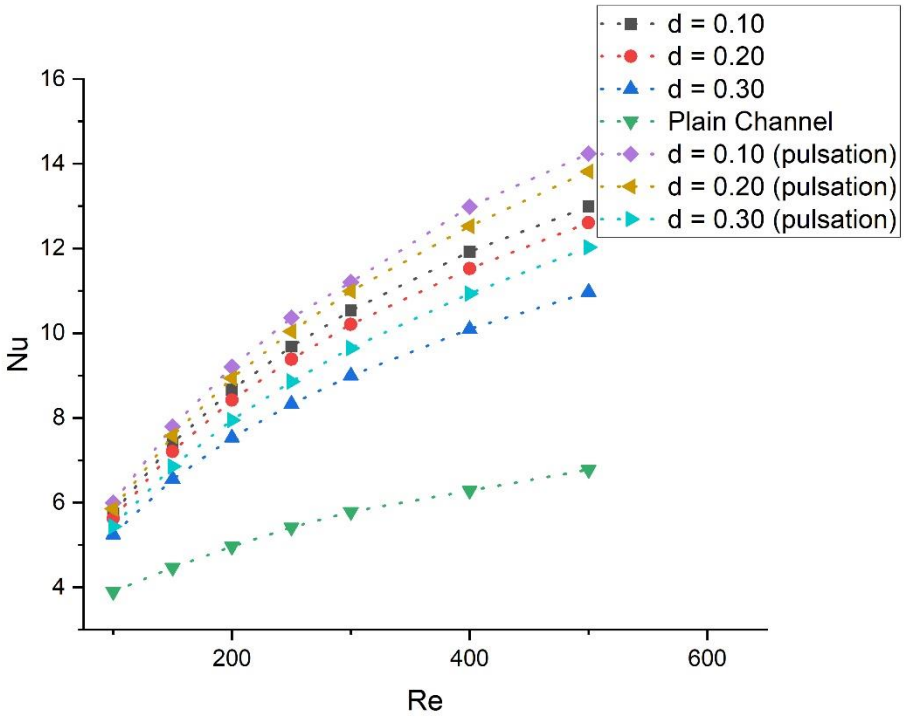

Figure 4.17(b). Comparison of Nu with Re for α=40 (converging diverging channel)

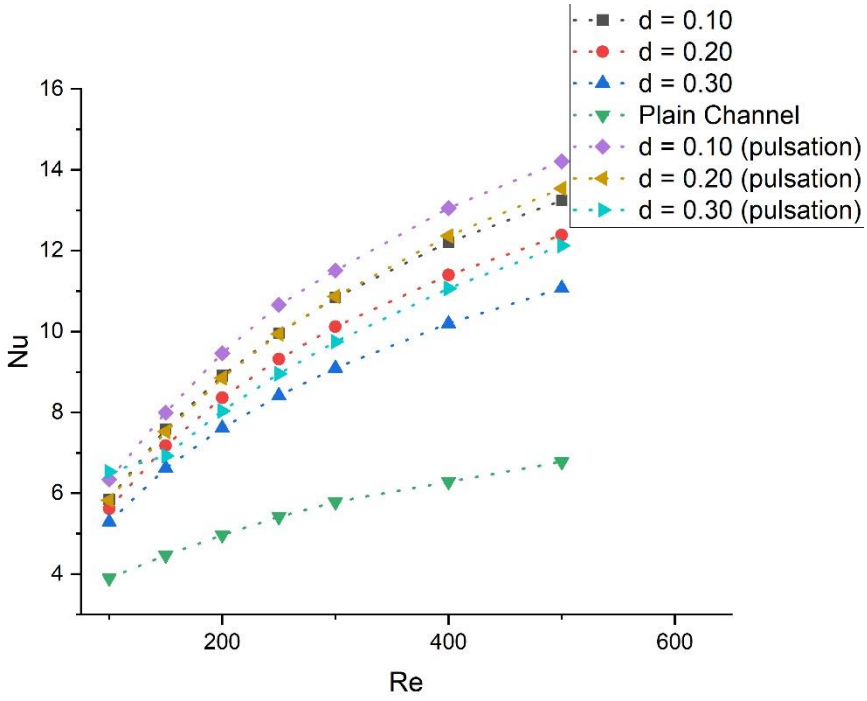

Figure 4.17(c). Comparison of Nu with Re for α=50 (converging diverging channel)

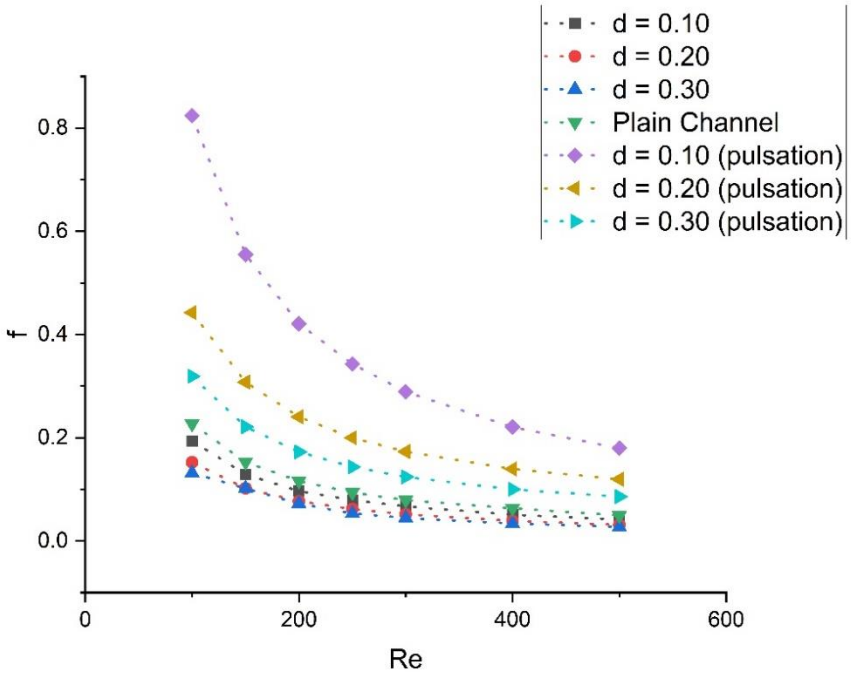

Figure 4.18(a). Comparison of *f* with Re for α=30 (converging diverging channel)

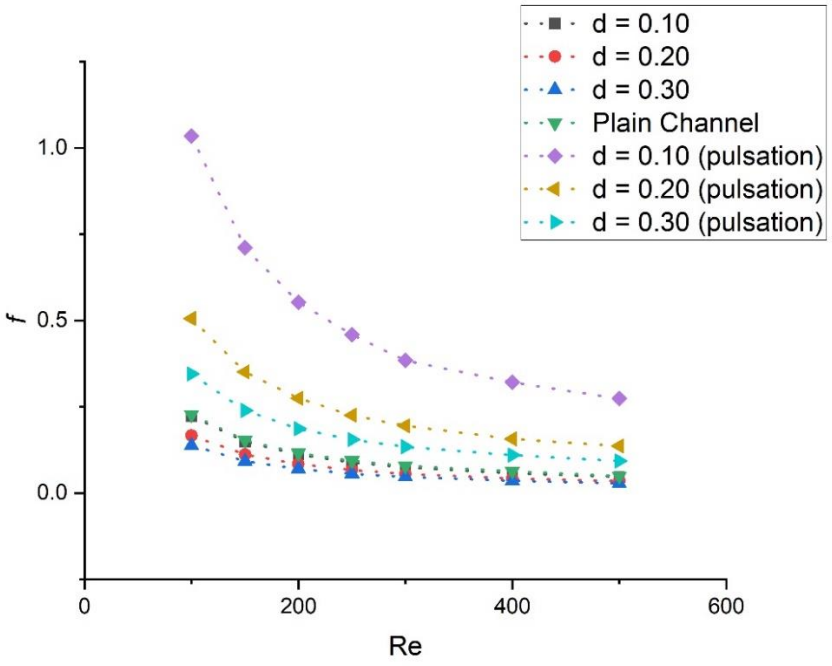

Figure 4.18(b). Comparison of *f* with Re for α=40 (converging diverging channel)

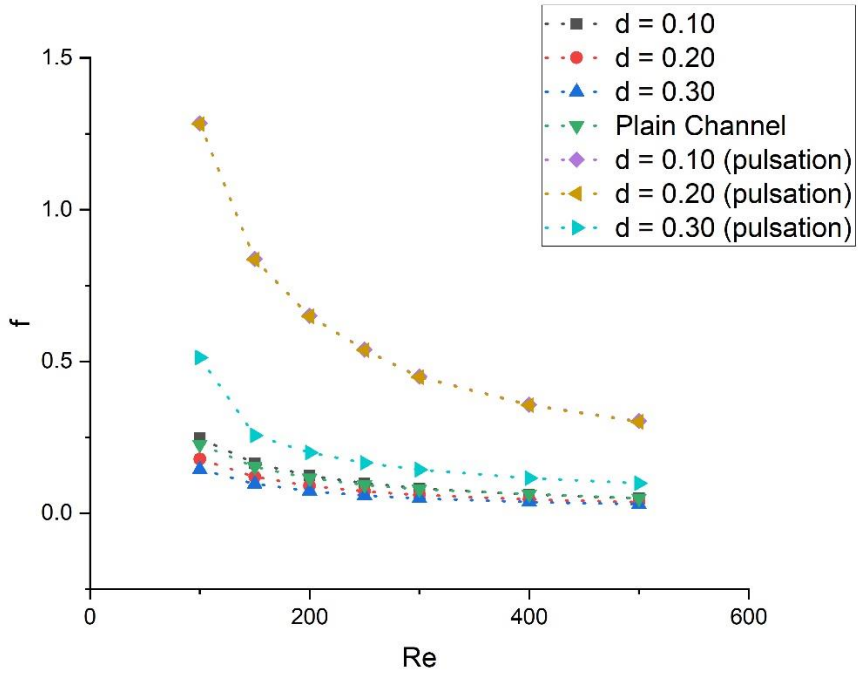

Figure 4.18(c). Comparison of *f* with Re for α=50 (converging diverging channel)

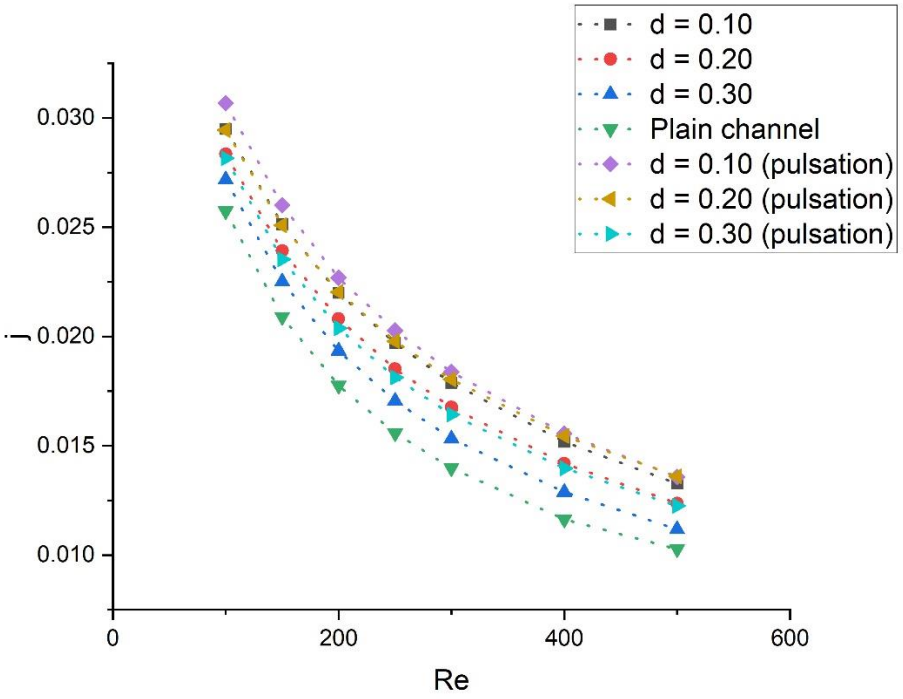

Figure 4.19(a). Comparison of j with Re for α=30 (converging diverging channel)

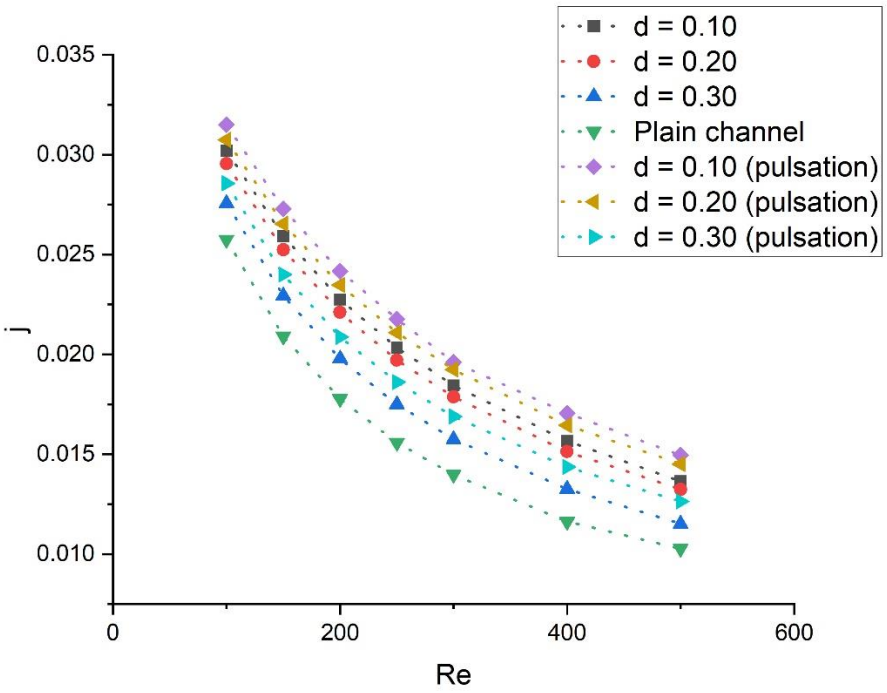

Figure 4.19(b). Comparison of j with Re for α=40 (converging diverging channel)

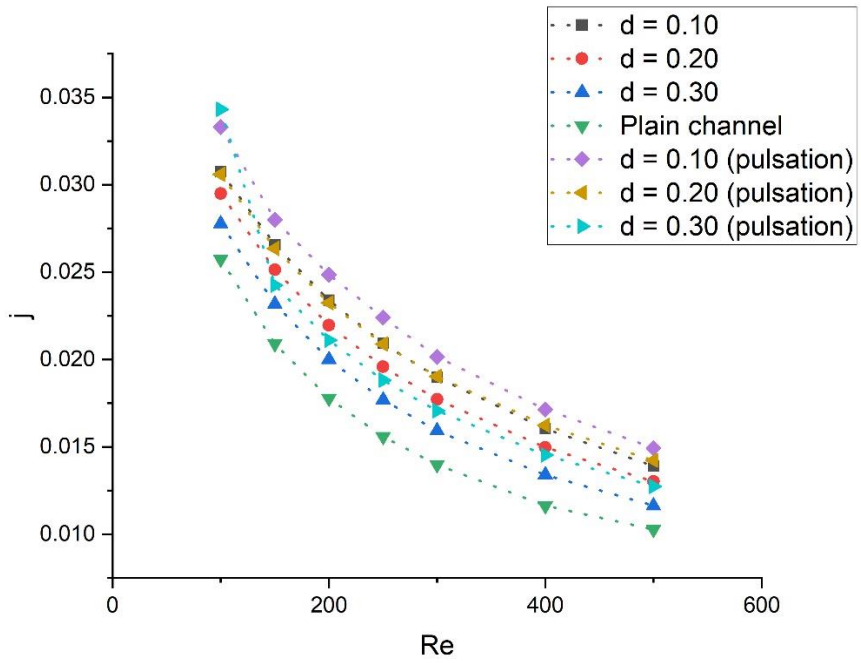

Figure 4.19(c). Comparison of j with Re for α=50 (converging diverging channel)

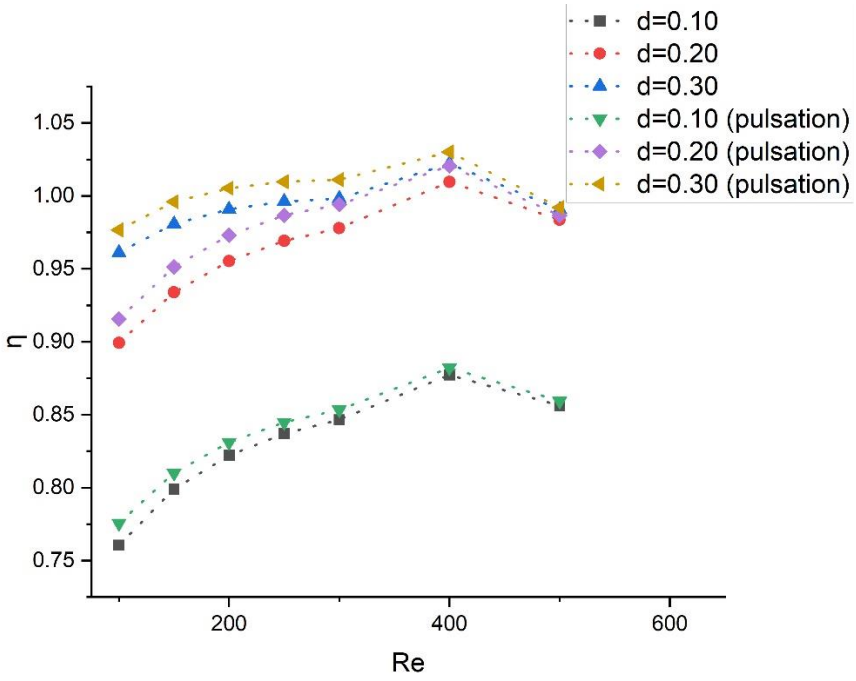

Figure 4.20(a). Variation of η with Re for α=30 (converging diverging channel)

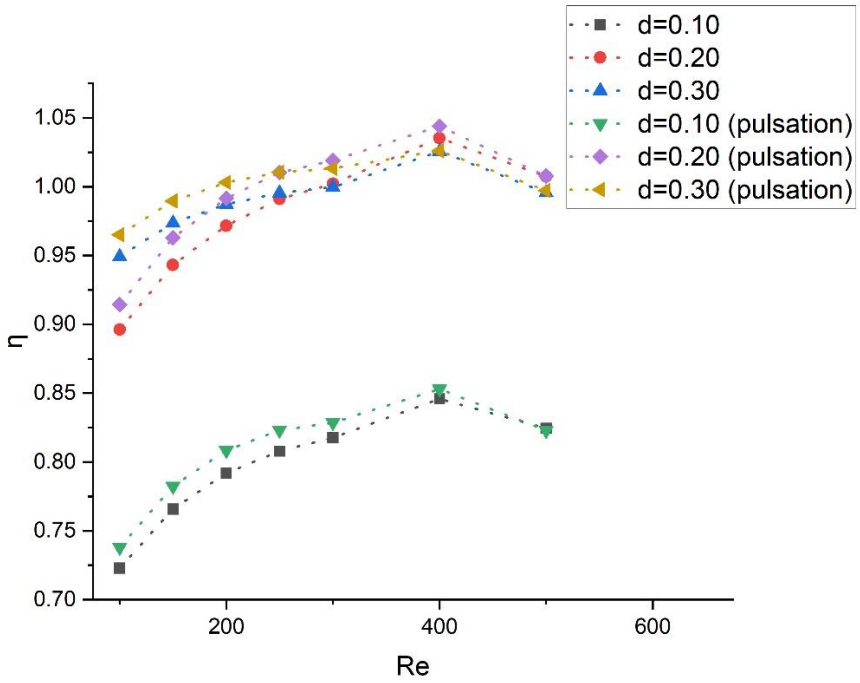

Figure 4.20(b). Variation of η with Re for α=40 (converging diverging channel)

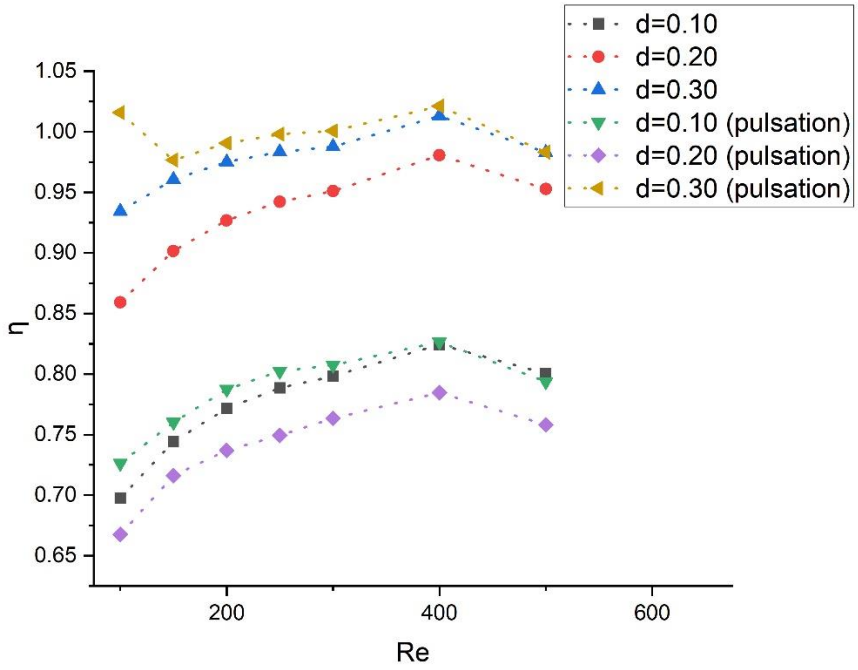

Figure 4.20(c). Variation of η with Re for α=50 (converging diverging channel)

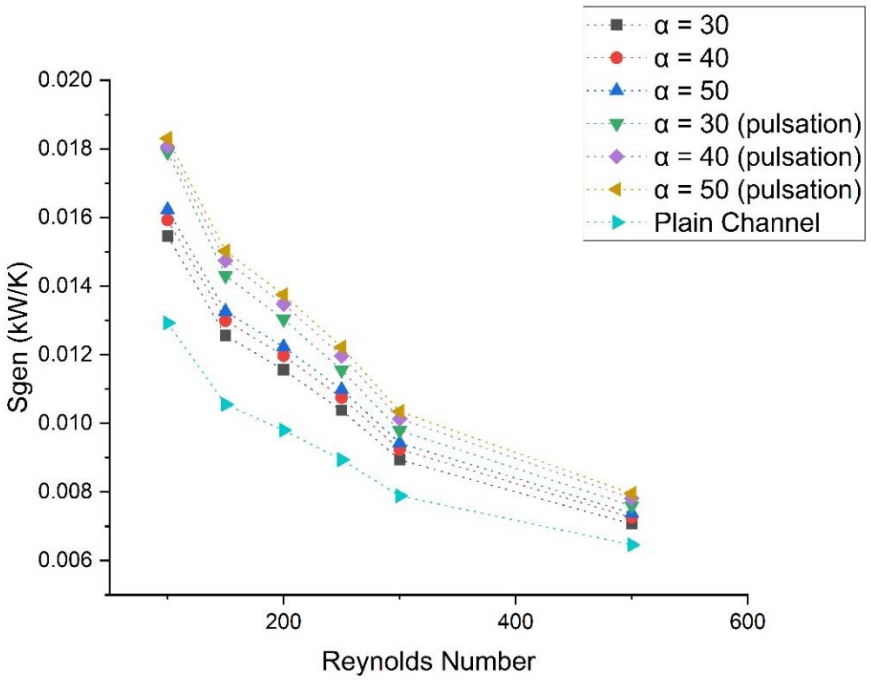

Figure 4.21. Variation of S_{gen} with Re for d=0.30 (converging diverging channel)

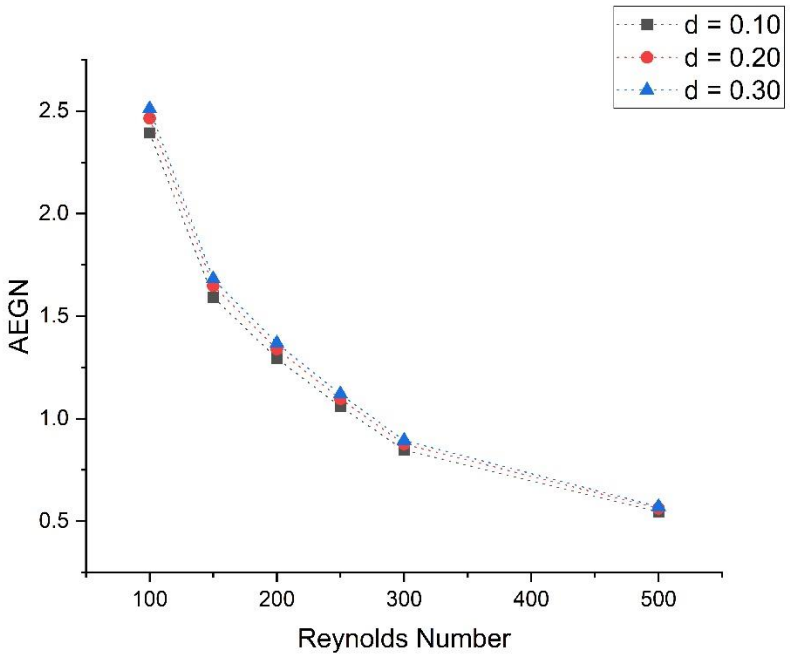

Figure 4.22. Variation of AEGN\with Re for α=50 (converging diverging channel)

Figure 4.21 demonstrates the character of entropy generation against Reynolds number for the suggested geometry for both steady and transient case. The figure indicates that with the Reynolds number (Re) increases, there is a noticeable decline in entropy generation, which is preferable as far as heat transfer augmentation is concerned. To compare the thermal performance of the converging diverging micro-channel with inlet flow pulsation to the steady one, a dimensionless quantity, composed of the ratio of entropy generation of the modified geometry to the entropy generation developed by the reference one i.e. the plain channel, taken into consideration. The quantity is termed as Augmentation Entropy Generation Number (AEGN). Figure 4.22 unfolds the variation of this quantity with increase in Reynolds number. As a matter of fact, to achieve greater heat transfer result, reduced value of thermal entropy generation is the objective. Therefore, a lower value of augmented entropy generation, less than one, would indicate a more favourable outcome. The figure illustrates that the present geometry with pulsating flow applied at inlet, exhibits Augmented Entropy Generation Number values below unity above Re value of 300 which is favourable. Whereas,

below 300, it is providing values greater than one. This illustrates that at low Reynolds number the inlet flow pulsation increases the entropy generation which is not favourable in terms of heat transfer augmentation.

4.5 Closure

Present investigation assesses the effect of contracted flow passage over heat transfer in two dimensional micro-channels. Computational simulation of Navier-Stokes equation was performed for this purpose. Also, a sinusoidal velocity component was implemented on the inlet velocity to achieve augmented thermal performance. The results of modified geometry were compared with the case of inlet flow pulsation with modified geometry, to prescribe optimum result. Both suddenly contracted channel (stepped micro-channel) and gradually contracted channel (converging diverging micro-channel) with different contraction ratio was analyzed for better result. The computation was performed for laminar flow regime with Reynolds number ranging 100 – 500. Constant temperature condition is maintained at the channel walls as thermal boundary condition. To validate the present scheme, previous well established results were compared with the current set of results. Dimensionless Nusselt number and friction factor were measured to assess the augmented heat transfer. The Performance Enhancement Criterion that heat transfer as well as pressure drop, was also examined to evaluate the performance of the present geometry. The proposed geometry showed better thermal result compared to plain channel. Optimum contraction ratio revealing the best overall thermal performance, was also prescribed.

CHAPTER FIVE

ENHANCEMENT OF HEAT TRANSFER WITH INLET FLOW PULSATION THROUGH TWISTED CHANNELS

5.1 Introduction

In the preceding section, some modified three dimensional geometries were analyzed to achieve augmented heat transfer performance. The channels were twisted (employing different twist combination) about its own axis to facilitate increased mixing of the fluid to generate swirl. Although these geometries brought flow disruption and enhanced fluid mixing resulting improved Nusselt number result, they also produced higher pressure drop penalty. As a result, no significant improvement in PEC was received. The results indicated that this kind of geometry modification may not be sufficient alone to overcome the limitations of laminar flow and thermal boundary layer development inside such tortuous flow passage.

To get through this challenge, along with twisted geometry, a sinusoidal pulsating flow also administered at the channel inlet and its influence on the overall thermal performance of the heat sink was assessed numerically in this chapter. Periodically pulsating inlet velocity can disrupt the boundary layer and promote fluid mixing as well as convective transport. The flow path was also made sinusoidally wavy and twisted about its own flow axis. A detailed investigation on the effect of pulsating flow on the thermal performance of the proposed Micro-Channel Heat Exchanger (MCHS) is presented in this section. The motive behind this investigation was to estimate the overall thermal performance of the MCHS and to determine whether such unsteady flow conditions can be proved to be a more effective strategy for producing enhanced heat transfer while maintaining the pressure drop within acceptable limits.

5.2 Problem Statement

In present section, analysis is performed with micro-channels where the channel cross section traces a twisted sinusoidal curve around a straight line, referred to as “main axis”. The specialty of the present contribution is that both Active as well as passive techniques are

applied in a combined manner. This means that the passage geometry is modified by twisting the channel

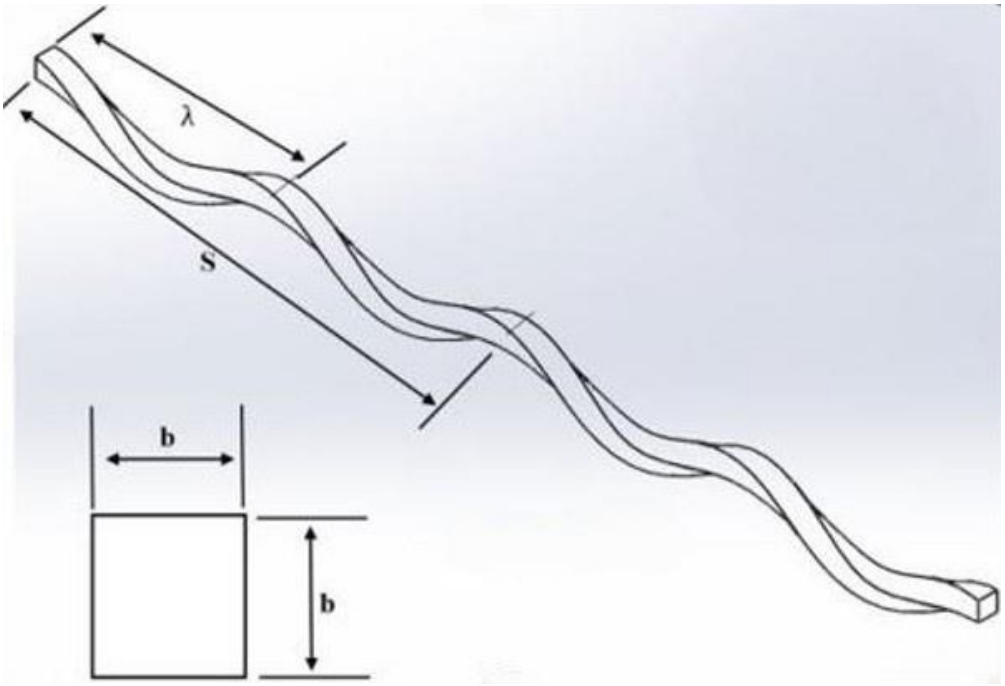

Figure 5.1(a) Schematic diagram of clockwise twisted channel

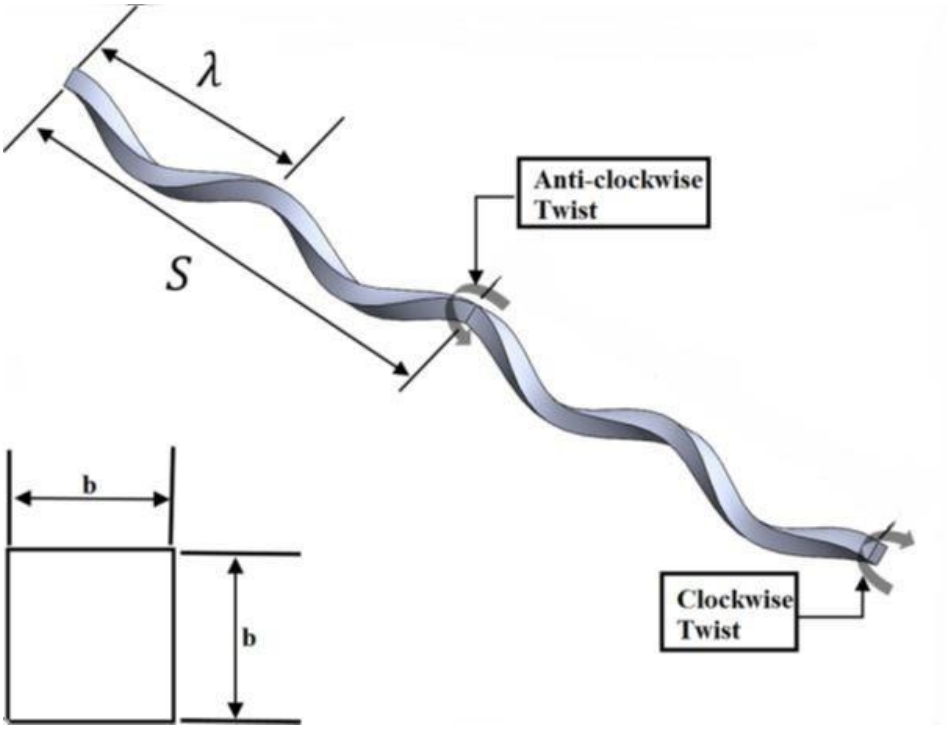

Figure 5.1(b) Schematic diagram of clockwise-anticlockwise twisted channel

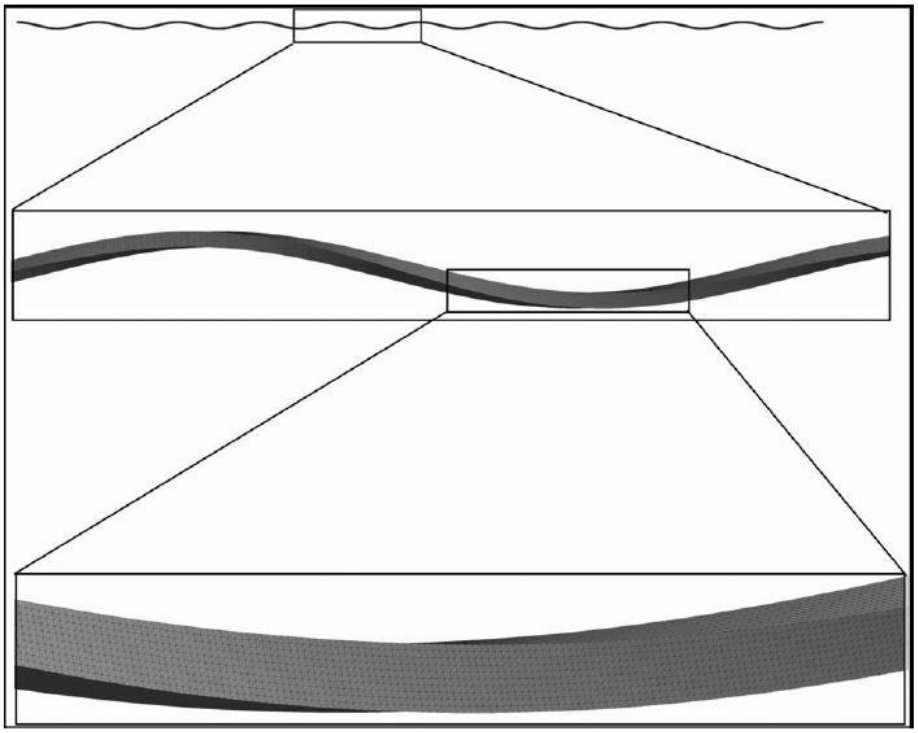

Figure 5.2(a) Mesh of the clockwise twisted channel

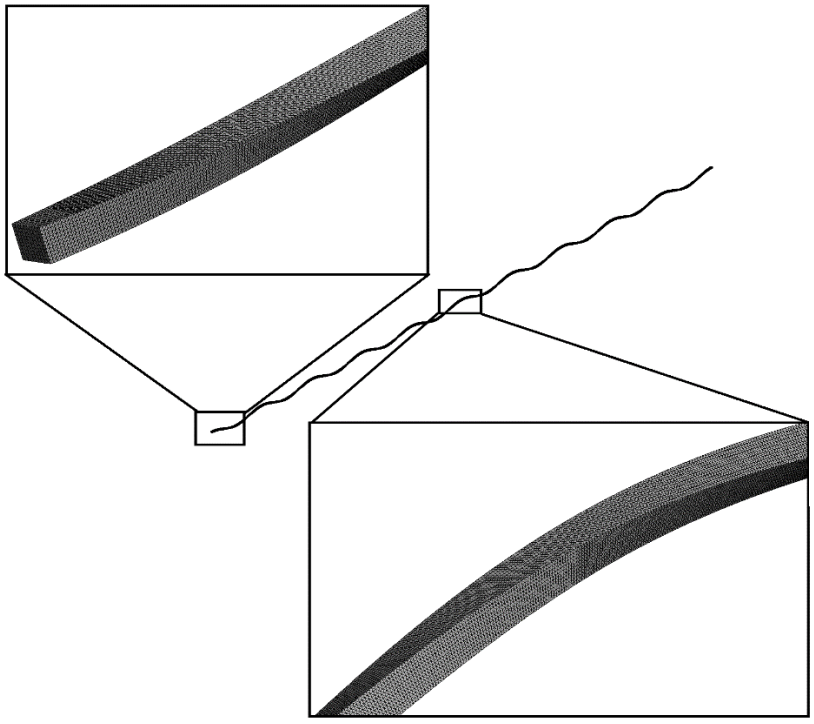

Figure 5.2(b) Mesh of the clockwise-anticlockwise twisted channel

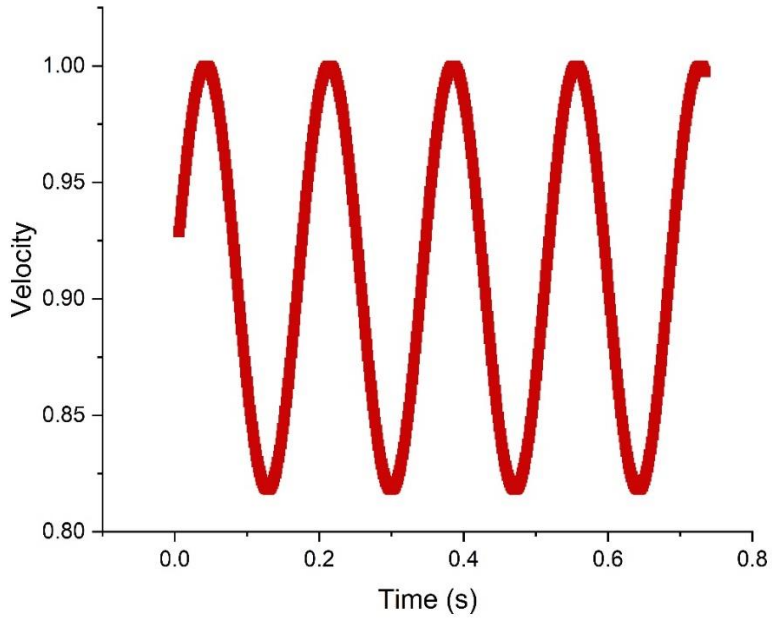

Figure 5.3 Periodical local axial non-dimensional velocity

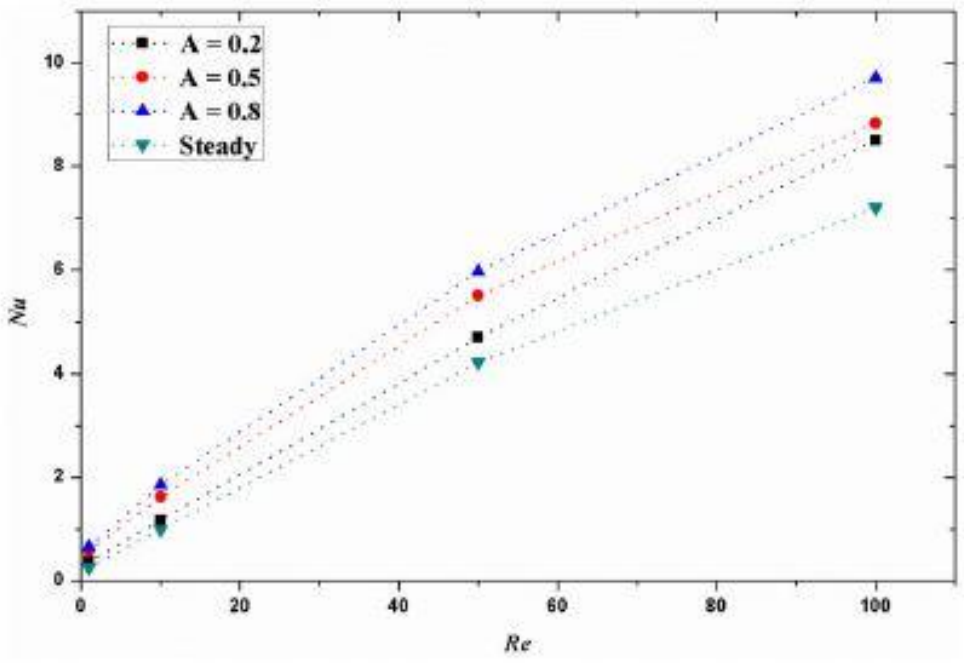

Figure 5.4 Comparison of time averaged *Nu* with Re for different amplitudes at *St* = 10.

to pertain out of plane mixing, while imposing pulsations onto the flow rate. Thus, twisted channels with fully three-dimensional geometries for unsteady flow, i.e. for pulsating flow rate, are computationally investigated in the present study. The focus of the study has been to achieve a heat transfer enhancement by a combined application of the both measures. Two separate channels with different twist pattern i.e., clockwise twisted for the first channel, while clockwise twist combined with anticlockwise twist for the second channel was incorporated. The first half length (starting from inlet) of the second channel was made clockwise twisted while the remaining half was made anticlockwise twisted. Figure 5.1(a) and 5.1(b) depicts the schematic diagram of these two micro-channels. Denoting the space coordinate along the main axis by x, the offset of the centre of the channel cross section from the main axis is given as –

$$\varepsilon = A_w \cos\left(\frac{2\pi}{\lambda}x\right) \tag{5.1}$$

For both the channels, cross section of the channel is square-shaped with 0.50 mm breadth. While the wave amplitude (A_w) was fixed at 1 mm, the total length was 25 cm. The pitch of the channel (S) was 5 cm with wavelength (λ) at 2.5 cm for both the cases.

For analysis purpose, we consider unsteady, laminar, incompressible flow with constant material properties. As typical application of such channels does not include high temperature, radiation is neglected and fluid properties was assumed to be temperature invariant.

For the microchannel walls, Dirichlet type boundary condition is used. No slip condition on the walls implies zero velocity and a fixed temperature was prescribed imposing isothermal conditions on boundary. For the inlet velocity, a sinusoidal time variation is assumed in the form

$$u_{in} = u_m + A\sin(2\pi f_r t)\} \tag{5.2}$$

In the above equation, u_{in} is the bulk inlet velocity, which varies around its time-averaged value (u_m) sinusoidally with an amplitude of A and a frequency of f_r. The latter is related to Strouhal number (St) through the relationship $St = f_r D_h / u_m$. It may be mentioned here that similar inlet condition is reported in literature e.g. in Nandi and Chattopadhyay (2013). As the outlet of the domain is free exit, pressure outlet boundary condition i.e. a zero gauge pressure was prescribed. The Reynolds number of flow is defined by $Re = \rho u_m D_h / \mu$.

A finite volume based solver, ANSYS Fluent 19.2 was used for obtaining the solution of the equation set. Simulations were performed for different Reynolds numbers in the range 1-100, for different pulsation frequencies and amplitudes.

Because of the complex geometry, it was necessary to deploy an unstructured grid. However, the mesh was generated with uniform structure density distribution. A rigorous grid independence test regime was ensured as illustrated in Table 1 and Table 2. Three major parameters, namely, the Nu, f and performance parameter (η) were considered for evaluating grid independence. Table 1 shows that the grid with 872,250 nodes deliver results, which can be deemed sufficient, as further refinement does not change the output significantly. Figure 6.2(a) and figure 6.2(b) represents a close view of the mesh for both the channels.

Solutions were obtained using SIMPLE algorithm (1977). For momentum equations, QUICK scheme and for energy equation MUSCL scheme was chosen following Nandi and Chattopadhyay (2013). For convergence, residual values at each time steps were ensured to be below 10^{-5} and 10^{-8} for the momentum and energy equations, respectively.

5.3 Grid Independence and Validation

Because of the complex geometry, it was necessary to deploy unstructured grid. However, mesh was generated with uniform structure density distribution. A rigorous grid independence

Table 5.1 Grid independence study (*St* = 10, *A* = 0.8 and *Re* = 10)

	Total number of grid nodes	***Nu***	***f***	***η***
Grid 1	872,250	1.8533	0.1706	1.6320
Grid 2	932,658	1.8537	0.1706	1.6321
Grid 3	995,326	1.8539	0.1707	1.6321

test regime was ensured as presented in table 5.1 and table 5.2 for these two geometries. For the first case (i.e. wavy twisted micro-channel) three major parameters, namely- Nusselt number, friction factor and performance parameter were considered for evaluating grid independence. Table 1 shows a grid with 8,72,250 nodes deliver results, which can be deemed sufficient, as further refinement does not change the output significantly. Whereas, for the second geometry (wavy clockwise and anticlockwise geometry) Nusselt number, friction factor, performance enhancement criteria and outlet temperature were considered for the purpose. Table 2 illustrates the GIS results and it is evident from the table that 8,99,852 nodes served the purpose

Table 5.2. Grid independence study (St = 10, A = 0.8 and Re = 10)

	Total number of grid nodes	**Nu**	**f**	**η**	**Outlet Temperature (K)**
Grid 1	899,852	1.8531	0.17055	1.641	325.5680
Grid 2	963,789	1.8537	0.17061	1.639	325.5683
Grid 3	982,369	1.8538	0.17081	1.641	325.5689
Grid 4	1,109,369	1.8539	0.17085	1.642	325.5693
Grid 5	1,153,633	1.8541	0.17089	1.645	325.5697
Grid 6	1,213,332	1.8543	0.17092	1.647	325.5699

5.4 Result and Discussion

The dimensionless frequency (i.e Strouhal number) and pulsation amplitude were kept within the range of $1 \leq St \leq 10$ and $0.1 < A < 1$ for the current study which corresponds to typical microchannel applications. Due to addition of periodic pulsation at inlet, the instantaneous

axial velocity in the middle of the microchannel should show periodic change in nature. The observed velocity signal in Figure 6.3 confirms that.

Figure 6.4 and Figure 6.5 depict the variation of time averaged *Nu* with *Re*. It is evident from the Figure 4 that lower values of *Re* and inlet pulsation amplitude, the *Nu* yields almost same result as of the steady one. This can be attributed to weak swirl generation inside the flow, at low *Re*. At low Reynolds number, the viscous force subjugates over the effect of the wavy and twisted nature of the channel. Also, at low amplitude of pulsation, the flow cannot be disrupted. With increase in *Re* and amplitude of pulsation, the Figure 4 and Figure 5 display an

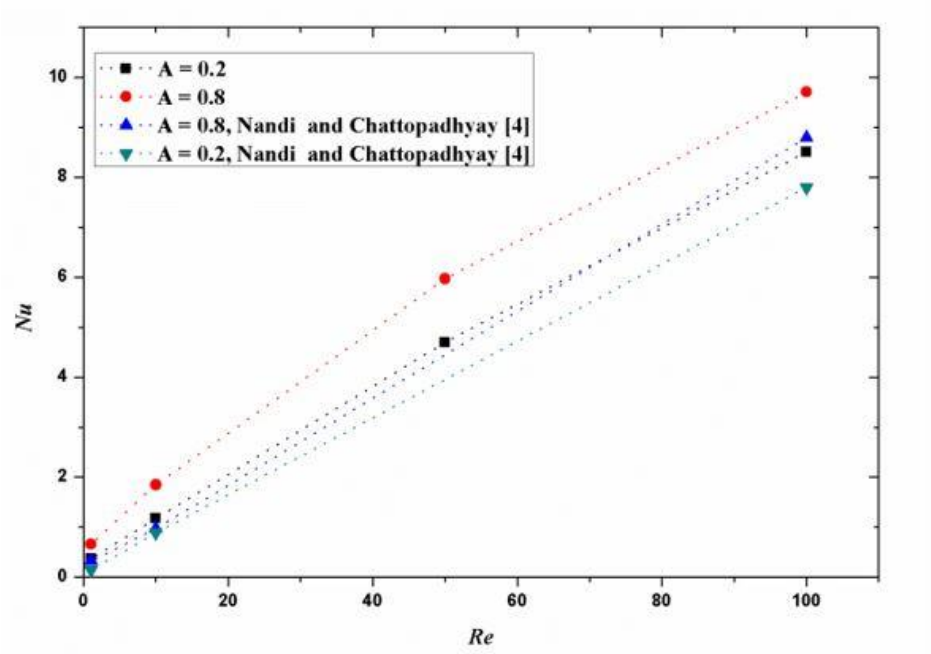

Figure 5.5 Comparison of time averaged *Nu* as a function of *Re* with the results of Nandi and Chattopadhyay (non-twisted wavy microchannel), at *St* = 10.

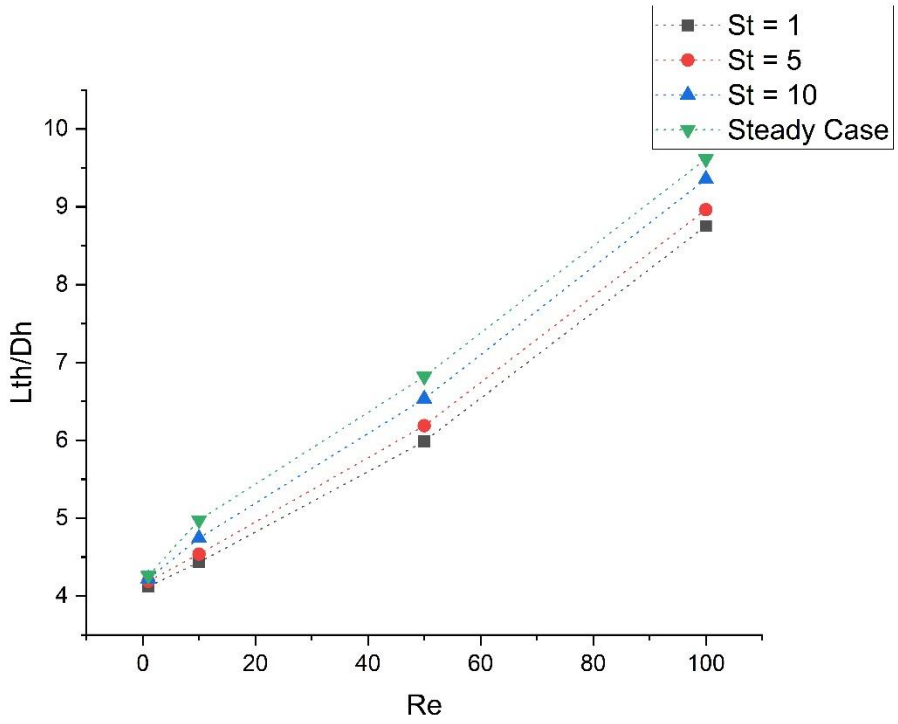

Figure 5.6 Comparison of thermal development length with varying *Re* for different *St* at *A* = 0.2

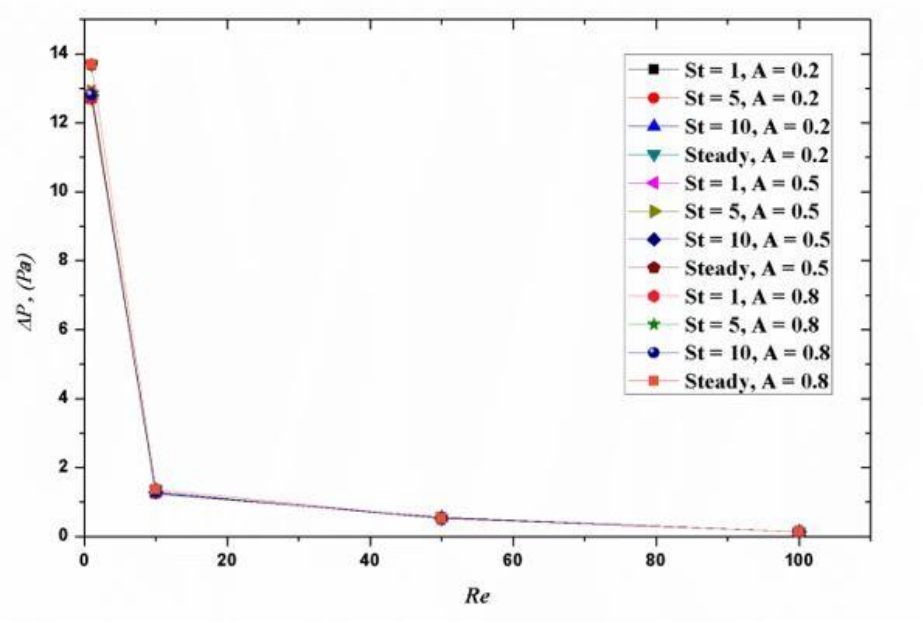

Figure 5.7 Variation of Δp with *Re* for different amplitude and *St*.

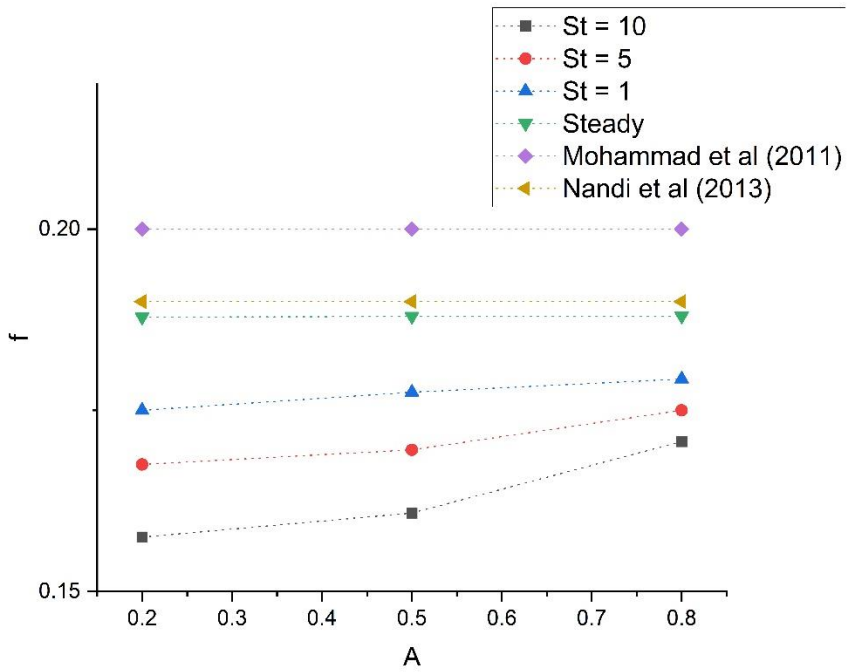

Figure 5.8 Variation of friction factor as a function of *A* for different *St*, at *Re*=10. Steady-state results of Mohammad et al. [2011] and Nandi and Chattopadhyay [2013] for *Re*=10 are also shown for comparison.

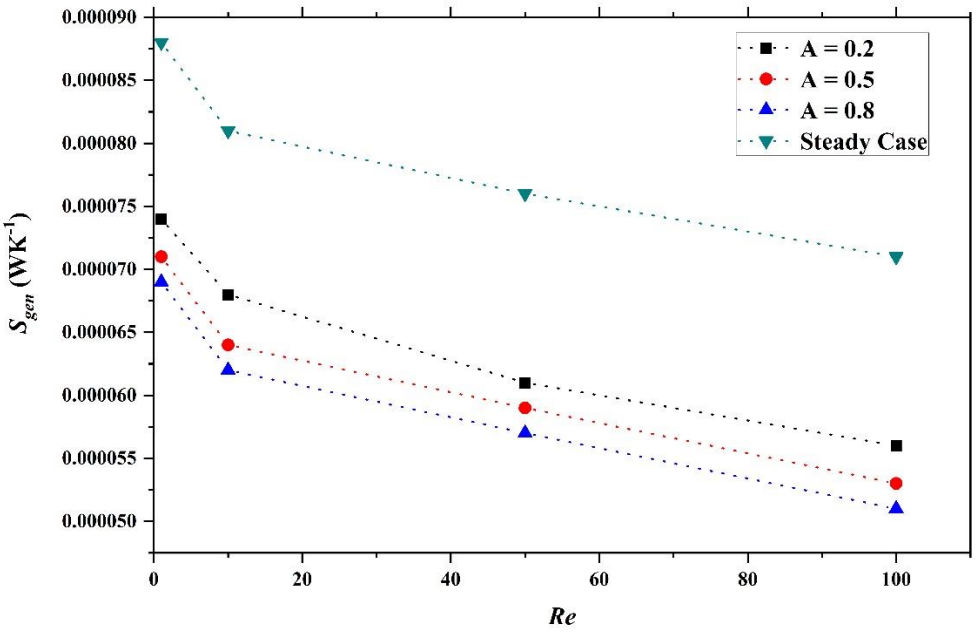

Figure 5.9(a) Variation of S_{gen} with *Re* for pulsating flow with different amplitudes at *St* = 10 and for steady-state flow

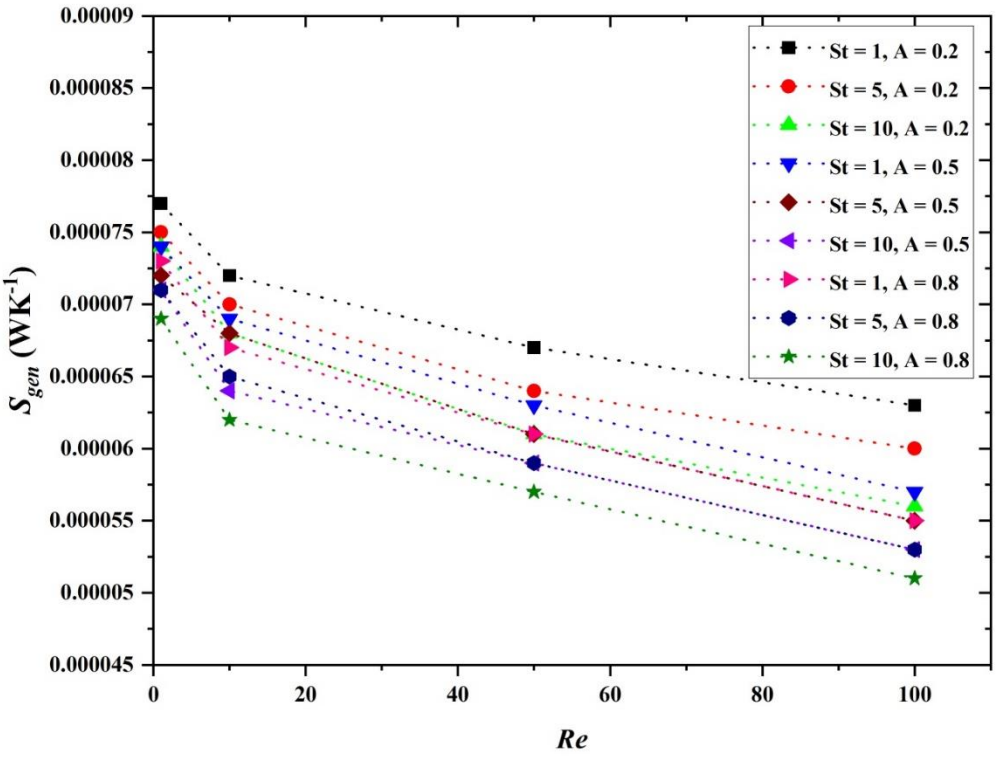

Figure 5.9(b) variation of S_{gen} with *Re* for different values of amplitude and St

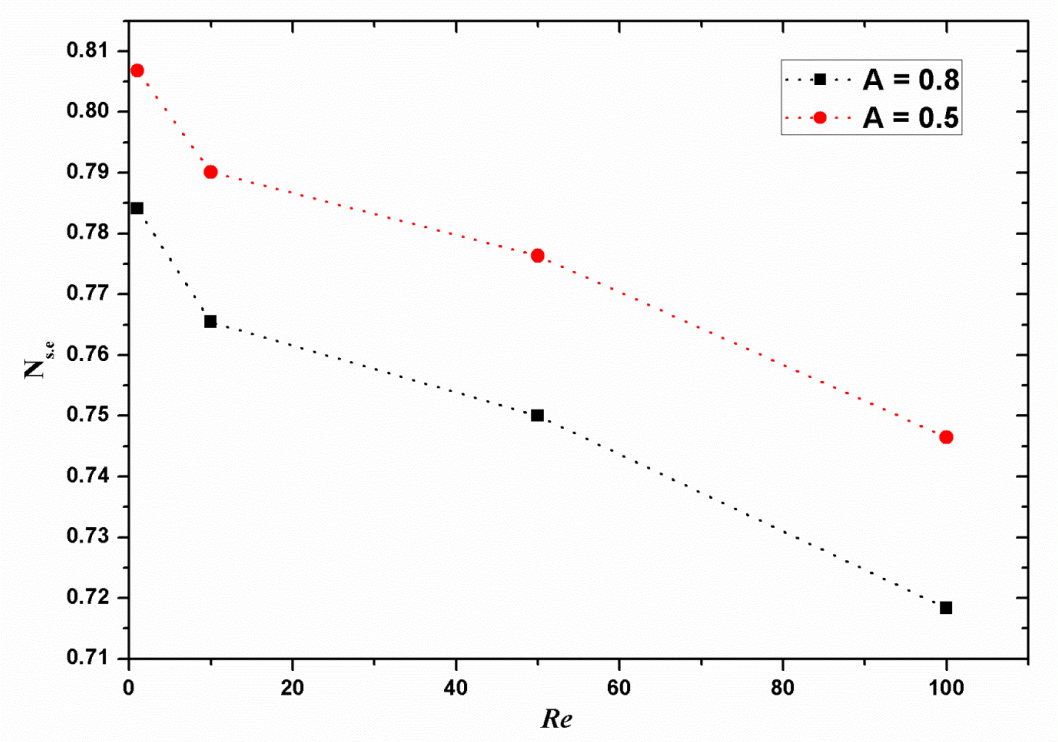

Figure 5.9(c) Variation of AEGN with *Re* for different amplitudes at *St* = 10.

accountable rise in the Nusselt number result as compared to that of the steady case. At higher *Re*, the flow pulsation seizes over the viscous force. Subsequently, better mixing of fluid occurs and the modified contour of the channel geometry provides generation of recirculation zones. So, one can interpret that at higher *Re* and amplitude of the pulsation of flow at inlet, the current model can provide better HT result. The current data is compared with previous well-established work of Nandi and Chattopadhyay (2013) in Figure 6.5. The microchannel described in the earlier work involved a two-dimensional sinusoidal wavy channel while the present geometry is twisted and hence the flow encounters a more tortuous path here. As a consequence, larger enhancement of heat transfer is noted in this case – about 100% higher at low *Re* and 10% higher at Re of 100. Overall, the proposed geometry shows a significant gain in performance vis-à-vis a simple wavy channel as presented in Nandi and Chattopadhyay (2013).

Thermal development length (L_{th}) is a parameter of importance in the field of heat transfer augmentation. This was inspected for a range of *St* and *Re*. Figure 6.6 establishes the time-averaged dimensionless thermal development length (L_{th}/D_h) as a function of *Re*. With increased frequency, the development length is found to grow. The steady case however shows highest development length. This can be caused due to the flow pulsation employed at inlet, which incorporates better mixing of the fluid situated near the wall with the core fluid. For a straight duct, the development length is given by L_{th}/D_h = 0. 05Re.Pr [34], which leads to much lower values compared to the present configuration. As an example, at *Re*=100 and *Pr* = 0.7, the straight duct has a development length of 3.5 [34]. But for the same parameters, L_{th} varies between 8.2 and 9.3 for the proposed geometry. This is expected to be due to tortuous passage of fluid flow.

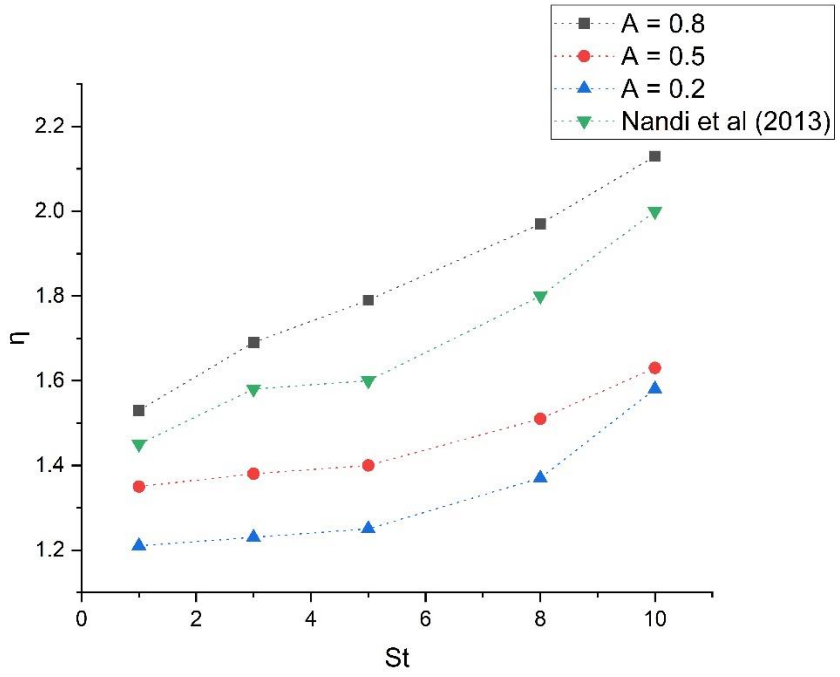

Figure 5.10. (a) Variation of η with *St* for different amplitudes: present results and the results of Nandi and Chattopadhyay (2013) (only *A*= 0.8) at *Re* = 10

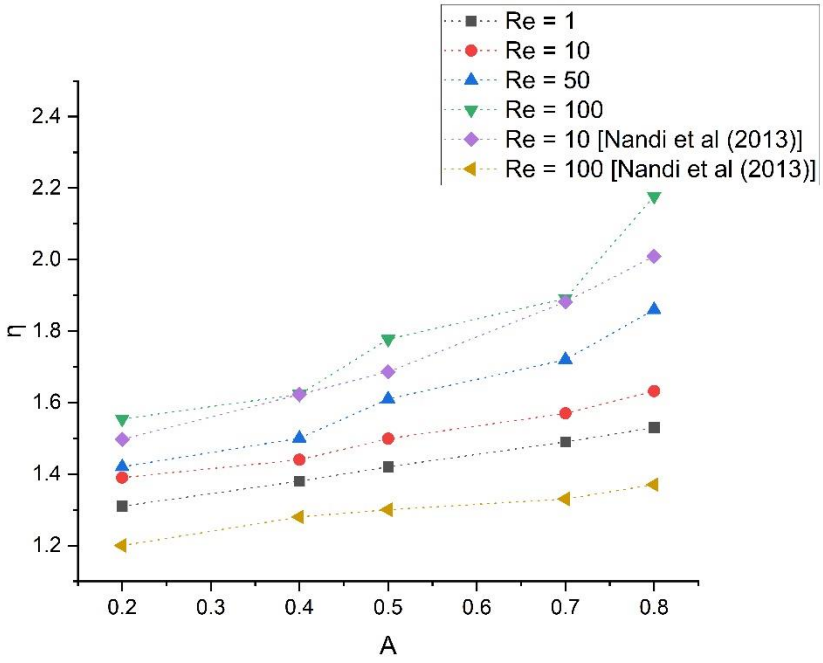

Figure 5.10(b) variation of η with amplitude for different *Re*: present results and the results of Nandi and Chattopadhyay (2013) (for *Re* = 100 and *Re* = 10) at *St* = 10

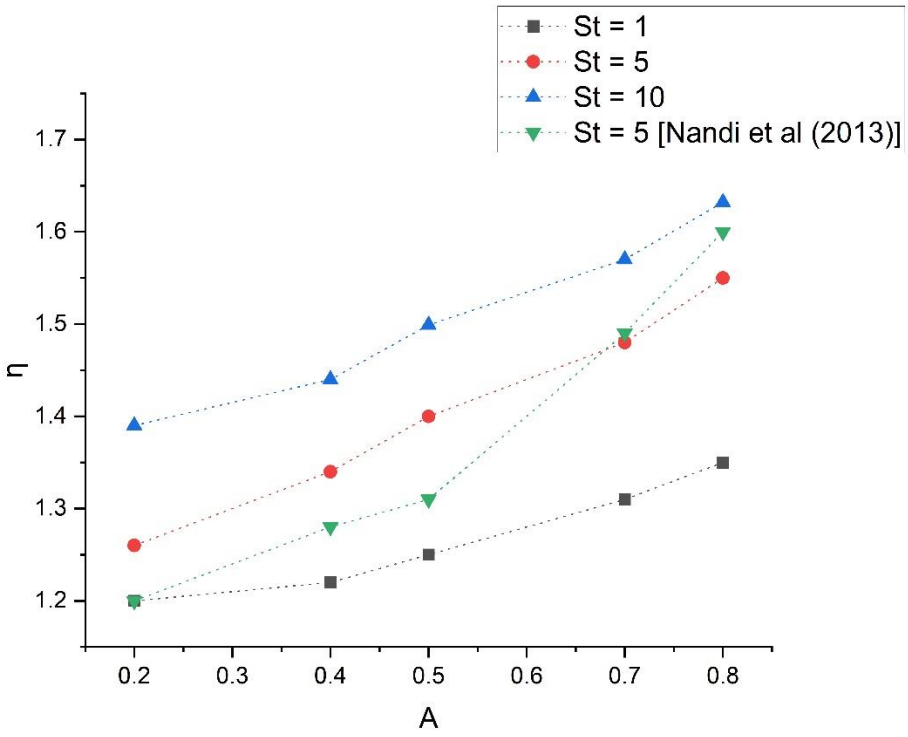

Figure 5.10(c) comparison of η with amplitude at different St, with Nandi and Chattopadhyay (2013) (for St = 5 and St = 10) at constant Re = 10.

Pressure drop is the penalty that has to be paid at the cost of enhanced heat transfer in enhancing techniques by employing wavy and twisted channel geometry. The narrow and fluctuating flow passage prevents the fluid mixing specially at low Reynolds number attributing high pressure drop. Figure 6.7 shows the fluctuation of the time-averaged Δp as a function of the amplitude at different frequencies. In Figure 8, it can clearly be seen that the time-averaged f of the steady-state case is larger compared to those of the cases with pulsations for the present geometry. It is depicted that with increase in frequency of the inlet flow pulsation (represented by Strouhal number), the friction factor decreases. However, with increase in the amplitude of the flow pulsation, an increasing trend for 'f' is observed, which can be due to the larger quantity of fluid incorporated with higher amplitude. The dependence of 'f' on A is observed to be more pronounced for higher values of St.

It is palpable from the figure that the present work is providing better result in terms of friction factor than the other published results for configurations [Nandi and Chattopadhyay (2013), Mohammad *et al* (2011)] with some similarity to the present one. The comparison to those results [Nandi and Chattopadhyay (2013), Mohammad *et al* (2011)] are presented for steady-state flow in Figure 6.8. The non-twisted two-dimensional wavy channel of Nandi and Chattopadhyay (2013) delivers slightly higher values compared to the present geometry, whereas the non-twisted three-dimensional wavy channel of Mohammad *et al.* (2011) exhibits even higher values. This comparison indicates the importance of the twisted geometry.

Figure 6.9(a) elaborates the variation of time-averaged thermal entropy generation, for TSWMC. The thermal entropy generation depends upon temperatures only. From the figure, it is clear that the thermal performance of a MCHE can be enhanced by employing sinusoidal pulsation at the inlet, thus minimizing the entropy generation. It can also be noted that with increase in pulsation amplitude the entropy generation result yields better performance. Figure 6.9(b) portrays the variation of time-averaged thermal entropy generation with *Re* at different amplitude and Strouhal number. It can be easily discerned from the figure that with increase in *Re*, the entropy generation is showing a downward trend which is desirable. The figure also illustrates that the case with maximum Strouhal number and pulsation amplitude is showing the best result. To compare the performance of the TSWMC with plain channel, a dimensionless quantity named augmentation entropy generation number is used. It may be defined as the ratio of total entropy generation furnished by TSWMC to the total entropy generation by the plain channel. Figure 6.9(c) depicts the comparison of augmentation entropy generation number with *Re*. The objective is to decrease the thermal entropy generation, hence, a augmentation entropy generation value less than unity would suggest better result. The figure displays that as an effect of inlet flow pulsation, the present case

always showing values less than 1. It is also noteworthy that at the highest amplitude (i.e. 0.8) the channel is showing best result.

To assess the effect of inlet flow pulsation, a parameter called thermal performance enhancement factor (η), is used in the current study, as already mentioned before. By definition, η is a measure for the improvement of the heat transfer performance by the flow pulsations compared to the steady-state flow. In Figure 6.10(a), the time-averaged η is shown as a function of *St* at different Amplitude (*A*) and constant Reynolds number (*Re* = 10). The figure shows that the present scheme offers η values larger than unity for all cases, showing that flow pulsations have a beneficial effect for all considered cases. One can also see that η increases with increasing *St* and increasing *A*. For comparison, the pulsating flow results in the non-twisted wavy channel of Nandi and Chattopadhyay (2013) are also included in the figure, for *A*=0.8. These values are smaller compared to the present results for *A*=0.8, indicating again, the important role of the twisted geometry.

In Figure 6.10(b), the time-averaged η is shown as a function of amplitude (*A*) at different *Re* and constant Strouhal number (*St* = 10). The results are also compared with the previous work of Nandi and Chattopadhyay (2013), for non-twisted wavy channel. Also from this perspective, one can see that pulsating flow always leads to a thermal performance improvement ($\eta > 1$). This increases with increasing *A* and *Re*. Compared for the same *Re*, the present results exhibit higher η values compared to those of Nandi and Chattopdhyay (2013), underlining again the important role of the twisted geometry.

Figure 6.10(c), shows η as a function of amplitude (*A*) at different St and constant Re (Re= 10). It is also obvious from the figure that at amplitude 0.80, the present setup is providing better result than the previous well-established work of Nandi and Chattopadhyay (2013). At St = 10, and amplitude of 0.8, it is providing a η value even greater than 2.0. In general, increased amplitude and frequency of pulsation at inlet can provide improved thermal performance. This can be attributed to the fact that the superimposing of the

pulsation at inlet with the main flow incorporates the required instability in the flow to enhance proper mixing of fluid. Also, at high amplitude (A) of pulsation the wavy and twisted nature of the channel geometry also contributes to the mixing of fluid and recirculation zones generated. Much more decrease in hydrodynamic, as well as thermal boundary layer thickness, occurs. Hence, the present geometry shows even a much more thermal enhancement.

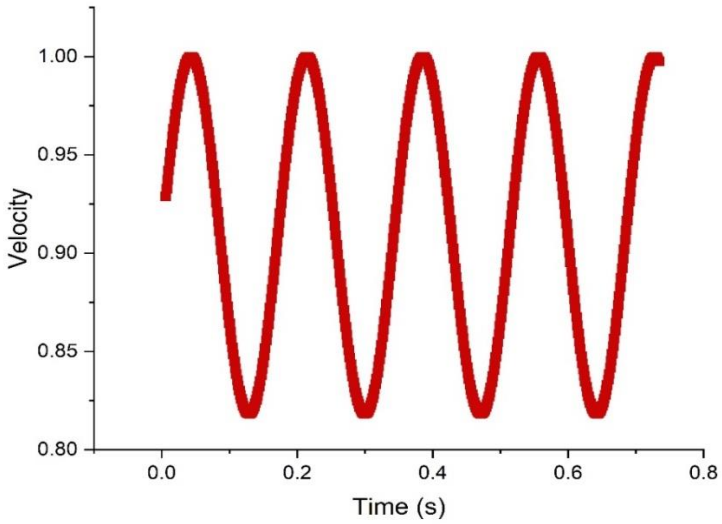

Figure 5.11 Periodical local axial non-dimensional velocity

Expecting further improvement, a second micro-channel with same features was also evaluated. The second channel was made clockwise twisted for half of the length and the remaining half-length was made anticlockwise twisted. The non-dimensional frequency (i.e. Strouhal number, St) and amplitude of pulsation (A) were kept within the range of $1 \leq St \leq 10$ and $0.1 < A \leq 0.8$ for the current investigation consistent with the prior works [Nandi & Chattopadhyay (2013)]. Due to addition of periodic pulsation at inlet, the immediate axial velocity in the middle portion (at 12.5 cm from the entrance along downstream) of the MC should exhibit periodic change in nature. The observed velocity signal in Figure 5.11 confirms that flow field remains periodic.

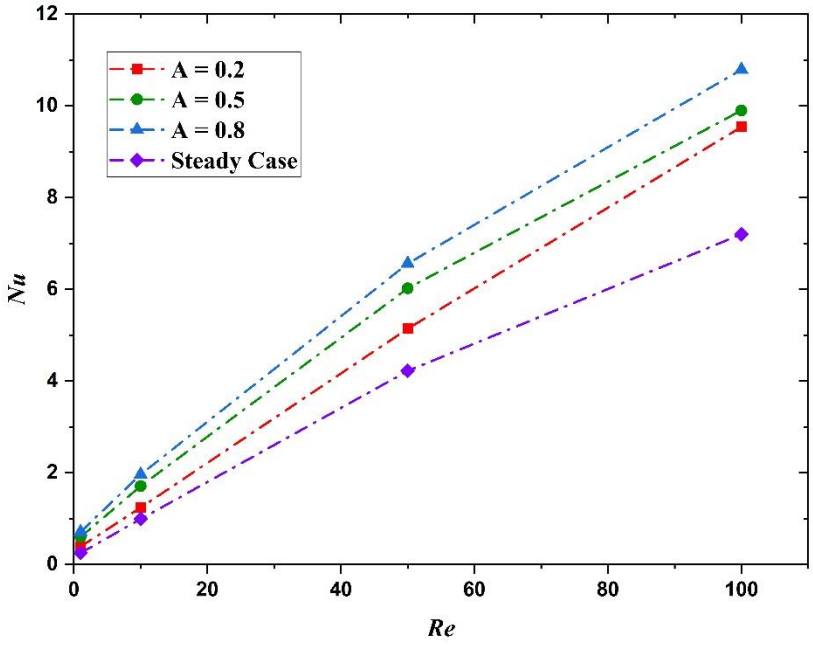

Figure 5.12 Comparison of time average Nusselt number with Reynolds number for different amplitudes at St = 10

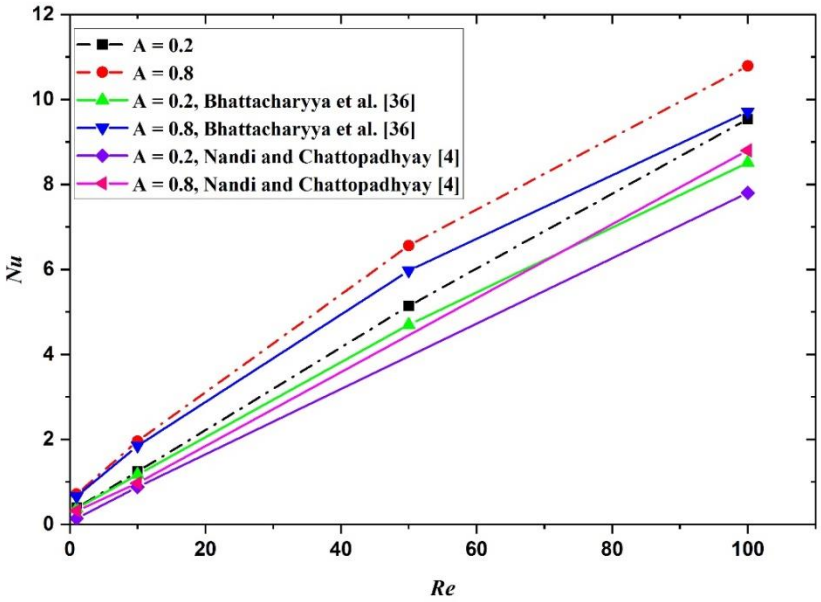

Figure 5.13 Comparison of time average Nusselt number with Reynolds number with previous study at constant St = 10.

Figure 5.12 and Figure 5.13 portrays the variation of time average Nusselt number with Reynolds number. It is evident from the Figure 4 that for low values of Reynolds number and inlet pulsation amplitude, the Nusselt number yields almost the same result as of the steady one. This can be attributed to weak swirl generation inside the flow, at low Reynolds number. At low Reynolds number, the viscous force subjugates over the effect of the wavy and twisted nature of the channel. With increase in Reynolds number and amplitude of pulsation, the Figure 5.12 and Figure 5.13 display an accountable rise in the Nusselt number result as compared to that of the steady case. At higher Reynolds number, the flow pulsation seizes over the viscous force. Subsequently, better mixing of fluid occurs and the modified contour of the channel geometry provides generation of recirculation zones. So, one can interpret that at higher Reynolds number and amplitude of the pulsation of flow at inlet, the current model can provide better HT result. The present data is compared with previous work of Nandi and Chattopadhyay (2013) and Bhattacharyya et al. (2019) on wavy microchannel with pulsating inlet in Figure 5.13 and an increase in Nusselt number by around 33% and 19% respectively are obtained. It is also clear that the novel geometry introduced by reversing the turn of the tube in the middle provides higher heat transfer over the case of the unidirectional twisted channel.

The thermal development length describes the distance for incoming flow in a pipe to form a fully developed temperature profile. Thermal development length is a parameter of importance in judging the effectiveness of mixing between fluid layers. This was studied for a range of Reynolds number and Strouhal number. Figure 5.14 establishes the thermal development length as a function of Reynolds number. The development length reduces when the flow field is under pulsating inlet condition compared to the case of steady laminar flow. The reason can be attributed to the increased interaction between fluid layers due to pulsations. With increased frequency, there is more mixing between fluid layers leading to shorter development length.

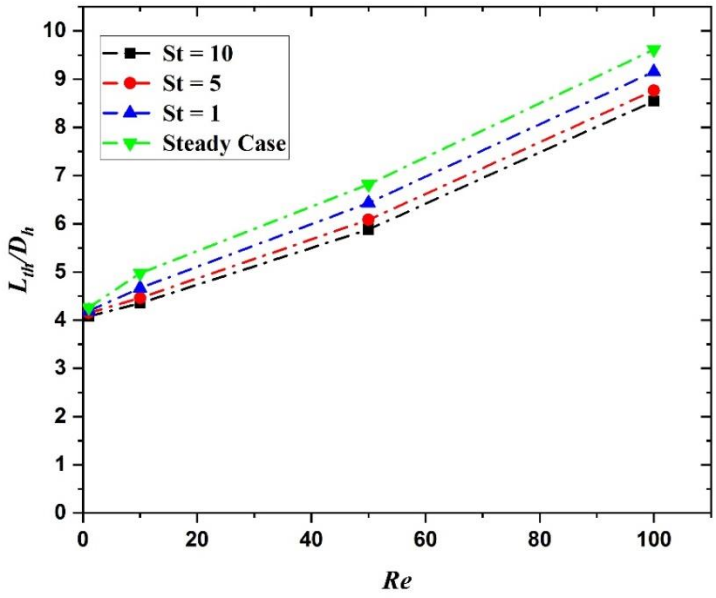

Figure 5.14 Comparison of L_{th}/Dh as a function of Reynolds number for different Strouhal number at constant A = 0.2

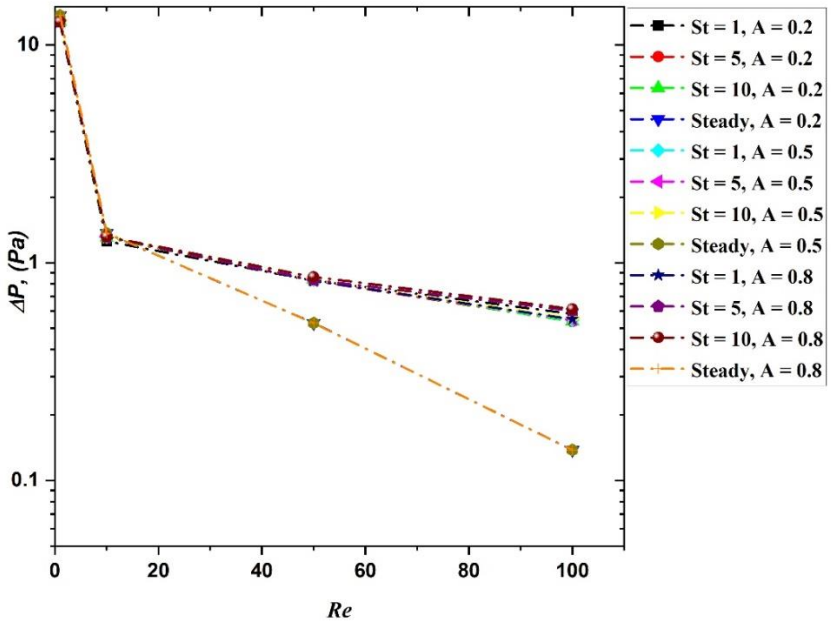

Figure 5.15. Variation of ΔP with Reynolds number for different amplitude and Strouhal number.

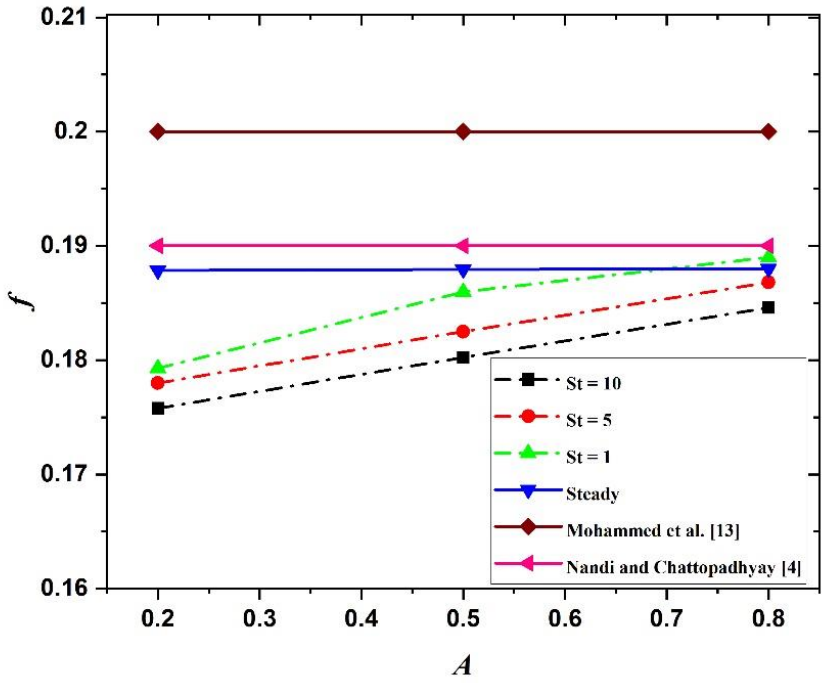

Figure 5.16 Variation of friction factor with amplitude (A) for different Strouhal number at constant Re = 10.

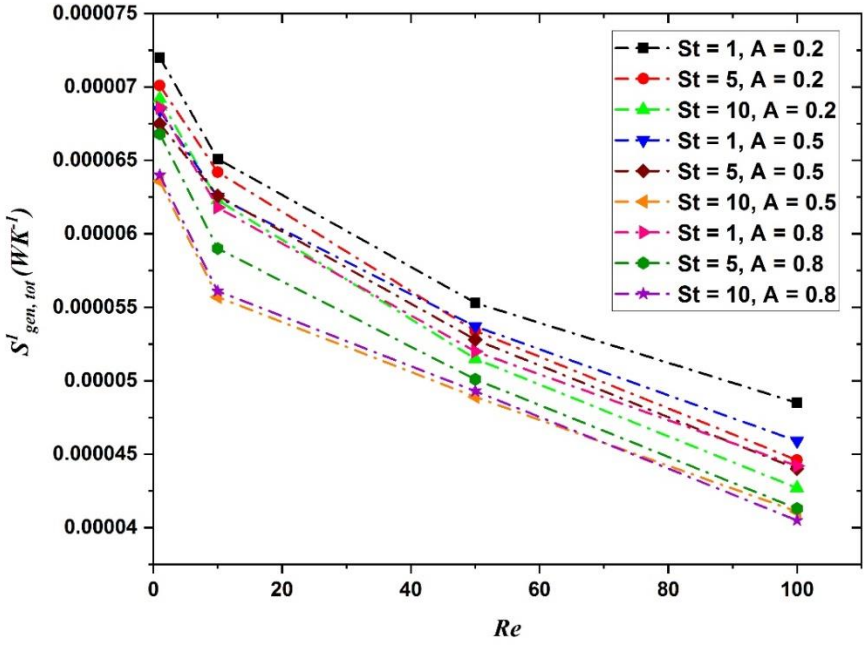

Figure 5.17 (a) Total entropy generation as a function of Re at different amplitude and Strouhal number

The deviation from the case of steady flow is more pronounced at higher Reynolds number corresponding to increased fluid momentum in the channel.

Pressure drop is the penalty that has to be paid at the cost of enhanced heat transfer in enhancing techniques by employing wavy and twisted channel geometry. The narrow and fluctuating flow passage obstructs the fluid mixing especially at low Reynolds number attributing high pressure drop but as the Reynolds number increases the pressure drop decreases and the differences among the parameters are negligible. The Figure 5.15 shows variation of $\Delta\mathbf{P}$ as a function of the Reynolds number at different amplitude (A) and different Strouhal number.

As in Figure 5.15, $\Delta\mathbf{p}$ is plotted against Reynolds number, now it is important to how friction factor behaves as a function of amplitude. In Figure 5.16, time-averaged friction factor as a function of amplitude is presented. From the figure one sees that the steady case provides higher friction factor over all the cases of pulsating flows. The present work depicts that with increase in frequency of the inlet flow pulsation (represented by Strouhal number for the present study), the present geometry gives high pressure drop result. However, with increase in amplitude of the flow pulsation, the present scheme exhibits increasing trends of pressure drop.

Figs. 5.17 (a) and (b) portrays the effects of the Re on the total entropy generation ($S^{\prime}_{gen,tot}$), and entropy generation number (EGN) for TSWMC. The S_{gen} depends on thermal entropy generation and friction entropy generation . An increase in Reynolds number is related to higher flow rate leading to higher fluid temperature. This leads to lower temperature difference between channel wall and fluid and as a result $S^{\prime}_{gen,T}$ decreases with increasing Reynolds number. However as velocity increases, the pressure drop in channel increases with Reynolds number and as a result $S^{\prime}_{gen,F}$ increases. From the figure, it is clear that the $S^{\prime}_{gen}$ decreases for all the tested cases with increase in Reynolds number. The

thermal performance of a MCHE can be improved by employing sinusoidal pulsation at the inlet, thus minimizing the entropy generation. It can also be noted that with increase in pulsation amplitude the entropy generation

result yields better performance. The figure also illustrates that the case with maximum Strouhal number and pulsation amplitude is showing the best result. To compare the performance of the TSWMC with plain channel, a dimensionless quantity named augmentation entropy generation number (EGN) is used. It may be defined as the ratio of total entropy generation furnished by TSWMC to the total entropy generation by the plain channel. Fig. 5.17(b) depicts the comparison of augmentation entropy generation number with Reynolds number. The objective is to decrease the total entropy generation, hence, the EGN value less than unity would suggest better result. The figure displays that as an effect of Strouhal number and pulsation amplitude, all the tested cases are showing values less than unity. It is also noteworthy that two cases with A= 0.8, St = 10 and A = 0.8, St = 5 are showing best result. This approach can thus help in finding the optimum situations.

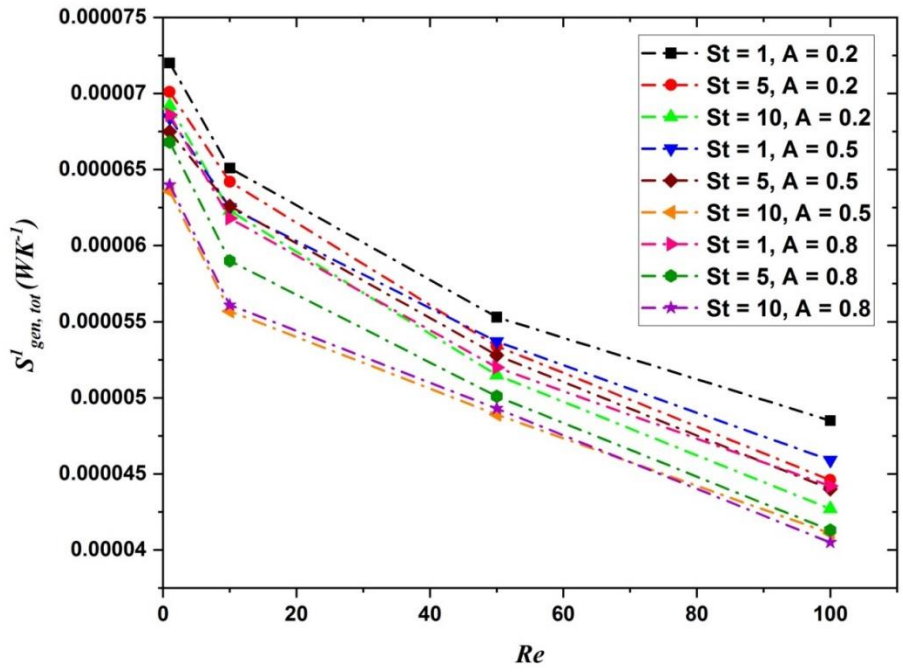

5.17(b) Entropy generation number (EGN) as a function of Re at different A and Strouhal number.

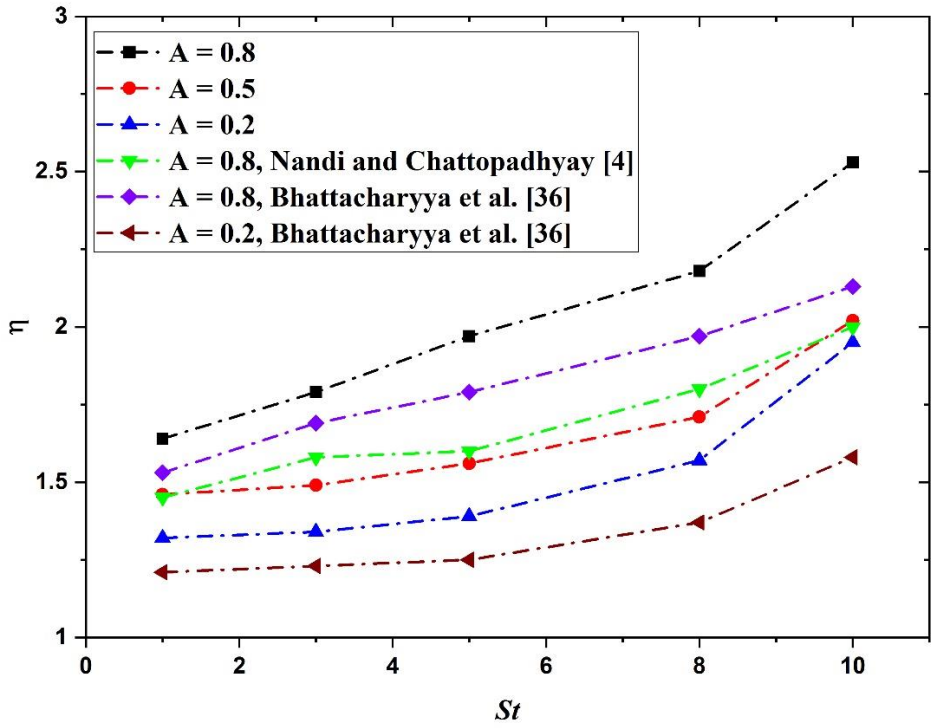

Figure 5.18(a) Comparison of η with St at different amplitude at constant Re = 100

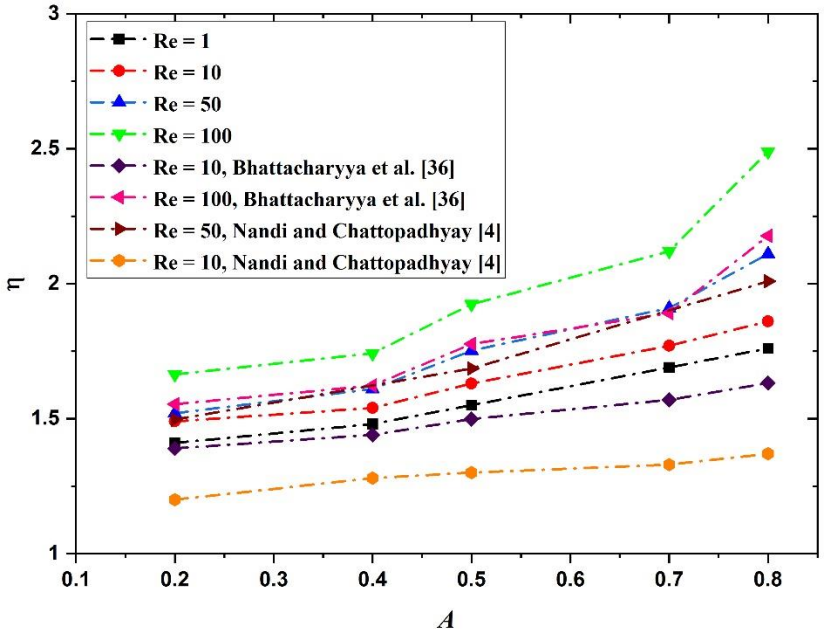

Figure 5.18(b) comparison of η with amplitude at different Re, at constant Strouhal number = 10

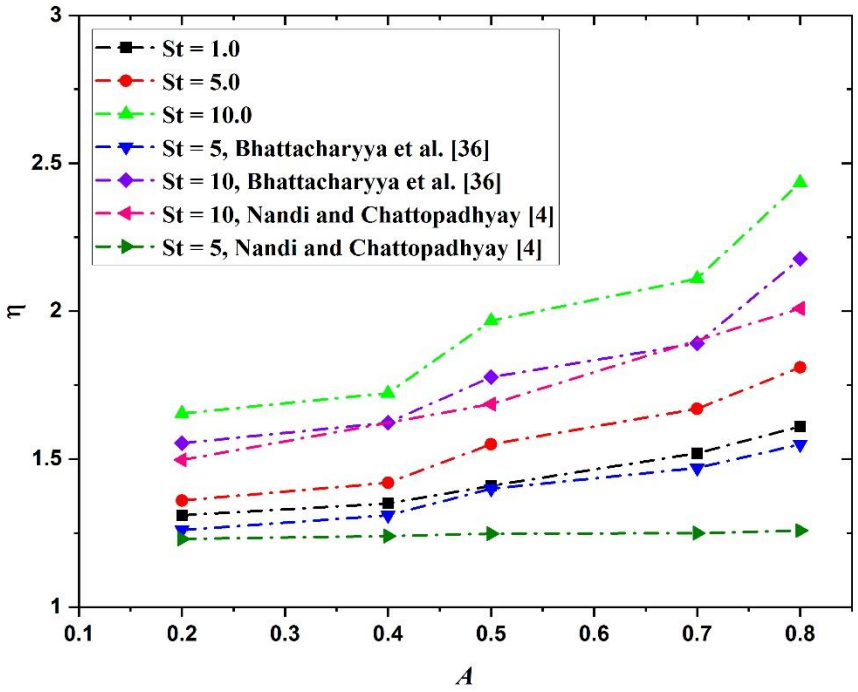

Figure 5.18(c) comparison of η with amplitude at different St, at constant Re = 100.

In Figure 5.18(a), η is shown as a function of Strouhal number at different Amplitude (A) and constant Reynolds number (Re = 10). The figure shows that at Re = 10, the present scheme offers η values more than unity. In Figure 5.18 (b), η is shown as a function of amplitude (A) at different Reynolds number and constant St = 10. The results also compared with the previous work of Nandi and Chattopadhyay (2013) and Bhattacharyya et al. (2019), for different channel geometry (straight channel with wavy surface corrugations). The present figure offers η values more than unity. Figure 5.18 (c), η is shown as a function of amplitude (A) at different Strouhal number and constant Reynolds number = 10. It is also obvious from the figure that at amplitude 0.80, the present set up is providing better result than the previous well-established work of Nandi and Chattopadhyay (2013) and

Bhattacharyya et al. (2019). At St = 10, and amplitude of 0.8 even it is providing a η value greater than 2.00. In general, increased amplitude and frequency of pulsation at inlet can provide improved thermal performance. This can be attributed to the fact that the

superimposing of the pulsation at inlet with the main flow incorporates the required instability in the flow to enhance proper mixing of fluid. Also, at high amplitude (A) of pulsation the wavy and twisted nature of the channel geometry contributes to the mixing of fluid and recirculation zones generated. Hence, the present geometry shows higher transport enhancement. The additional tortuosity in the flow passage by reversing the turn at the middle of the channel for this novel geometry leads to improved overall thermal performance compared to the channel with one directional twist.

5.5 Closure

In present work, the impact of sinusoidal pulsating flow rate in the proposed sinusoidal wavy and twisted microchannel is investigated by analysing transient three dimensional Navier – Stokes equations, for the laminar flow regime, for Reynolds numbers from 1 to 100. The inlet velocity was prescribed by superimposing a sinusoidal fluctuating component to the mean flow. Investigations were performed for a range of frequency and amplitude. As thermal wall boundary condition, constant temperature is maintained at the channel walls. Time averaged Nusselt numbers were obtained to assess the heat transfer augmentation results. To compare the efficiency of the proposed scheme with previous well-established works, thermal performance enhancement Criteria (η) combining heat transfer rate and pressure drop was also examined. The proposed geometry showed better results in terms of thermal performance and also with minimal pressure drop. The influence of flow rate pulsations on the thermal development length was also examined.

CHAPTER SIX

CONCLUSION

AND

FUTURE SCOPE OF WORK

7.1 Summary & Closure

The present work explores the transport phenomena in various micro-channel geometries with and without inlet pulsation for simultaneously developing flow in micro-channels. Both two dimensional and three dimensional geometries were considered for the analysis purpose. Two types of two dimensional channels with contraction in flow passage namely stepped channel and converging diverging channel were investigated. Further, two types of three dimensional wavy and twisted micro-channels were studied. Assessment of the effect of contraction (both sudden and gradual contraction) inside the flow passage over heat transfer was the goal of the two dimensional micro-channel analysis. For further improved thermal performance, and to obtain a better insight of the transport phenomena, a novel three dimensional microchannel was proposed. For three dimensional cases also, two separate channels were designed with different twist combination. The channel with square section is twisted clockwise for the first case whereas, the second geometry was twisted clockwise for half of the length and for the rest half, the twist is reversed. Computational simulation of Navier-Stokes equation was performed for all the cases. Also, a sinusoidal velocity component was superimposed over the inlet velocity to achieve augmented thermal performance. For the two-dimensional cases, the results of modified geometry were compared with the case of inlet flow pulsation with modified geometry, to prescribe optimum result. Different contraction ratio was analyzed to study the effect. The computation was performed for laminar flow regime with Reynolds number ranging 100 – 500. Constant temperature condition was maintained at the channel walls as thermal boundary condition. To validate the present scheme, previous well established results were compared with the current set of results. Dimensionless Nusselt number and friction factor were measured to assess the augmented heat transfer. The performance enhancement criterion (η) that combines heat transfer as well as pressure drop, was also examined to evaluate the performance of the present geometry. The proposed geometry showed better thermal result compared to plain

channel. Optimum contraction ratio revealing the best overall thermal performance, was also prescribed.

For the three dimensional cases also, two separate channels with different twist pattern i.e., clockwise twisted for the first channel, and clockwise twist combined with anticlockwise twist for the second channel was incorporated. The first half length (starting from inlet) of the second channel was made clockwise twisted while the remaining half was made anticlockwise twisted. For both the cases, a sinusoidal pulsating velocity component was superimposed over the main flow at the channel inlet. The solution of the governing equations for mass, momentum and energy were obtained using the SIMPLE algorithm of Patankar (1977). The focus of the study has been to achieve a heat transfer enhancement by a combined application of the both measures.

One important objective of the study was to determine the potential heat transfer enhancement for such unsteady flow condition over the steady flow. The effect of varying Strouhal number and amplitude of pulsation was computed at different Reynolds number values. Analysis of the fluid flow and heat transfer phenomena in micro channels was conducted by solving relevant governing equations for observing the effect of flow pulsation over the transport processes in the laminar regime of developing microchannel flow. Both two dimensional and three dimensional convective heat transfer calculations are performed at low and moderate Reynolds number ($Re \leq 100$) appropriate for microchannel flows. The phenomena of wall slip were not considered in this present work. A performance parameter combining the enhancement in heat transfer and pressure drop were used to assess the overall performance of the MCHS.

For three dimensional cases also, the impact of a sinusoidally pulsating flow at the inlet of the micro-channels were investigated by analyzing transient Navier – Stokes equations. The inlet velocity was prescribed by superimposing a sinusoidal fluctuating

component to the mean flow. Investigations were performed for a range of frequency and amplitude. Time average Nusselt number values were calculated to assess the heat transfer enhancement results. To compare the efficiency of the proposed scheme with previous well-established works, performance enhancement criteria (η) combining heat transfer and pressure drop was also investigated. Enhanced value of η has been found possible though with a slight penalty in terms of entropy generation. The effect of inlet flow pulsation on thermal development length of the novel microchannel was also examined. For the two dimensional cases an inflated enhancement criterion up to 30% was reported. The three dimensional geometries provided much better results instead. The inlet pulsation enhanced the Nusselt number greatly, while keeping the pressure drop almost same as of the plain channel in spite of, the tortuous flow passage. A maximum increase in performance enhancement criteria about 63% was obtained as a result of inlet flow pulsation at these three dimensional twisted micro-channels.

7.2 Future Scope of Work

Present study is an effort of numerical modeling and analysis of transport phenomena in micro-channels with various geometrical configuration for simultaneously developing flow condition with inlet pulsation. This work gains a greater understanding of the process by means of rigorous numerical simulation by solution of full Navier- Stokes equation. It is expected that the true potential of thermal management of MCHS employing the inlet velocity pulsation would be realized in practical applications. However, further research is necessary to compliment and validate the present findings. Following are some of the examples that would be a logical successor of the present approach.

1. In this numerical investigation, wall slip boundary conditions were not incorporated. This study can be further developed by considering the slip at the wall, which is important for rarefied flows.

2. Temperature jump plays an important role in case of rarefied flows in channels. Incorporation of this type of boundary condition would be subject of interest.
3. The study considered only isothermal channel walls as the thermal wall boundary condition. Non-isothermal wall boundary conditions with specified heat flux and mixed boundary conditions may be an interesting extension in this field.
4. This study was limited to only one working fluid i.e. water. It should be extended to analyses with multiple cooling fluid.
5. This study is carried out with numerical procedures only. Rigorous experimentation is required for confirming the outcome from this study.
6. This study is limited to single phase flow in microchannel. Further studies on two phase flow in microchannel is possible.

References

Ahmad, T. and Hassan, I. (2010) 'Experimental analysis of microchannel entrance length characteristics using microparticle image velocimetry', *Journal of Fluids Engineering, Transactions of the ASME*, 132(4), pp. 0411021–04110213. Available at: https://doi.org/10.1115/1.4001292.

Al-Neama, A.F. (2025) 'Improving heat transfer in micro-heat exchangers using the dynamic wall technique', *International Communications in Heat and Mass Transfer*, 167(PA), p. 109259. Available at: https://doi.org/10.1016/j.icheatmasstransfer.2025.109259.

Ali, N. *et al.* (2024) 'Heat dissipation and fluid flow in micro-channel heat sink equipped with semi-elliptical pin-fin structures: A numerical study', *International Communications in Heat and Mass Transfer*, 155(April), p. 107492. Available at: https://doi.org/10.1016/j.icheatmasstransfer.2024.107492.

Avci, M. and Aydin, O. (2007) 'Mixed convection in a vertical parallel plate microchannel with asymmetric wall heat fluxes', *Journal of Heat Transfer*, 129(8), pp. 1091–1095. Available at: https://doi.org/10.1115/1.2737483.

Awad, M.M. (2015) *A reviewof entropy generation in microchannels*, *Advances in Mechanical Engineering*. Available at: https://doi.org/10.1177/1687814015590297.

Chang, S.W., Jan, Y.J. and Liou, J.S. (2007) 'Turbulent heat transfer and pressure drop in tube fitted with serrated twisted tape', *International Journal of Thermal Sciences*, 46(5), pp. 506–518. Available at: https://doi.org/10.1016/j.ijthermalsci.2006.07.009.

Chattopadhyay, H., Durst, F. and Ray, S. (2006) 'Analysis of heat transfer in simultaneously developing pulsating laminar flow in a pipe with constant wall temperature', *International Communications in Heat and Mass Transfer*, 33(4), pp. 475–481. Available at: https://doi.org/10.1016/j.icheatmasstransfer.2005.12.008.

Chen, C.K. and Cho, C.C. (2007) 'Electrokinetically-driven flow mixing in microchannels

with wavy surface', *Journal of Colloid and Interface Science*, 312(2), pp. 470–480. Available at: https://doi.org/10.1016/j.jcis.2007.03.033.

Croce, G., D'agaro, P. and Nonino, C. (2007) 'Three-dimensional roughness effect on microchannel heat transfer and pressure drop', *International Journal of Heat and Mass Transfer*, 50(25–26), pp. 5249–5259. Available at: https://doi.org/10.1016/j.ijheatmasstransfer.2007.06.021.

Cui, K. *et al.* (2026) 'Investigations into flow and heat transfer performance of bifurcated-divergent micro-channels', *International Journal of Heat and Fluid Flow*, 117(PA), p. 110030. Available at: https://doi.org/10.1016/j.ijheatfluidflow.2025.110030.

Das, S.G. *et al.* (2021) 'Transport Phenomenon of Simultaneously Developing Flow and Heat Transfer in Twisted Sinusoidal Wavy Microchannel under Pulsating Inlet Flow Condition', *Heat Transfer Engineering*, 43(3–5), pp. 410–422. Available at: https://doi.org/10.1080/01457632.2021.1875166.

Ebrahim Qomi, M., Sheikhzadeh, G.A. and Fattahi, A. (2020) 'Heat transfer enhancement in a microchannel using a pulsating MHD hybrid nanofluid flow', *Energy Sources, Part A: Recovery, Utilization and Environmental Effects*, 00(00), pp. 1–16. Available at: https://doi.org/10.1080/15567036.2020.1834031.

Faraji, M. and El Qarnia, H. (2010) 'Numerical study of free convection dominated melting in an isolated cavity heated by three protruding electronic components', *IEEE Transactions on Components and Packaging Technologies*, 33(1), pp. 167–177. Available at: https://doi.org/10.1109/TCAPT.2009.2029086.

Ganguly, S. *et al.* (2015) 'Thermally developing combined electroosmotic and pressure-driven flow of nanofluids in a microchannel under the effect of magnetic field', *Chemical Engineering Science*, 126, pp. 10–21. Available at: https://doi.org/10.1016/j.ces.2014.11.060.

Ghaedamini, H., Lee, P.S. and Teo, C.J. (2013) 'Developing forced convection in converging-diverging microchannels', *International Journal of Heat and Mass Transfer*, 65, pp. 491–499. Available at: https://doi.org/10.1016/j.ijheatmasstransfer.2013.06.036.

Guo, Z.Y. and Li, Z.X. (2003) 'Size effect on single-phase channel flow and heat transfer at microscale', *International Journal of Heat and Fluid Flow*, 24(3), pp. 284–298. Available at: https://doi.org/10.1016/S0142-727X(03)00019-5.

Haider, S.M.M. *et al.* (2025) 'Effects of rib geometry on hydrothermal performance of composite secondary micro-channels', *International Communications in Heat and Mass Transfer*, 168(August), p. 109501. Available at: https://doi.org/10.1016/j.icheatmasstransfer.2025.109501.

Han, Y., Lee, Y.J. and Zhang, X. (2013) 'Trapezoidal microchannel heat sink with pressure-driven and electro-osmotic flows for microelectronic cooling', *IEEE Transactions on Components, Packaging and Manufacturing Technology*, 3(11), pp. 1851–1858. Available at: https://doi.org/10.1109/TCPMT.2013.2272478.

Hanafi, M.Z.M., Ismail, F.S. and Rosli, R. (2015) 'Radial plate fins heat sink model design and optimization', *2015 10th Asian Control Conference: Emerging Control Techniques for a Sustainable World, ASCC 2015* [Preprint]. Available at: https://doi.org/10.1109/ASCC.2015.7244448.

Harms, T.M., Kazmierczak, M.J. and Gerner, F.M. (1999) 'Developing convective heat transfer in deep rectangular microchannels', *International Journal of Heat and Fluid Flow*, 20(2), pp. 149–157. Available at: https://doi.org/10.1016/S0142-727X(98)10055-3.

Hetsroni, G. *et al.* (2009) 'Heat transfer of gas-liquid mixture in micro-channel heat sink', *International Journal of Heat and Mass Transfer*, 52(17–18), pp. 3963–3971.

Available at: https://doi.org/10.1016/j.ijheatmasstransfer.2009.03.027.

Hrnjak, P. and Tu, X. (2007) 'Single phase pressure drop in microchannels', *International Journal of Heat and Fluid Flow*, 28(1 SPEC. ISS.), pp. 2–14. Available at: https://doi.org/10.1016/j.ijheatfluidflow.2006.05.005.

Huang, B. *et al.* (2020) 'Experimental investigation of the flow and heat transfer performance in micro-channel heat exchangers with cavities', *International Journal of Heat and Mass Transfer*, 159. Available at: https://doi.org/10.1016/j.ijheatmasstransfer.2020.120075.

Huang, Y. *et al.* (2024) 'Investigation of thermo-hydrodynamic characteristics in micro-oscillating heat pipe by alternatively-arranged ratchet microchannels', *International Journal of Heat and Mass Transfer*, 222(December 2023), p. 125134. Available at: https://doi.org/10.1016/j.ijheatmasstransfer.2023.125134.

Judy, J., Maynes, D. and Webb, B.W. (2002) 'Characterization of frictional pressure drop for liquid flows through microchannels', *International Journal of Heat and Mass Transfer*, 45(17), pp. 3477–3489. Available at: https://doi.org/10.1016/S0017-9310(02)00076-5.

Klank, H. *et al.* (2002) 'INSTITUTE OF PHYSICS PUBLISHING JOURNAL OF MICROMECHANICS AND MICROENGINEERING PIV measurements in a microfluidic 3D-sheathing structure with three-dimensional flow behaviour', *J. Micromech. Microeng*, 12, pp. 862–869. Available at: http://iopscience.iop.org/0960-1317/12/6/318.

Li, J. and Peterson, G.P. (2006) 'Geometric optimization of a micro heat sink with liquid flow', *IEEE Transactions on Components and Packaging Technologies*, 29(1), pp. 145–154. Available at: https://doi.org/10.1109/TCAPT.2005.853170.

Liu, D. and Garimella, S. V. (2002) 'Investigation of liquid flow in microchannels', *8th*

AIAA/ASME Joint Thermophysics and Heat Transfer Conference, 18(1), pp. 65–72. Available at: https://doi.org/10.2514/6.2002-2776.

Lori, M.S. and Vafai, K. (2022) 'Heat transfer and fluid flow analysis of microchannel heat sinks with periodic vertical porous ribs', *Applied Thermal Engineering*, 205(January), p. 118059. Available at: https://doi.org/10.1016/j.applthermaleng.2022.118059.

Lu, H., Gong, L. and Xu, M. (2013) 'Thermal performance of microchannels with dimples for electronics cooling', *ASME 2013 4th International Conference on Micro/Nanoscale Heat and Mass Transfer, MNHMT 2013*, 1(7), pp. 1029–1035. Available at: https://doi.org/10.1115/MNHMT2013-22198.

Maynes, D. and Webb, B.W. (2003) 'Fully developed electro-osmotic heat transfer in microchannels', *International Journal of Heat and Mass Transfer*, 46(8), pp. 1359–1369. Available at: https://doi.org/10.1016/S0017-9310(02)00423-4.

Meinhart, C.D., Wereley, S.T. and Santiago, J.G. (1999) 'PIV measurements of a microchannel flow', *Experiments in Fluids*, 27(5), pp. 414–419. Available at: https://doi.org/10.1007/s003480050366.

Mohammed, H.A., Gunnasegaran, P. and Shuaib, N.H. (2011) 'Numerical simulation of heat transfer enhancement in wavy microchannel heat sink', *International Communications in Heat and Mass Transfer*, 38(1), pp. 63–68. Available at: https://doi.org/10.1016/j.icheatmasstransfer.2010.09.012.

Morini, G.L. *et al.* (2006) 'Thermal performance of silicon micro heat-sinks with electrokinetically-driven flows', *International Journal of Thermal Sciences*, 45(10), pp. 955–961. Available at: https://doi.org/10.1016/j.ijthermalsci.2006.01.009.

Morini, G.L. and Spiga, M. (2007) 'The role of the viscous dissipation in heated microchannels', *Journal of Heat Transfer*, 129(3), pp. 308–318. Available at: https://doi.org/10.1115/1.2430725.

Nandi, T.K. and Chattopadhyay, H. (2013) ‘Numerical investigations of simultaneously developing flow in wavy microchannels under pulsating inlet flow condition’, *International Communications in Heat and Mass Transfer*, 47, pp. 27–31. Available at: https://doi.org/10.1016/j.icheatmasstransfer.2013.06.008.

Nandi, T.K. and Chattopadhyay, H. (2014) ‘Numerical investigations of developing flow and heat transfer in raccoon type microchannels under inlet pulsation’, *International Communications in Heat and Mass Transfer*, 56, pp. 37–41. Available at: https://doi.org/10.1016/j.icheatmasstransfer.2014.04.017.

Nandi, T.K. and Duari, S. (2022) ‘A Numerical Study on Fluid Flow and Heat Transfer in a Flow Interrupting Ribbed Microchannel under Inlet Flow Pulsation’, *International Journal for Research in Applied Science and Engineering Technology*, 10(7), pp. 5006–5012. Available at: https://doi.org/10.22214/ijraset.2022.46086.

Narrein, K., Sivasankaran, S. and Ganesan, P. (2016) ‘Numerical investigation of two-phase laminar pulsating nanofluid flow in a helical microchannel’, *Numerical Heat Transfer; Part A: Applications*, 69(8), pp. 921–930. Available at: https://doi.org/10.1080/10407782.2015.1090834.

Ničeno, B. and Nobile, E. (2001) ‘Numerical analysis of fluid flow and heat transfer in periodic wavy channels’, *International Journal of Heat and Fluid Flow*, 22(2), pp. 156–167. Available at: https://doi.org/10.1016/S0142-727X(01)00074-1.

Obot, N.T. (2002) ‘Toward a better understanding of friction and heat/mass transfer in microchannels - A literature review’, *Microscale Thermophysical Engineering*, 6(3), pp. 155–173. Available at: https://doi.org/10.1080/10893950290053295.

Parida, P.R. *et al.* (2010) ‘Experimental investigation of cooling performance of metal-based microchannels’, *Heat Transfer Engineering*, 31(6), pp. 485–494. Available at: https://doi.org/10.1080/01457630903409654.

Patankar, S. V., Liu, C.H. and Sparrow, E.M. (1977) 'Fully developed flow and heat transfer in ducts having streamwise-periodic variations of cross-sectional area', *Journal of Heat Transfer*, 99(2), pp. 180–186. Available at: https://doi.org/10.1115/1.3450666.

Peng, X.F. and Peterson, G.P. (1996) 'Convective heat transfer and flow friction for water flow in microchannel structures', *International Journal of Heat and Mass Transfer*, 39(12), pp. 2599–2608. Available at: https://doi.org/10.1016/0017-9310(95)00327-4.

Persoons, T. *et al.* (2009) 'Heat transfer enhancement due to pulsating flow in a microchannel heat sink', *15th International Workshop on Thermal Investigations of ICs and Systems, THERMINIC 2009*, (October), pp. 163–167.

Pfahler, J. *et al.* (1991) 'Gas and liquid flow in small channels', *American Society of Mechanical Engineers, Dynamic Systems and Control Division (Publication) DSC*, 32(June 2016), pp. 49–60.

Qu, W. and Mudawar, I. (2002) 'Experimental and numerical study of pressure drop and heat transfer in a single-phase micro-channel heat sink', *International Journal of Heat and Mass Transfer*, 45(12), pp. 2549–2565. Available at: https://doi.org/10.1016/S0017-9310(01)00337-4.

Ramgadia, A.G. and Saha, A.K. (2013) 'Numerical study of fully developed flow and heat transfer in a wavy passage', *International Journal of Thermal Sciences*, 67, pp. 152–166. Available at: https://doi.org/10.1016/j.ijthermalsci.2012.12.005.

Rhie, C.M. and Chow, W.L. (1983) 'Numerical study of the turbulent flow past an airfoil with trailing edge separation', *AIAA Journal*, 21(11), pp. 1525–1532. Available at: https://doi.org/10.2514/3.8284.

Rostami, J. and Abbassi, A. (2016) 'Conjugate heat transfer in a wavy microchannel using nanofluid by two-phase Eulerian-Lagrangian method', *Advanced Powder Technology*, 27(1), pp. 9–18. Available at: https://doi.org/10.1016/j.apt.2015.10.003.

Sakanova, A., Keian, C.C. and Zhao, J. (2015) ‘Performance improvements of microchannel heat sink using wavy channel and nanofluids’, *International Journal of Heat and Mass Transfer*, 89, pp. 59–74. Available at: https://doi.org/10.1016/j.ijheatmasstransfer.2015.05.033.

Sakkay, M. *et al.* (2024) ‘Enhancing heat transfer efficiency and entropy generation minimization in Micro-Channel Heat Sinks through pillar spacing and diameter optimization’, *International Journal of Heat and Fluid Flow*, 108(May), p. 109492. Available at: https://doi.org/10.1016/j.ijheatfluidflow.2024.109492.

Sheikholeslami, M. and Rokni, H.B. (2017) ‘Nanofluid two phase model analysis in existence of induced magnetic field’, *International Journal of Heat and Mass Transfer*, 107, pp. 288–299. Available at: https://doi.org/10.1016/j.ijheatmasstransfer.2016.10.130.

Sivasankaran, S. and Narrein, K. (2016) ‘Numerical investigation of two-phase laminar pulsating nanofluid flow in helical microchannel filled with a porous medium’, *International Communications in Heat and Mass Transfer*, 75, pp. 86–91. Available at: https://doi.org/10.1016/j.icheatmasstransfer.2016.03.016.

Steinke, M.E. and Kandlikar, S.G. (2004) ‘Single-phase heat transfer enhancement techniques in microchannel and minichannel flows’, *Proceedings of the Second International Conference on Microchannels and Minichannels (ICMM2004)*, pp. 141–148. Available at: https://doi.org/10.1115/icmm2004-2328.

Sui, Y. *et al.* (2010) ‘Fluid flow and heat transfer in wavy microchannels’, *International Journal of Heat and Mass Transfer*, 53(13–14), pp. 2760–2772. Available at: https://doi.org/10.1016/j.ijheatmasstransfer.2010.02.022.

Sui, Y., Teo, C.J. and Lee, P.S. (2012) ‘Direct numerical simulation of fluid flow and heat transfer in periodic wavy channels with rectangular cross-sections’, *International*

Journal of Heat and Mass Transfer, 55(1–3), pp. 73–88. Available at: https://doi.org/10.1016/j.ijheatmasstransfer.2011.08.041.

Taylor, P. and Grande, W.J. (2010) 'Evolution of Microchannel Flow Passages--Thermohydraulic Performance and Fabrication Technology Evolution of Microchannel Flow Passages — Thermohydraulic Performance and', *Mechanical Engineering*, (February 2012), pp. 37–41. Available at: https://doi.org/10.1080/01457630390116077.

Tretheway, D.C. and Meinhart, C.D. (2002) 'Apparent fluid slip at hydrophobic microchannel walls', *Physics of Fluids*, 14(3). Available at: https://doi.org/10.1063/1.1432696.

Tuckerman, D.B. and Pease, R.F.W. (1981) 'High-Performance Heat Sinking for VLSI', *IEEE Electron Device Letters*, EDL-2(5), pp. 126–129. Available at: https://doi.org/10.1109/EDL.1981.25367.

Wang, B.X. and Peterson, G.P. (1994) 'Heat transfer characteristics of water flowing through microchannels', *Experimental Heat Transfer*, 7(4), pp. 265–283. Available at: https://doi.org/10.1080/08916159408946485.

Wang, C.S. *et al.* (2020) 'Lattice Boltzmann study of flow pulsation on heat transfer augmentation in a louvered microchannel heat sink', *International Journal of Heat and Mass Transfer*, 148, p. 119139. Available at: https://doi.org/10.1016/j.ijheatmasstransfer.2019.119139.

Wang, G. and Vanka, S.P. (1995) 'Convective heat transfer in periodic wavy passages', *International Journal of Heat and Mass Transfer*, 38(17), pp. 3219–3230. Available at: https://doi.org/10.1016/0017-9310(95)00051-A.

Wang, S.L. *et al.* (2022) 'Heat transfer enhancement of symmetric and parallel wavy microchannel heat sinks with secondary branch design', *International Journal of*

Thermal Sciences, 171(July 2021). Available at: https://doi.org/10.1016/j.ijthermalsci.2021.107229.

Wu, H.Y. and Cheng, P. (2003) 'Friction factors in smooth trapezoidal silicon microchannels with different aspect ratios', *International Journal of Heat and Mass Transfer*, 46(14), pp. 2519–2525. Available at: https://doi.org/10.1016/S0017-9310(03)00106-6.

Wu, W., Zhao, L. and Dong, H. (2025) 'Study on enhanced heat transfer of a micro-channel radiator with flexible microcolumn clusters by CFD', *Applied Thermal Engineering*, 264(November 2024), p. 125445. Available at: https://doi.org/10.1016/j.applthermaleng.2025.125445.

Wu, Y. *et al.* (2024) 'Experimental investigations of flow boiling heat transfer performance in finned micro-channels', *International Journal of Heat and Fluid Flow*, 110(October), p. 109610. Available at: https://doi.org/10.1016/j.ijheatfluidflow.2024.109610.

Xie, G. *et al.* (2013) 'Comparative study of thermal performance of longitudinal and transversal-wavy microchannel heat sinks for electronic cooling', *Journal of Electronic Packaging, Transactions of the ASME*, 135(2), pp. 1–9. Available at: https://doi.org/10.1115/1.4023530.

Xu, C. *et al.* (2021) 'Experimental investigation of flow and heat transfer characteristics of pulsating flows driven by wave signals in a microchannel heat sink', *International Communications in Heat and Mass Transfer*, 125, p. 105343. Available at: https://doi.org/10.1016/j.icheatmasstransfer.2021.105343.

Yan, X. *et al.* (2025) 'Experimental study of flow boiling heat transfer in rectangular ribbed micro-channels with rectangular cavities', *International Journal of Heat and Mass Transfer*, 236(P2), p. 126402. Available at: https://doi.org/10.1016/j.ijheatmasstransfer.2024.126402.

Yang, C. *et al.* (2019) 'Heat transfer characteristics of magnetohydrodynamic electroosmotic flow in a rectangular microchannel', *European Journal of Mechanics, B/Fluids*, 74, pp. 180–190. Available at: https://doi.org/10.1016/j.euromechflu.2018.11.015.

Yeh, C.T. and Yang, C.Y. (2009) 'Performance comparison of rectangular and air-foil shapes offset strip flow paths micro-heat exchangers', *Heat Transfer Engineering*, 30(1–2), pp. 54–61. Available at: https://doi.org/10.1080/01457630802293373.

Zhang, D. *et al.* (2024) 'Experimental study of heat transfer performance in rectangular microchannels enhanced by ultrasound', *International Journal of Heat and Mass Transfer*, 228(April), p. 125626. Available at: https://doi.org/10.1016/j.ijheatmasstransfer.2024.125626.

Zhang, Z. *et al.* (2024) 'Experimental investigations into flow boiling heat transfer in a micro-channel with hybrid of fin and porous coating structure', *International Journal of Heat and Mass Transfer*, 229(May), p. 125704. Available at: https://doi.org/10.1016/j.ijheatmasstransfer.2024.125704.

Zhang, Z. *et al.* (2025) 'Experimental investigation into flow boiling heat transfer in ribbed micro-channel with porous-decorated sidewalls', *International Journal of Thermal Sciences*, 214(December 2024), p. 109883. Available at: https://doi.org/10.1016/j.ijthermalsci.2025.109883.

Zhou, T., Xin, Z. and Wang, L. (2026) 'Heat transfer enhancement in a microchannel via passive vortex generators combining with cylinder and symmetrically clamped elastic flaps', *International Journal of Thermal Sciences*, 220(PA), p. 110262. Available at: https://doi.org/10.1016/j.ijthermalsci.2025.110262.

Sampad Lokinda Das
23/06/25.